Identifying vulnerabilities in sugar nucleotide metabolism of cancer cells

Identifying vulnerabilities in sugar nucleotide metabolism of cancer cells

A Dissertation Presented

By

MIHIR B. DOSHI

Submitted to the Faculty of the

Morningside Graduate School of Biomedical Sciences at UMass Chan Medical School

in partial fulfillment of the requirements for the degree of

DOCTOR OF PHILOSOPHY

October 20, 2023

CANCER BIOLOGY

Identifying vulnerabilities in sugar nucleotide metabolism of cancer cells

A Dissertation Presented

By

MIHIR B. DOSHI

This work was undertaken in the Morningside Graduate School of Biomedical Sciences

Cancer Biology Program

Under the mentorship of

_____
Dohoon Kim, Ph.D., Thesis Advisor

_____
Arthur M. Mercurio, Ph.D., Member of Committee

_____
Michael J. Lee, Ph.D., Member of Committee

_____
David Guertin, Ph.D., Member of Committee

_____
Nada Kalaany, Ph.D., External Member of Committee

_____
Cole Haynes, Ph.D., Chair of Committee

_____
Mary Ellen Lane, Ph.D.,

Dean of the Graduate School of Biomedical Sciences
October 20, 2023

DEDICATION

To my late grandparents, Chhotalal M. Doshi and Kantaben Doshi, whose unconditional love and wisdom greatly contributed to the person I have become.

ACKNOWLEDGEMENTS

The GSBS program at UMass Chan Medical School has been an exceptional experience, marking a special chapter in my life where I had the privilege of collaborating with highly supportive and brilliant individuals.

First and foremost, I express my sincere gratitude to my thesis advisor, **Dohoon Kim (Do)**, for being an exceptional mentor. Do has consistently been generous with his time, providing guidance and allowing me the freedom to explore innovative experiments. His mentorship style, a blend of encouraging creativity and offering thoughtful direction through brainstorming sessions, has been instrumental in bringing out the best in me. I appreciate the numerous opportunities he provided for collaboration with other lab members and university peers, emphasizing participation in scientific meetings and conferences to foster critical thinking. I am truly grateful for having him as my mentor.

A heartfelt thank you goes to my thesis committee members: **Art Mercurio, Dave Guertin, Cole Haynes, and Mike Lee**. They have been a continual source of inspiration, offering valuable feedback, advice, and unwavering support. Special recognition is due to my TRAC committee chair, **Art Mercurio**, for his exceptional guidance throughout the cancer biology course and up until the submission of my PhD thesis. I extend my gratitude to the collaborators of my thesis project—**Hira Goel, Tenzin Tseyang, Olga Ponomarova, Rui Li, Julie Zhu, Christopher Ashwood, Karl Simin, Choolsoon Jang, Mariam Walhout, and Jessica Spinelli**—who played integral roles in various aspects of the project, contributing to a high-impact publication. I also acknowledge the support from Dean **Mary Ellen Lane** and the entire GSBS admin team, including **Mindy Donovan, Irina Parker,**

and Annette Stratton. I would like to express my gratitude to the external examiner, **Dr. Nada Kalaany**, for dedicating time to attend my defense, posing insightful questions, and offering valuable feedback on my thesis.

Special recognition goes to the members of the Kim lab with whom I shared the lab space: **Namgyu Lee, Anne Carlisle, Meghan Spears, Faith Conroy, Austin Peppers, Brennon Berard, Minoh Lim, and Valarie Bausemer**. **Namgyu**, with whom I collaborated when I first joined as a rotation student in the lab, along with **Anne and Meghan**—two graduate students who warmly welcomed me into the lab—played a significant role in shaping my experience. All three of them provided valuable scientific feedback during lab meetings and posed insightful questions that contributed to the development of my project. I extend special thanks to **Namgyu** for his assistance with in-vivo experiments. The new lab members, **Brennon Berard, Minoh Lim, and Valarie Bausemer,** have been outstanding lab mates, and I consider myself fortunate to have had the opportunity to work alongside such a supportive and exceptional team. I couldn't have asked for better lab mates.

I would like to express my gratitude to numerous friends both in the US and back in India. The list is extensive, I think it will be difficult to name all of them. Special thanks go to **Sumeet Nayak**, who was my first point of contact when I joined UMass and has been a steadfast friend since. Additionally, I want to acknowledge my graduate school colleagues, including **Anand Desai, Melanie Walker, Levi Ali, Havisha Honwad, Karthik Ramesh, Eleni Jaeklein, Michelle Mosqueda, Christine Carbone, Shivani Nanda, Megan Honeywell, Alexandria Lee, Silvia Lee, Brittany Rosener**, and many others. I am

incredibly grateful to have such amazing friends who have shared in the joys and provided valuable advice, offered encouragement, and celebrated the good times with me. Their friendship throughout the years has been truly invaluable.

Finally, my heartfelt thanks go to my family for their unwavering support throughout my Ph.D. journey. I express my deepest gratitude to my parents, **Bhavik Doshi and Vaishali Doshi**, whose unconditional love and constant encouragement have been my driving force. They have consistently inspired me to dream big, motivated me to pursue all my goals and ambitions, and supported me through every decision. My lovely partner in crime (read life**) Radha Kalekar,** has been a rock-solid support who not only helped me scientifically through my graduate journey but also kept me sane and fun. She has been supporting me from the day I set foot in the US and has always believed in me. **Radha** has been my biggest critic and strongest ally. I love you all.

ABSTRACT

Cancer cells exhibit elevated metabolic demands, imposing a need for metabolic reprogramming. The aim of the thesis is to identify a targetable metabolic vulnerability using an approach that leverages the altered pathways in cancer cells to induce the accumulation of inherently toxic metabolites to eliminate cancer cells selectively. Through a systematic analysis of transcriptomics and cancer dependency data, we identified UXS1, a Golgi enzyme responsible for converting UDP-glucuronic acid (UDPGA) to UDP-xylose that is conditionally essential in cells expressing high levels of its upstream enzyme UGDH. Here, we demonstrate that UGDH high cancer cells are dependent on UXS1 to prevent excess buildup of UDPGA, generated by UGDH. Excess UDPGA causes disruption of the structure and function of the Golgi, leading to aberrant protein glycosylation and improper protein trafficking of critical glycoproteins within cancer cells. We find that UGDH expression is elevated in various cancers, including lung adenocarcinoma and breast carcinoma. Furthermore, elevating UGDH expression is beneficial to cancer cells, because UDPGA functions as a substrate in the detoxification of chemotherapeutic agents. Therefore, chemo-resistant cells upregulate UGDH expression, enhancing their susceptibility to UXS1 ablation. Consequently, this study reveals the therapeutic potential of targeting UXS1 in cancer treatment, offering a novel approach to exploit the metabolism of sugar nucleotides in cancer cells.

TABLE OF CONTENTS

LIST OF FIGURES

LIST OF ABBREVIATIONS

2-DG	2-deoxyglucose
2-DG6P	2-deoxyglucose-6-phosphate
3KDS	3-ketodihydrosphingosine
4MU	4-methylumbelliferone
5-FU	5-Fluorourail
AKT	Protein Kinase B (PKB)
ALL	Acute lymphoblastic leukemia
ARF4	ADP Ribosylation Factor 4
Asn	Aspargine
ATP	Adenosine triphosphate
CCLE	Cancer Cell Line Encyclopedia
CDP	Cytidine diphosphate
CGN	Cis-golgi network
CMP	Cytidine monophosphate
CRISPR	Clustered regularly interspaced short palindromic repeats
CSPG	Chondroitin sulfate proteoglycans
CTG	CellTiter-Glo
CTRL	Non-targeting control guide
DEPMAP	Dependency Map
DNA	Deoxyribonucleic Acid
dox	Doxycycline
dTMP	deoxythymidine monophosphate
dUMP	deoxyuridine monophosphate
ECM	Extracellular matrix
EGF	Epidermal growth factor

EGFR	Epidermal growth factor receptor
EMT	Epithelial-mesenchymal transition
ER	Endoplasmic Reticulum
FASN	Fatty acid synthase
FGFR	Fibroblast growth factor receptor
Fuc	Fucose
GA	Golgi apparatus
GAG	Glycosaminoglycans
Gal	Galactose
GALE	UDP-galactose-4-epimerase
GalNAc	N-acetyl galactose
GBM	Glioblastoma multiforme
GDP	Guanosine diphosphate
GEPIA2	Gene Expression Profiling Interactive Analysis Program
Glc	Glucose
GlcA	Glucuronic acid
GlcNAc	N-acetyl glucose
GLDC	Glycine decarboxylase
GO	Gene Ontology
GPX4	Glutathione peroxidase 4
gRNA	guide RNA
GSD	Glycogen storage disease
GSEA	Gene set enrichment analysis
GT	Glycotransferases
GTEX	Genotype-Tissue Expression project
HA	Hyaluronic acid
HSPG	Heparan sulfate proteoglycans
IACUC	Institutional Animal Care and Use Committee

IdoA	Iduronic acid
iKO	inducible Knockout
IRB	Institutional Review Board
KDSR	3-ketodihydrosphingosine reductase
KO	Knockout
LC-MS	Liquid Chromatography-Mass Spectrometry
Man	Mannose
MDR	Multidrug reseistance receptor
MMA	methylmalonic acid
MMUT	methyl malonyl-CoA mutase
MRP	Multidrug resistance-associated protein
NAD	Nicotinamide adenine dinucleotide
NADH	Nicotinamide adenine dinucleotide-hydrogen (Reduced)
NeuAc	Neuraminic acid
NSCLC	Non small cell lung cancer
OGT	O-linked N-acetylglucosaminyltransferase
PBS	Phosphate buffered saline
PDGF	Platelet-derived growth factor
PDO	Patient-derived organoid
PDX	Patient-derived xenograft
PFA	Paraformaldehyde
PGM	Phosphogluco mutase
PHGDH	Phosphoglycerate dehydrogenase
PI3K	phosphatidylinositol 3-kinase
PKM2	Pyruvate kinase 2
pLCv2	lentiCRISPR v2 construct
PRPP	5-phosphoribosyl-1-pyrophosphate
RHAMM	Receptor for hyaluronan-mediated motility

ROS	Reactive oxygen species
RR	Ribonucleotide reductase
RTK	Receptor tyrosine kinase
SEPHS2	Selenophosphate synthetase 2
Ser	Serine
SHMT2	Serine hydroxymethyltransferase 2
SLC35	solute carrier family 35
TCA	Tricarboxylic acid
TCGA	The Cancer Genome Atlas
TCGA	The Cancer Genome Atlas
TEM	Transmission electron microscopy
TGN	Trans-golgi network
Thr	Threonine
TME	tumor micoenvironment
TP53	Tumor protein 53
TPM	Transcripts per million
Trp	Tryptophan
TYMS	Thymidylate Synthase
UDP	Uridine diphosphate
UDPGA	Uridine diphosphate-glucuronic acid
UGDH	UDP-glucose dehydrogenase
UGT	UDP-glucuronosyltransferase
UMP	Uridine monophosphate
UPR	Unfolded Protein Response
UXS1	UDP-xylose synthase 1 or UDP-glucuronic acid decarboxylase
VEGFR	Vascular endothelial growth factor receptor
VNTR	Variable number of tandem repeats

Xyl	Xylose

COPYRIGHT INFORMATION

Figures 1.4 and 1.5 are adapted from the following:

Varki A, Cummings RD, Esko JD, et al., editors. **Essentials of Glycobiology**. 2nd edition. Cold Spring Harbor (NY): Cold Spring Harbor Laboratory Press; 2009. Available from: https://www.ncbi.nlm.nih.gov/books/NBK1908/

PREFACE

The work presented in Chapter II represents published work:

Doshi MB, Lee N, Tseyang T, Ponomarova O, Goel HL, Spears M, Li R, Zhu LJ, Ashwood C, Simin K, Jang C, Mercurio AM, Walhout AJM, Spinelli JB, Kim D. **Disruption of sugar nucleotide clearance is a therapeutic vulnerability of cancer cells.** Nature. 2023 Oct 25. doi: 10.1038/s41586-023-06676-3. Epub ahead of print. PMID: 37880368.

The contributions of the authors are as follows.

M.B.D. and D.K. conceived the project; M.B.D. and D.K. designed the research. M.B.D. (with assistance described below) performed experiments involving metabolic gene knockouts; knockouts with concomitant overexpression; and combination knockouts, examining as readouts: cell viability, cell cycle analyses, organelle morphology, protein expression and size shift, protein localization, xenograft growth and mouse survival, glycosaminoglycan levels, hyaluronic acid levels and 13C labelling experiments. N.L. assisted in carrying out and analyzing cell viability and xenograft growth / mouse survival-based experiments. M.S. assisted with carrying out the cell viability-based experiments. K.S. provided tumor samples, assisted in experimental design, and assisted in analyses of experiments determining protein levels in patient derived tumor tissues and normal tissues. R.L. and L.J.Z. conducted the analyses of RNA-Seq data. O.P. performed GC-MS analyses and A.J.M.W. assisted in experimental design and in analyses. H.G. produced chemo-resistant organoids, and along with A.M.M. assisted with experimental design using these. C.A. carried out N-glycan profiling and quantitative analysis. T.T. and J.B.S. advised the design and carried out analyses of the 13C labeling experiments with assistance from C.J. M.B.D. and D.K. wrote the manuscript with consultation from all authors.

CHAPTER I:

INTRODUCTION

Targeting Cancer Metabolism

Cancer is a complex disorder that involves dysregulation of various processes, including gene expression, immune recognition, and metabolism. For nearly a century, it has been understood that cancer cells exhibit elevated metabolic and energy requirements, leading to metabolic reprogramming in tumor cells[1]. More recently, we've discovered that this metabolic transformation in tumors also impacts the metabolism of non-cancer cells and immune cells residing within the tumor microenvironment (TME)[2]. Metabolic reprogramming in tumors also mediates resistance to anti-tumor drugs[3]. Ever since Sidney Farber, a pioneer in modern chemotherapy, published his groundbreaking paper in 1948 about anti-folates inducing remission in children with acute lymphoblastic leukemia (ALL), cancer metabolism has remained a critical target in cancer treatment[4]. Although new insights regarding metabolic dependencies have unveiled innovative therapeutic approaches for exploiting metabolic liabilities, addressing cancer metabolism in the precision oncology era necessitates considering the metabolic vulnerability of non-cancer cells as well[5].

Metabolic alterations in cancer and therapeutic approaches

Otto Warburg reported that cancer cells exhibit high glucose consumption, with the majority of glucose being converted into lactate, even when oxygen is available[6]. This is known as the Warburg effect or aerobic glycolysis. Later Sidney

Weinhouse showed that the rates of oxidative phosphorylation are similar in cancer and normal cells[7]. Rates of lactic acid production exceed the rates of anaerobic glycolysis only in tumor cores where oxygen is limited[8]. Nevertheless, glucose metabolism is remarkably different between cancer and most normal tissues, and a substantial amount of work has been done to target glucose metabolism and increased glycolysis[8,9]. 2-deoxyglucose (2-DG) is a glucose molecule with 2 hydroxyl groups replaced by a hydrogen atom. 2-DG is phosphorylated by hexokinase to produce 2-deoxyglucose-6-phosphate (2-DG6P), which cannot undergo glycolysis further[10]. Therefore, 2-DG acts as a competitive inhibitor of hexokinase by accumulating 2-DG6P and blocking glucose metabolism. 2-DG has been explored as an anticancer agent. Although early testing yielded promising responses in pre-clinical models[11], overall, it was limited by hypoglycemia-related toxicities[12], as glucose metabolism is important in normal tissues, including the brain[13].

Increased biosynthetic processes represent a crucial aspect of metabolic reprogramming because cancer cells have a constant demand for producing macromolecules required for DNA replication, cell division, and tumor growth. Amino acids are involved in the synthesis of proteins, lipids, and nucleic acids[14]. Glutamine is a non-essential amino acid and an important nitrogen donor for nucleotides. It has been suggested that elevated rates of glutaminolysis can facilitate rapid proliferation by providing precursor molecules for biosynthetic pathways[15]. Various oncogenic signaling pathways, such as MYC, promote the

upregulation of glutamine metabolism[16]. Correspondingly, inhibiting the entry of glutamine into the TCA cycle in MYC-driven cancers has been observed to hinder tumor growth in pre-clinical models[16,17] but this approach has had limited success in the clinic so far[18,19]. Similarly, increased activity of *de novo* serine synthesis enzymes has been observed in cancer, in the form of increased expression of phosphoglycerate dehydrogenase (PHGDH) [20]. Increased PHGDH expression results in higher serine synthesis from glucose in breast cancer and lung adenocarcinoma[20,21]. The serine biosynthesis pathways also contribute to essential metabolic processes, such as the production of glycine and glutathione[22]. Considering the significance of serine in cancer cells, the *de novo* synthesis of serine is a prospective target for cancer treatment. However, PHGDH inhibition causes overall growth retardation with severe brain microcephaly and leads to embryonic lethality in mice[23]. PHGDH inhibition still remains an active area of research, with a combined use of serine dietary restriction and other medications to target serine metabolism being explored[24].

Fatty acids are another important class of macromolecules required for cell growth and survival. Although only a limited number of tissues, including the liver and adipose, can naturally synthesize fatty acids in normal physiological conditions[25], certain tumors possess the capacity for *de novo* lipid synthesis[26]. Fatty acids are manufactured within the cytosol, originating from acetyl CoA generated from mitochondrial citrate. Two key enzymes participating in this process are ACLY and FASN[27]. Many inhibitors have been developed to target

these enzymes for inhibiting fatty acid synthesis, but they have shown limited success[28]. Ongoing efforts are being made to understand better and effectively target fatty acid synthesis in tumors.

Another important class of macromolecules is nucleotides. Nucleotides can be synthesized *de novo* or acquired through salvage pathways to support the metabolic needs of cancer cells[29]. One of the strategies for targeting nucleotide metabolism is to target *de novo* nucleotide synthesis. The enzyme ribonucleotide reductase (RR), for instance, plays a pivotal role in converting ribonucleotides into deoxyribonucleotides, a crucial step in DNA synthesis[30]. Small molecule inhibitors of RR, such as hydroxyurea and gemcitabine, have shown efficacy in slowing cancer cell growth by limiting the availability of deoxyribonucleotides. Another key enzyme in nucleotide metabolism is thymidylate synthase (TS), which converts deoxyuridine monophosphate (dUMP) to deoxythymidine monophosphate (dTMP), a precursor of thymidine[31]. Thymidine is necessary for DNA replication, and inhibitors of TS, like 5-fluorouracil (5-FU) disrupt this process, making it a valuable chemotherapeutic agent in various cancers[32]. Alternative approaches to target nucleotide biosynthesis involve inhibiting enzymes within the salvage pathway, including deoxycytidine kinase (dCK) and other relevant factors[33-35]. Ongoing research is focused on exploring challenges like therapy resistance and the potential side effects linked to perturbing nucleotide metabolism in healthy cells.

Cancer cell metabolism diverges from that of healthy cells in various other ways, including distinct requirements for NAD^+/NADH balance and the antioxidant defense mechanisms, among other factors[36-39]. Although targeting pathways that are involved in macromolecule biosynthesis due to their elevated requirements of cancer cells has been an effective strategy, it faces limitations related to the therapeutic window and the ability of cancer cells to circumvent these demands through salvage pathways.

Targeting cancer cells by inducing the buildup of toxic metabolites

Our laboratory has recently unveiled a novel alternative approach for targeting cancer metabolism. This approach doesn't rely on inhibiting the production of macromolecules required for meeting the increased demands of cancer cells. Instead, it promotes the accumulation of toxic intermediates within metabolic pathways to eliminate cancer cells. Unexpectedly, endogenously produced metabolites, often integral to cellular structures, can possess toxic properties[40]. For example, the folate-dependent one-carbon (1C) cycle enables the production of nucleotides and amino acids, leading to the release of formaldehyde[41]. Formaldehyde's toxic properties are well known, as it can cross-link proteins and DNA.

Under normal physiological conditions, potentially toxic metabolites within cells are typically kept at non-toxic levels through either additional metabolism by

downstream metabolic enzymes or efficient secretion mechanisms. Supporting this concept, numerous metabolic disorders, such as methylmalonic acidemia, Gaucher disease, or glycogen storage disease (GSD), result from loss-of-function mutations or enzyme deficiencies within those pathways[42,43]. Vitamin B12 deficiency, a cofactor for the enzyme methyl malonyl-CoA mutase (MMUT) responsible for converting methyl malonyl-CoA into succinyl-CoA, as well as loss-of-function mutations in MMUT, results in the harmful accumulation of methylmalonic acid (MMA)[44]. In type I GSD, patients are unable to convert fructose and galactose into glucose, resulting in unwanted glycogen deposits accompanied by uric acid, which can be harmful if they accumulate in excessive amounts within the body[45]. Dietary modulation in patients, such as the restriction of high-protein and sugar intake, are therapeutic approaches to alleviate the pathology in conditions like methylmalonic acidemia and type I GSD, respectively[44,45]. This also indicates the potential to induce toxicity in cancer cells through the accumulation of toxic metabolites produced by the cancer cells themselves. This can be achieved by targeting the detoxification enzymes responsible for the metabolism of ‘potential’ toxic metabolites.

In a typical linear metabolic pathway, where metabolites undergo sequential chemical conversions, the absence of an enzyme responsible for converting the toxic metabolite into a non-toxic metabolite can lead to the buildup of toxic levels within the cell. Furthermore, the extent of detoxification should correspond to the production of the toxic metabolite. This concept can be compared to a 'kitchen sink'

model (Figure 1). In this model, upstream metabolic enzymes (Enzyme1) act as a faucet, and detoxifying enzymes (Enzyme2) that are responsible for converting the toxic product of the faucet enzyme act as a drain by preventing the overflow of the sink. If cancer cells undergo metabolic reprogramming to upregulate a pathway containing a toxic metabolite, we may potentially exploit this by inhibiting the downstream detoxifying enzyme. This would lead to the accumulation of toxic metabolites in cancer cells, offering a potential method to eliminate them selectively.

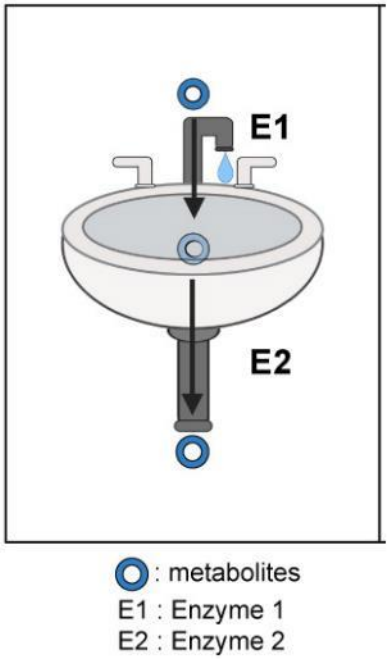

Figure 1.1: Kitchen-sink model in toxic metabolite theory. Metabolites and enzymatic reactions are symbolized by blue circles and arrows, respectively. In this analogy, the kitchen sink's faucet and drain correspond to the upstream and downstream metabolic enzymes' enzymatic reactions, while the basin signifies the level of accumulation of the toxic metabolite.

Over the past few years, our laboratory has confirmed the viability of this approach by inducing the accumulation of toxic metabolites in cancer cells within upregulated pathways. For instance, in human glioblastoma multiforme (GBM), cancer cells are dependent on the glycine processing enzyme GLDC, as its inhibition causes the accumulation of excess levels of toxic metabolites aminoacetone and methylglyoxal. In GBM, there is an upregulation of mitochondrial serine hydroxymethyltransferase (SHMT2) and glycine decarboxylase (GLDC). While cancer cells derive an advantage from elevated SHMT2 activity, which inhibits pyruvate kinase (PKM2) and provides a survival benefit to poorly vascularized tumor regions, they also exhibit an increasing dependency on GLDC to eliminate excess glycine and prevent its conversion into toxic metabolites[46]. In another example, some cancer cells gain an advantage by importing selenium, enabling the production of selenoproteins, including GPX4, which serve to protect them against ferroptosis[47]. Our lab has shown that senelophillic cancer cells depend upon SEPHS2 to prevent the buildup of toxic selenide by following the ‘kitchen-sink’ model[48]. Recently, our laboratory has also uncovered that cancer cells with increased *de novo* sphingolipid biosynthesis need to detoxify 3KDS, a toxic intermediate within the pathway[49]. These instances advocate that the strategy of inducing toxic accumulation can be effective, particularly in the selective targeting of cancer cells, and there may be numerous additional cases yet to be discovered.

In addition to its selective targeting of cancer cells, this strategy offers several other advantages. By focusing on pathways that are upregulated in cancer cells, it becomes possible to predict which patients will derive the greatest benefit from the pharmacological inhibition of a specific detoxifying enzyme. Unlike conventional approaches that target essential building block pathways, the ‘toxic metabolite’ approach prevents cancer cells from resolving the issue through macromolecule salvage, a common challenge, as previously discussed. Moreover, it allows for the potential adjustment of toxic metabolite accumulation levels through dietary restrictions and modifications. The approach involving toxic metabolites does come with possible drawbacks. For instance, if the toxic metabolite under consideration can be transported or secreted from cells, it might harm neighboring cells, including healthy host cells. Additionally, if a subset of healthy cells utilizes the same upregulated pathway being targeted, this could lead to host toxicity. Cancer cells exhibit metabolic diversity, meaning that resistance to treatment may emerge if a portion of cancer cells proves invulnerable due to this metabolic heterogeneity. However, tackling treatment resistance remains a formidable challenge in cancer therapy, and exploring drug combination strategies should be considered in such cases. Despite these potential limitations, the toxic metabolite theory represents a novel approach for selectively and predictively eliminating cancer cells and should be further investigated.

Introduction to Sugar Nucleotide Metabolism

Sugar nucleotides, also known as NDP-sugars (nucleoside diphosphate sugars) or nucleotide sugars, comprise a sugar molecule (usually a monosaccharide) linked to a nucleotide. They play pivotal roles in numerous metabolic processes, serving as primary constituents of carbohydrates and their derivatives. Additionally, sugar nucleotides contribute to essential processes such as nucleic acid synthesis and cell signaling[50].

Sugar nucleotides consist of two main components:

1. Sugar Moiety: This part of the molecule is typically a monosaccharide, such as glucose, galactose, mannose, or others. Sugar moiety provides the diversity necessary for different glycosylation reactions and cellular processes.

2. Nucleotide Moiety: The nucleotide moiety consists of a nitrogenous base (usually adenine, guanine, cytosine, or uracil), a ribose or deoxyribose sugar, and one or more phosphate groups. The phosphate group provides energy and helps in the transfer of sugar molecules during glycosylation reactions.

Monosaccharides cannot function as sugar donors and must undergo activation through attachment to nucleotides consisting of phosphate groups[50]. There are nine common sugar nucleotides involved in the human metabolome (Figure 1.2). Various sugars exhibit preferences for specific nucleotide attachments to facilitate their activation. For instance, glucose (Glc), galactose

(Gal), N-acetyl glucose (GlcNAc), N-acetyl galactose (GalNAc), glucuronic acid (GlcA), and xylose (Xyl) are activated as UDP-sugars. Mannose (Man) and fucose (Fuc) are activated as GDP sugars and neuraminic acid (NeuAc) undergoes activation as cytidine monophosphate[51]. While most of the sugar nucleotides are synthesized in the cytosol, UDP-Xyl is synthesized in the Golgi apparatus[52], and CMP-NeuAc is produced in the nucleus[53].

a

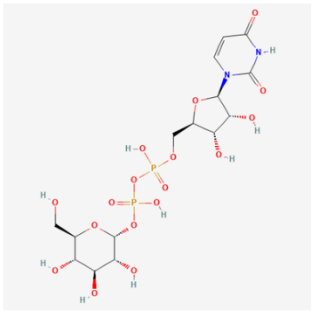

b

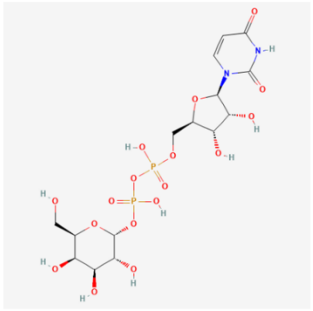

c

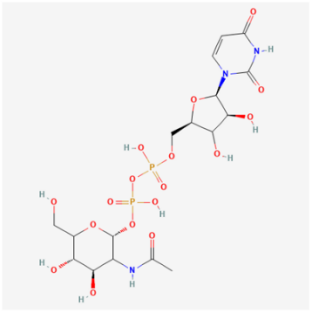

d

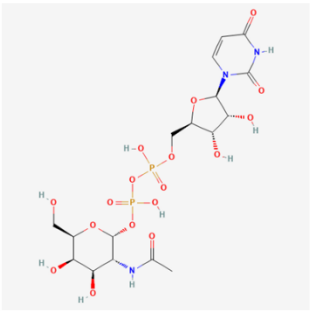

e

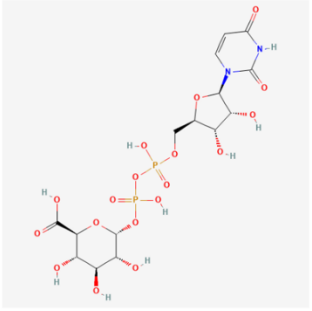

f

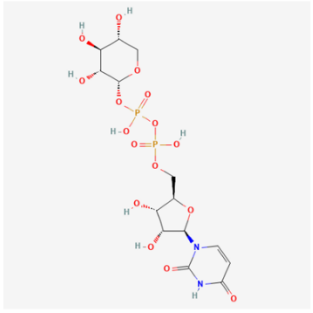

g

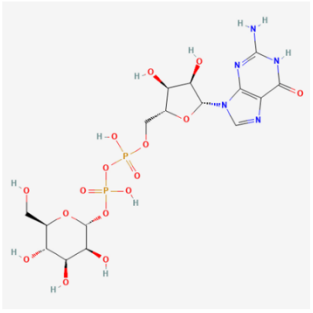

h

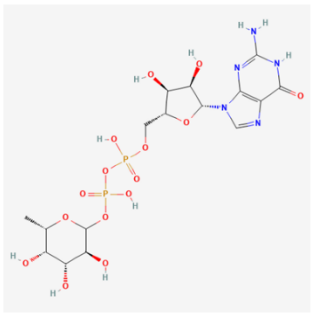

i

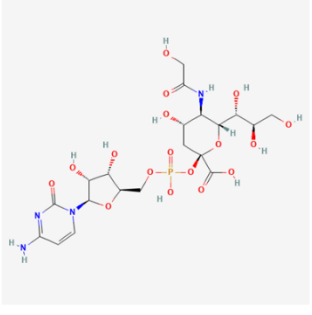

Figure 1.2: Sugar Nucleotides involved in glycosylation reactions within human metabolome. a. UDP-glucose b. UDP-galactose c. UDP-GlcNAc d. UDP-GalNAc e. UDP-glucuronic acid (UDPGA) e. UDP-xylose f. GDP-Mannose g. GDP-fucose h. CMP-Neu5Ac. The structures are downloaded from PubChem (https://pubchem.ncbi.nlm.nih.gov/).

Biosynthetic routes of sugar nucleotides

The synthesis of sugar nucleotides begins with the generation of nucleotide precursors, such as uridine diphosphate (UDP), guanosine diphosphate (GDP), and cytidine diphosphate (CDP)[54]. Nucleotides are comprised of phosphorylated five-carbon sugars bonded to nucleic acid bases. They can be either synthesized from carbohydrates and amino acids, acquired from dietary sources, or recycled after nucleic acid breakdown. The initial step in nucleotide biosynthesis starts with ribose-5-phosphate, a sugar derived from glucose-6-phosphate[55]. Through the utilization of 5-phosphoribosyl-1-pyrophosphate (PRPP), enzymes in the de novo pathway synthesize purine and pyrimidine nucleotides from basic molecules like CO2, amino acids and tetrahydrofolate[56]. Alternatively, nucleotides can be generated via salvage pathways by breaking down nucleic acids. These nucleotide precursors are fundamental building blocks that are further modified to form a wide array of sugar nucleotides, post-sugar addition.

Similarly, sugar components can either be obtained through diet or salvaged via catabolism of polysaccharides[57]. Among dietary sources, glucose and fructose sugars are particularly important. Once they are internalized by a cell, they undergo phosphorylation to form sugar 6-phosphates.

Glucose 6-phosphate is subsequently converted into glucose 1-phosphate, which, in a reaction with uridine triphosphate (UTP), yields UDP-glucose (UDP-Glc). The conversion of UDP-Glc is a reversible process facilitated by UDP-glucose pyrophosphatase (UGP1). UDP-Glc can be oxidized to UDP-glucuronic acid (UDPGA) by UDP-glucose dehydrogenase (UGDH). UDPGA is then decarboxylated to produce UDP-xylose (UDP-Xyl) inside golgi apparatus. UDP-galactose (UDP-Gal) is produced through an exchange reaction involving galactose-derived galactose 1-phosphate and UDP-Glc[58] (Figure 1.3).

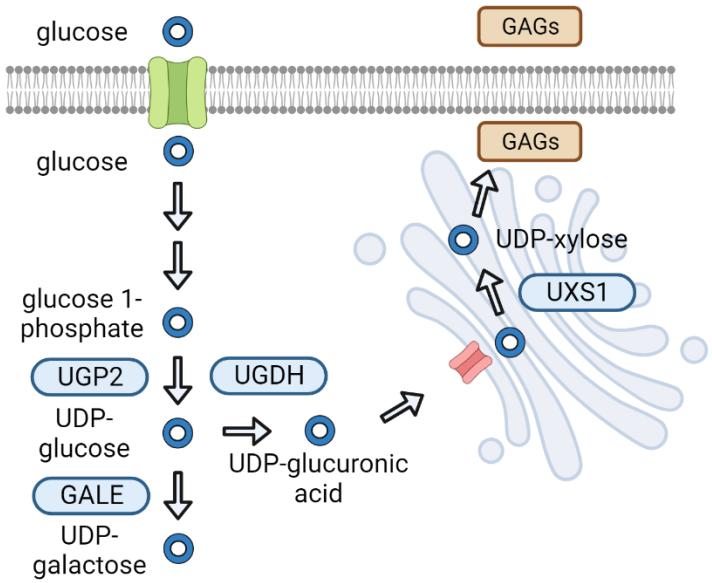

Figure 1.3: Synthesis of sugar nucleotide precursor UDP-Glc, UDP-gal, UDPGA, and UDP-Xyl and enzymes involved. Inside the cell, glucose is transported and converted into glucose-6-phosphate. Subsequently, glucose-6-phosphate undergoes conversion to glucose-1-phosphate. The synthesis of UDP-glucose occurs from glucose-1-phosphate, serving as a precursor for the generation of various other sugar nucleotides. This figure is generated using biorender.

Fructose 6-phosphate serves as a precursor in the biosynthesis of N-acetyl glucosamine and mannose 1-phosphates, which are subsequently converted into their corresponding UDP and GDP sugars[53]. UDP-GlcNAc can further undergo isomerization to produce UDP-GalNAc. In a similar manner, GDP-mannose can isomerize to yield GDP-fucose. The synthesis of CMP-NeuAc involves three sequential steps starting from UDP-GlcNAc[59]. Additionally, GDP-fucose, GDP-mannose, UDP-GalNAc, and UDP-GlcNAc can also be generated via salvage pathways that utilize recycled monosaccharides and ATP[58].

Role of sugar nucleotides in cellular processes and diseases

Sugar nucleotides are critical molecules within cells that act as building blocks for the biosynthesis of complex carbohydrates, glycolipids, glycoproteins, and other essential cellular components. Major roles of sugar nucleotides include carbohydrate synthesis, Glycosylation and protein modification, and cell signaling[53].

Sugar nucleotides serve as precursors for the biosynthesis of various carbohydrates, including polysaccharides like cellulose, chitin, and glycogen. For example, UDP-glucose is a key substrate for glycogen synthesis in the liver and muscle tissues, playing a pivotal role in energy storage. UDP-glucose serves as the primary glucose donor for the synthesis of glycogen. The extension of this initial glycogen sequence is catalyzed by glycogen synthase, which transfers a glycosyl group from UDP-glucose to elongate the growing glycogen strand[60]. Disruptions in carbohydrate metabolism due to defects in sugar nucleotide synthesis can lead to

diseases like glycogen storage disorders (GSDs)[61]. Sugar nucleotides also take part in the biosynthesis of glycoproteins and proteoglycans (also discussed in the next section). Alterations in protein glycosylation have been implicated in modulating the malignancy of cancer cells[62]. Altered sialylation patterns have also been linked to cancer and neurodevelopmental disorders[63].

Furthermore, to enhance the diversity of sugar nucleotides, a significant number of interconversions take place within them[64]. These conversions predominantly involve epimerization reactions. For instance, UDP-galactose-4-epimerase (GALE), an enzyme involved in galactose metabolism and glycosylation, facilitates two reversible reactions: the conversion of UDP-galactose to UDP-glucose and the conversion of UDP-GalNAc to UDP-GlcNAc. Mutations in GALE result in a mild form of galactosemia, a condition that requires patients to reduce their dietary galactose intake to mitigate the accumulation of toxic intermediates like galactitol[65]. GALE variants have also been associated with hematological manifestations, including anemia, febrile neutropenia, and severe thrombocytopenia[66]. Iduronic acid (IdoA), an epimer of glucuronic acid, serves as a crucial monosaccharide building block for glycosaminoglycans (discussed in the subsequent section). Initially, Jacobson et al. hypothesized that UDP-Glucuronate 5-Epimerase (UGA5E) catalyzed an epimerization reaction from UDPGA to produce UDP-IdoA[67]. However, subsequent research debunked this hypothesis, revealing that the epimerization of glucuronic acid to iduronic acid occurs at the polysaccharide level rather than at the UDP-sugar level[68]. This is catalyzed by

glucuronyl C5-epimerase (GCLE) (20807641). Mutations in GCLE are associated with lower BMI, elevated hemoglobin levels, and a higher incidence of cerebrovascular events[69]. Furthermore, these mutations have been found to impact the proliferation, angiogenesis, and metastasis of Ewing sarcoma (ES) by affecting the biosynthesis of heparan sulfate and heparin[70].

In summary, nucleotide sugars are critical in mediating a wide range of biological processes, from the modification of proteins and lipids to cell recognition, structural support, and energy storage.

Protein glycosylation

Glycosylation is a form of post-translational modification in which a carbohydrate is covalently attached to proteins or lipids to form a glycoconjugate, with further sugar modifications subsequently occurring. Most glycans are found on the outermost surfaces of cellular and secreted macromolecules and are remarkably diverse. Glycans are not only essential to protein folding, cellular homeostasis, and immune regulation but are involved in multiple disease conditions[71]. The impact of glycosylation on the folding and stability of glycoproteins has a dual role. Firstly, the presence of highly soluble glycans can directly contribute to the physical and chemical stabilization of proteins. The covalent attachment of glycans to the surface of the protein can increase the thermal stability of the proteins[72]. For instance, glycosylation of an antibody affects its circulatory half-life, which can substantially affect its in-vivo efficacy by directly

modulating its clearance from the bloodstream[73]. Secondly, N-linked glycans play a pivotal role as a quality control checkpoint during glycoprotein folding in the endoplasmic reticulum[74]. It is noteworthy that although glycans can assist in protein folding, the removal of glycans does not always impact protein folding or its function[72].

Types of protein glycosylation

About 50% of human proteins are glycosylated to some extent[75]. There are primarily two main types of glycosylation: N-linked and O-linked glycosylation, which constitute the majority of glycosylation events. Additionally, less common forms of glycosylation, like C-mannosylation, also exist. While most glycosylation reactions are enzymatic, non-enzymatic glycation processes are also observed in mammals.

N-linked glycosylation

N-linked glycosylation refers to the attachment of GlcNAc to the nitrogen atom of asparagine (Asn) residue of a protein by an amide bond with Asn-X-Ser/Thr motif, where Asn: aspargine, Ser: serine, Thr: threonine and X can be any amino acid except proline[75]. N-linked glycans are primarily classified into three major categories: high mannose, complex, and hybrid oligosaccharides, collectively constituting approximately 90% of the glycans found in eukaryotic cells[76]. The initiation of N-linked glycosylation involves the creation of a dolichol-linked GlcNAc sugar. GlcNAc is connected to dolichol, a lipid molecule, through a phosphate bond. Subsequently, sugar molecules are incrementally added to form

a precursor oligosaccharide. The lipid precursor is flipped to orient itself towards the lumen of the endoplasmic reticulum (ER). Within the ER lumen, mannose and glucose units are sequentially attached, resulting in the formation of a 14-sugar structure-Glc3Man9GlcNAc2[77]. This precursor is subsequently transferred to an asparagine (Asn) residue on a protein by an oligosaccharyltransferase enzyme within the ER. Following this attachment, the protein-carbohydrate complex undergoes additional modifications within the ER, typically including the removal of glucose residues as part of the quality control process. Following this, the conjugate proceeds to the Golgi apparatus, where it undergoes further modifications. This process begins with the pruning of mannose residues in the cis-Golgi by mannosidases, resulting in the core structure GlcNAc2Man3. In medial and trans-Golgi, further additions such as GlcNAc, galactose, sialic acid, and fucose sugars are made with a specific set of enzymes that determine whether the final structure is classified as high mannose, hybrid, or complex glycan (Figure 1.4)[77]. Fucose and sialic acids are frequent terminal carbohydrate residues and are very important in the biological function of proteins, as exemplified by their significance in recently developed SARS-Cov2 antibodies[78].

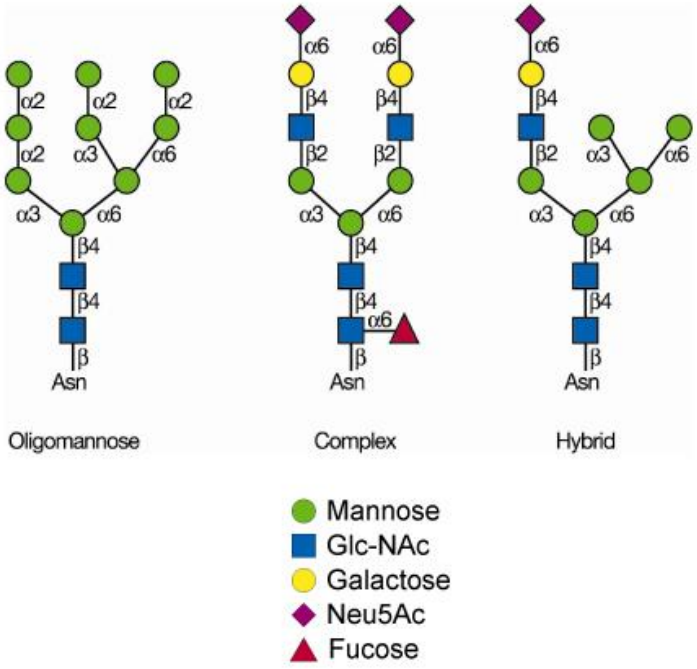

Figure 1.4: Types of N-glycosylations. The N-glycans are classified based on their final carbohydrate composition. They all contain the common core GlcNAc2Man3 on Asn residue. High-mannose glycans consist solely of mannose and N-acetylglucosamine residues. In contrast, complex glycans feature added sugars like galactose, while hybrid glycans encompass both unmodified terminal mannose residues and substituted mannose residues connected by an N-acetylglucosamine linkage. This figure is adapted from the Essentials of Glycobiology, 2nd edition[77].

O-linked glycosylation

O-linked glycosylations can take place on amino acids having functional hydroxyl groups, primarily Serine (Ser) and Threonine (Thr). The most common sugar linked to ser and Thr is GalNac, and the resulting proteins are called mucins. Mucin glycoproteins are prevalent components found in mucous secretions on cell

surfaces and within body fluids. They have recurring peptide segments known as "variable number of tandem repeats" (VNTR) regions. These VNTR regions are notably rich in serine or threonine O-glycosylation acceptor sites and are characterized by dense clusters of mucin O-glycans, which can constitute a substantial portion, up to 80%, of the molecule's total weight. The secretion of mucins serves the vital function of safeguarding both glycoproteins and cellular surfaces against external stresses and microbial infections and plays a role in self-recognition by the immune system. GalNAc transferases (GALNTs) start the synthesis of O-glycans with the transfer of the first GalNac. Although GALNTs present a degree of promiscuity, they also exhibit some degree of specificity for specific amino acid motifs[77]. Subsequently, non-templated sequential glycan addition to the initial GalNAc occurs, resulting in the generation of a diverse array of carbohydrate structures. Unlike N-glycans, most O-glycans do not undergo pre/post-processing, which involves pruning of specific sugar moieties. Instead, glycopeptide O-glycan chains undergo modifications facilitated by distinct glycosyltransferases. These enzymes have the capacity to extend the existing structure by incorporating galactose, GlcNAc, sialic acid, and fucose. This stepwise addition and expansion of sugar moieties (GalNAc, fucose, xylose, GlcNAc, mannose, galactose, or glucose) occur as the protein traverses through the cis-, medial-, and trans-Golgi compartments, contributing to the complex and diverse repertoire of O-glycan structures observed in mucin-type glycoproteins and

other proteins[77]. In rare instances, O-glycans may also incorporate glucuronic acid, as observed in Drosophila melanogaster[79].

Proteoglycans and glycosaminoglycans

Although proteoglycans are classified as a subclass of O-glycans due to the attachment of glycosaminoglycans chains via O-glycosidic bonds, they represent a class of extensively glycosylated glycoproteins that play a pivotal role as essential components within the extracellular matrix of animal connective tissues. The fundamental building block of a proteoglycan comprises a core protein accompanied by one or more covalently linked sugar chains, along with N-glycans and O-glycans[80].. These elongated sugar chains, known as glycosaminoglycans (GAGs), constitute a significant portion of the proteoglycan's total mass. While N-glycans typically comprise up to two dozen monosaccharides, a glycosaminoglycan motif can encompass a significantly larger range, with chain lengths ranging from 50 to 200 sugar units. Proteoglycans can end up at one of three locations: secretion into the extracellular matrix (ECM), insertion into the plasma membrane, or storage within secretory granules. These proteoglycans exhibit significant variability in the number of GAG chains they possess, with some, like decorin, containing only a single GAG chain, while others, such as aggrecan, can have over a hundred GAG chains[80]. Glycosaminoglycans are linear polysaccharides composed of disaccharide building blocks. These disaccharide units include an amino sugar, such as Glc-NAc or GalNAc, along with either a uronic acid, such as glucuronic acid or iduronic acid, or galactose[77]. There are five

major classes of glycosaminoglycans, including heparan sulfate, chondroitin sulfate, keratan sulfate, dermatan sulfate, and hyaluronic acid (figure 1.5). Within eukaryotic cells, the synthesis of sulfated glycosaminoglycans (heparan sulfate, chondroitin sulfate, and keratan sulfate) occurs as core proteins of proteoglycans pass through the Golgi apparatus. In contrast, hyaluronan synthesis, non-sulfated glycosaminoglycan, is synthesized at the inner surface of the plasma membrane, which is a disaccharide polymer of UDPGA and UDP-GlcNAc[81].

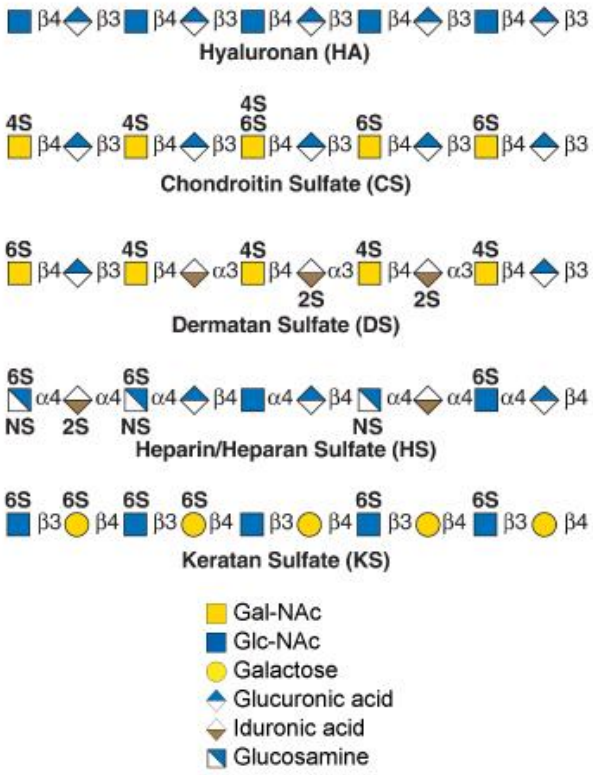

Figure 1.5: Types of Glycosaminoglycans. Glycosaminoglycans are composed of alternating glucosamine units, which can be either (GlcNAc or GalNAc) or N-sulfated (GlcNS), along with either a uronic acid (GlcA or IdoA) or galactose (Gal). Hyaluronan is unique in that it does not contain sulfate groups, whereas other

glycosaminoglycans incorporate sulfates at various positions within their structures. This figure is adapted from the Essentials of Glycobiology, 2nd edition[77].

C-mannosylation and O-GlcNAcylation

C-mannosylation is a protein glycosylation that occurs within the endoplasmic reticulum. In this process, individual α-mannose molecules are attached to designated tryptophan (Trp) residues, typically the first Trp within the Trp-x-x-Trp/Cys (W-x-x-W/C) motif found on substrate proteins. This enzymatic modification is carried out by C-mannosyltransferases[82]. While the majority of protein glycosylation occurs in the endoplasmic reticulum (ER) and Golgi apparatus, O-GlcNAc glycosylation reactions also take place in the cytoplasm. It is a process catalyzed by O-linked N-acetylglucosaminyltransferase (OGT). This enzyme adds GlcNAc to serine and/or threonine residues and uses UDP-GlcNAc as a substrate made from the hexosamine pathway[83,84]. This pathway is particularly sensitive to glucose levels, and in diabetic tissues, its flux is notably upregulated. This heightened activity results in increased levels of UDP-GlcNAc and consequently leads to elevated O-GlcNAc glycosylation[85].

Protein glycosylation in cancer

The growth of tumors hinges on cancer cells' capacity to circumvent cellular division checkpoints, elude signals for cell death, evade immune surveillance, and migrate to distant metastatic sites. Glycosylation plays a significant role in each of these critical processes[86]. Cells receive external signals that dictate their proliferation, survival, or apoptosis through interactions with ligands, such as

growth factors, cytokines, hormones, and death-inducing molecules. These ligands bind to specific cell surface receptors, primarily receptor tyrosine kinase receptors (RTKs). Upon ligand binding, RTKs form homo- or heterodimers, leading to autophosphorylation of tyrosine residues within the receptor's cytoplasmic domain, initiating intracellular signaling cascades and ultimately regulating gene transcription[87]. Post-translational mechanisms, including glycosylation, finely regulate the activity, turnover, and interaction of these receptors with adaptor molecules[88].

As an example, EGFR possesses a total of 15 N-glycosylation sites, with N-glycans contributing approximately 40 kDa to its overall molecular mass[89]. The remaining ERBB family members exhibit varying numbers of potential N-glycosylation sites, ranging from 8 in ERBB2 (also known as HER2) to 11 in ERBB4[89]. Notably, site-directed mutagenesis experiments have demonstrated that specific N-glycans, located on the extracellular region of ERBB receptors, can directly influence their biological activity. This is believed to be achieved through mechanisms such as changes in intracellular protein trafficking and the prevention of ligand-independent dimerization[90-92]. Vascular endothelial growth factors (VEGFs) and their corresponding receptor tyrosine kinases (VEGFRs) represent another important signaling system critical for angiogenesis. VGFR signaling plays a crucial role in cancer progression and metastasis. The number of N-glycosylation sites of VEGFR1-3 is 13, 18, and 12, respectively[93]. The glucose analog, 2-DG, inhibits angiogenesis at lower non-toxic concentrations with time-dependent

inhibition of Akt and Erk phosphorylation by altering N-linked glycosylation of VEGFR2[94].

Fibroblast growth factor receptors (FGFRs) comprise a family of four receptor tyrosine kinases (FGFR1-4) that interact with 18 fibroblast growth factors (FGFs). These FGFs are widely expressed and play pivotal roles in embryonic development and tissue repair. FGFs bind to heparan sulfate proteoglycans (HSPGs), forming a ternary complex alongside FGFRs on the cell surface, aiding in the dimerization of inactive FGFRs[95]. While the absence of N-glycans on FGFRs may enhance the formation of the FGF-FGFR-HSPG complex, potentially leading to the overactivation of FGFR signaling[96], inhibition of mannose phosphate isomerase, an enzyme involved in the initial stages of N-glycan biosynthesis, results in reduced activation of the FGFR receptor family[97].

Since most cell-surface proteins are glycosylated, changes in the glycosylation patterns of proteins, which result in neo-glycan epitopes, can help in the immune detection of tumor cells[98,99]. Terminal carbohydrate structures, in particular, hold significance in oncology, as they can act as cancer markers and influence the characteristics of cancer cells. The Sialyl Lewis antigen is one such terminal carbohydrate structure, which is frequently elevated in cancer cells due to alterations in their glycosylation profiles and is used in the diagnosis of gastrointestinal cancers[100]. Hence, aberrant glycosylation of crucial glycoproteins holds significant implications in cancer and offers opportunities for the development of targeted drugs.

Golgi apparatus

The Golgi apparatus (GA) is an organelle found in most eukaryotic cells. It was identified in 1897 by the Italian biologist and pathologist Camillo Golgi and was named after him in 1898[101]. GA serves as the central hub for cellular glycosylation. It plays a pivotal role not only in the classical secretory pathway but also in various endocytic pathways.

Morphology

The typical Golgi apparatus (GA) is characterized by a series of flattened cisternal membranes closely interconnected, arranged in parallel, and forming a stacked configuration. It also includes an abundance of tubular-reticular networks and vesicles. In the perinuclear region, numerous Golgi stacks are interconnected to create a ribbon-like structure, essentially functioning as a unified organelle[102].

GA exhibits a tubular morphology made up of stacks of cisternae. The assembly of cisternae is divided into three distinct compartments: the cis, medial, and trans regions, constituting the core components of two primary networks, namely, the cis-Golgi network (CGN) and the trans-Golgi network (TGN)[103]. The CGN is the entry point of vesicles containing proteins from the endoplasmic reticulum (ER). It acts as a receiving station for newly synthesized proteins. The TGN functions as the exit point for proteins leaving the Golgi apparatus. It directs

vesicles containing processed proteins to their appropriate destinations within the cell[102]. The Golgi apparatus is organized into four functionally distinct regions, and there are distinct Golgi markers for the study of their morphology. For instance, GM130 serves as a marker for the cis-Golgi region, Giantin is employed as a marker for the medial-Golgi region, and TGN46 is utilized as a marker for the trans-Golgi region[104-106].

The transition from cis to trans compartments involves alterations in the thickness of the cisternae. It reduces initially, moving from cis-to-medial Golgi, and again increases as we move towards trans-golgi and become more pierced[107]. Additionally, various other gradients are notable within the Golgi apparatus, including the distribution of Golgi enzymes, pH levels, and cholesterol concentration across the Golgi stacks. The concentration of cholesterol is higher at the trans side of a Golgi stack[108]. Enzymes responsible for the initial stages of glycosylation are predominantly situated on the cis-Golgi stacks. In contrast, the late-stage and terminal glycosylation enzymes responsible for sialylation are primarily located on the trans side of these stacks[109]. Golgi apparatus's unique structural organization and morphology, consisting of distinct cisternae and compartments, enables precise and coordinated cellular activities.

Functions

Glycosylation and other post-translational modifications

One of the Golgi apparatus's primary functions is post-translational protein processing and modification. Newly synthesized proteins in the ER, undergo a

series of transformative changes within the Golgi. The initial attachment of sugars to glycoproteins or glycolipids takes place in the ER. However, the subsequent addition of the diverse array of sugars that constitute a mature glycan occurs within the GA. The Golgi membranes are decorated with glycosyltransferases, glycosidases, and nucleotide sugar transporters, arranged in an organized manner from the cis-Golgi to the trans-Golgi network (TGN)[110]. This spatial arrangement enables each enzymatic activity to act on specific substrates. The specific spectrum of glycosyltransferases and related activities governing glycosylation may differ depending on the cell type, resulting in a variable repertoire of glycans on glycoconjugates. Moreover, the process of glycan synthesis is influenced by factors such as the pH within the Golgi, the integrity of peripheral membrane proteins associated with the Golgi, signaling from growth factors, dynamics of the Golgi membrane, and cellular stress conditions[111,112].

Within mammals, a diverse group of over 250 glycosyltransferases (GTs) are present inside the Golgi apparatus, where they catalyze the transfer of one sugar to another sugar, typically covalently linked to a glycan acceptor that is attached to a protein or lipid[110]. Most GTs facilitate the transfer of a single sugar to an acceptor molecule. However, there are exceptions where some GTs perform the transfer of two different sugars, generating a polymer with repeating units, such as in the case of proteoglycans (10984485). The Golgi-resident GTs are generally type II transmembrane proteins, featuring a short cytoplasmic tail, a transmembrane domain, a stalk-like stem region, and a catalytic domain situated

within the Golgi lumen. Several GalNAc GTs also contain dual functional domains where one domain binds to GalNAc, and the other domain is responsible for the transfer of GalNAc to an acceptor[113,114]. It is noteworthy that GTs can undergo glycosylation themselves, mediated either by other GTs or, in some instances, by autocatalytic transferase activity important for its own protein folding, stability, and function[115].

In essence, glycosylation is essential for the proper structure, function, solubility and, stability of proteins, enabling them to fulfill their designated roles within and outside the cell. Additionally, Golgi-mediated post-translational modifications such as phosphorylation, sulfation, and proteolysis fine-tune protein activity and signaling pathways[116-118].

Protein sorting trafficking

The Golgi apparatus is at the forefront of cellular sorting and trafficking. It acts as a dispatch center, ensuring that proteins and lipids are directed to their designated cellular destinations. Once the proteins have achieved proper folding and assembly within the endoplasmic reticulum (ER), they are transported to the Golgi complex through coat protein II (COPII) vesicles[119]. Upon reaching the Golgi apparatus, these proteins are further glycosylated and then undergo sorting processes based on their intended final destinations[120-122].

There are distinct subsets of proteins with different trafficking pathways from the Golgi apparatus: 1. Some proteins are transported back to the endoplasmic reticulum (ER) via COPI vesicles. This group includes soluble resident ER

chaperones, which are reclaimed from the cis Golgi stacks through interactions with the KDEL receptor. This process ensures their stable localization within the ER[123,124]. 2. Another subset comprises Golgi resident enzymes that remain within the Golgi apparatus[125]. 3. A third subset is transported via clathrin-coated vesicles from the Golgi apparatus. These vesicles are directed to the endo-lysosomal system and contain lysosomal hydrolases along with their receptors[126]. 4. The final subset of proteins exits the Golgi apparatus and is directly transported to the plasma membrane[127].

In summary, the Golgi apparatus is a versatile organelle involved in diverse functions, including protein processing, sorting, and trafficking. It also plays a crucial role in glycosylation and modulation of the immune response, contributing significantly to the cell's essential processes.

Golgi dysfunction and stress response

The Golgi apparatus is responsible for processing secretory and membrane proteins, applying post-translational modifications, and directing them to their respective locations within the cell. However, when the production of these proteins exceeds the Golgi's capacity, leading to inadequate modification and transport, a condition known as "Golgi stress" occurs. To address Golgi stress, cells activate adaptive mechanisms that enhance the Golgi's capacity in response to specific cellular demands, referred to as the Golgi stress response[128]. The Golgi apparatus is a remarkably intricate organelle characterized by its complexity and a multitude

of functions. Therefore, the mammalian Golgi stress response includes various response pathways, including TFE3, proteoglycan, CREB3-ARF4, and HSP47.

The TFE3 pathway primarily governs the overall Golgi functionality, including structural maintenance, N-glycosylation, and vesicular transport[129]. Further examination of several genes associated with its pathway, such as GCP60 and SIAT4A, unveiled the presence of an enhancer element known as the Golgi Apparatus Stress Response Element (GASE), characterized by the consensus sequence ACGTGGC. GASE plays a pivotal role in governing the transcriptional upregulation of genes related to Golgi stress[130,131]. Nevertheless, the mechanisms by which Golgi stress is detected and how these molecules trigger the Golgi stress response have not yet been fully elucidated[132]. In response to Golgi stress, dephosphorylated TFE3 binds to a Golgi Apparatus Stress Response Element (GASE), consequently triggering the activation of gene transcription within the TFE3 pathway[131].

In contrast, the proteoglycan pathway focuses on enhancing the expression of glycosylation enzymes for proteoglycans[129]. Likewise, the examination of genes related to the proteoglycan pathway, including B3GAT3, GLCE, and NDST2, unveiled another enhancer element known as the proteoglycan-type Golgi stress response element (PGSE). Subsequent research has revealed that both the overexpression and insufficiency of core proteins necessary for proteoglycan synthesis can activate PGSE, potentially resulting in the perturbation of Golgi morphology[133].

Additionally, the CREB3-ARF4 and HSP47 pathways are responsible for regulating pro- and anti-apoptotic functions, respectively[129]. Brefeldin A (BFA), a compound known to halt protein transport from the ER to the Golgi[134], induces the activation of the CREB3-ARF4 pathway while inhibiting ARF protein function. Consequently, the cytoplasmic segments of CREB3 dissociate from the ER membrane and translocate into the nucleus, where they promote the expression of Golgi-associated genes, including ARF4. This ultimately leads to apoptosis triggered by Golgi stress[135,136]. Furthermore, Mitogen-activated protein kinases/erythroblast transformation specific (MAPK/ETS), and the protein kinase R (PKR)-like ER kinase (PERK) pathways are also recently implicated in Golgi stress response[132]. HSP47 functions as an ER chaperone, and its increased expression in reaction to Golgi stress provides cellular protection against apoptosis[137].

Several small compounds that induce Golgi stress through various mechanisms have been identified. These stressors include ionophores like monensin and nigericin, which alter luminal pH and disrupt intra-Golgi trafficking[138,139]. Golgicide A (GCA) targets ADP ribosylation factor (ARF) proteins and causes Golgi stress by dispersing cis and medial Golgi via redistribution of COPI from the Golgi[140]. Exo2 hinders the anterograde movement of the glycoproteins from the ER to the Golgi, disrupting the Golgi[141].

These observations highlight the dynamic nature of the Golgi apparatas. While significant Golgi stress can trigger apoptosis and cell demise, low-grade

Golgi stress may protect cells through the PERK pathway by reprogramming cysteine metabolism in Huntington's disease[142]. This implies that the Golgi stress response, like other stress responses, functions as a defensive mechanism that enables cells to adjust or overcome stress in brief and moderate situations but acts as an exacerbating factor contributing to disease in cases of prolonged stress.

A sugar nucleotide: UDP-glucuronic acid

Structure, chemical properties, and biosynthesis of UDP-glucuronic acid

UDP glucuronic acid (UDPGA; chemical formula: C15H22N2O18P2) is a sugar nucleotide that plays a vital role in various biochemical reactions within the body, including detoxification of xenobiotics, metabolism of various substances, and glycosylation reactions.

UDP-Glucuronic acid is a nucleotide sugar, which means it consists of a nucleotide linked to a sugar molecule. Its structure is composed of four fundamental components: a uracil base, a ribose sugar, phosphates, and a glucuronic acid moiety. The uracil base consists of the nucleotide portion of UDP-GlcA, while the ribose sugar connects the nucleotide portion to the glucuronic acid moiety via two phosphates (figure 1.2). UDP-Glucuronic acid exhibits a high degree of polarity due to its exposed hydroxyl groups, allowing it to form hydrogen

bonds readily. This property contributes to its water solubility, which extends to approximately 18 milligrams per liter of water[143].

While UDP-Glucuronic acid can be sourced from various food items like herbs (parsley, and, chervil), and some fruits, its primary origin is through biosynthesis from glucose in animal cells. A portion of glucose is consumed within our cells through glycolysis to generate ATP, while the remaining glucose is transformed into glucose-1-phosphate. UDP-glucose dehydrogenase (UGDH) functions as a hexameric cytosolic enzyme, driving the conversion of UDP-glucose into UDP-glucuronic acid in the cytoplasm. This enzymatic process entails two consecutive oxidations that transform the 6'-hydroxyl group of UDP-glucose into a carboxylate group, concomitantly reducing two moles of NAD+ to NADH. It was first documented by Strominger and colleagues over six decades ago[144].

UDP-glucuronic acid (UDPGA), synthesized in the cytoplasm, serves multiple purposes. It functions as a precursor for glycosylation, contributing to the production of hyaluronic acid[145]. Additionally, UDPGA can be imported into ER, where it acts as a substrate in reactions catalyzed by a group of ER-bound enzymes known as uridine glucuronosyl transferases (UGTs)[146]. Furthermore, within the Golgi apparatus, UDPGA can either be employed as a substrate in glycosylation reactions for the generation of O-glycans and proteoglycans or undergo carboxylation, catalyzed by UXS1, to transform into another glycosylation precursor, UDP-xylose (UDP-Xyl)[77,147].

Functions of UDPGA

While UDPGA is known for its roles in detoxifying endogenous insoluble metabolites and xenobiotics, as well as facilitating glycosylation of proteins and lipids, it also plays a significant role in plant cells and in several non-human mammals. Notably, most primates, including chimpanzees and gorillas, guinea pigs, certain bird species, and plant cells, possess the ability to synthesize ascorbic acid, commonly known as vitamin C, from UDPGA[148,149]. UDPGA serves as a precursor in this process, initially transforming into l-gulonolactone, which is subsequently oxidized to produce ascorbic acid[150]. However, it is noteworthy that in humans, the gene responsible for ascorbic acid synthesis, namely gulonolactone oxidase, is present but non-functional due to the accumulation of several mutations[149]. Thus, humans require exogenous sources of Vitamin C.

UDPGA in xenobiotic detoxification

Numerous substances, including pharmaceuticals and non-pharmaceutical xenobiotics (like those found in the diet, and environment), that humans encounter are non-polar and lipophilic in nature. This lipophilicity facilitates their diffusion through biological membranes and enables them to reach their intended sites of action. However, this very property impedes their removal from the body via renal excretion. Consequently, the conversion of lipophilic compounds into more polar and hydrophilic forms becomes crucial for their elimination from the body. This transformative process is commonly referred to as Xenobiotic metabolism[151,152].

Xenobiotic metabolism is divided into two distinct phases I and II. In phase I reactions, molecules undergo modifications through processes such as oxidation, reduction, and hydrolysis, which introduce polar groups to the compounds. Phase II reactions involve conjugation reactions where resulting metabolites from phase I or parental compounds themselves are attached to hydrophilic substances like glucuronic acid, sulfate, or glutathione. These phase II conjugation reactions increase the water solubility of the compounds and help with excretion from the body via bile or urine while deactivating the biological activity of the compound[153-155]. UDPGA is employed by a superfamily of enzymes known as Human UDP-glucuronosyltransferase (UGT), consisting of roughly two dozen proteins. These enzymes transfer a glucuronic acid moiety to a diverse array of endogenous compounds, environmental pollutants, and pharmaceutical drugs, a process referred to as glucuronidation[156-158]. Among the endogenous substances are bilirubin, bile acids, dihydroxysteroids, as well as fat-soluble vitamins. A wide range of structurally diverse drugs from various classes, including analgesics, antiretrovirals, antipsychotics, NSAIDs, and many others, undergo glucuronidation through enzymes within the UGT1A or UGT2B enzyme families[158]. About 11.7% of the total 125 compounds tested by a study that were approved between 2006-2015 relied on glucuronidation for excretion[159]. A wide variety of chemotherapeutic drugs, including tamoxifen, epirubicin, etoposide, belinostat, and irinotecan, are subject to glucuronidation[160]. Some compounds that undergo glucuronidation in humans may not necessarily undergo the same process in other mammals, such

as rats[161]. Consequently, the evaluation of glucuronidation for each drug should exclusively rely on human studies. While the majority of detoxification processes take place in hepatic tissues, various other organs like the kidneys, colon, lungs, epithelium, and gonads also express a range of UGTs to varying degrees[162,163]. UGTs are situated on the endoplasmic reticulum (ER) membrane within cells, with their active site positioned inside the ER lumen, where the transfer of UDPGA to the acceptor compounds takes place[164].

A deficiency or impairment in the activity of UGT1A1, the enzyme responsible for glucuronidation and bilirubin clearance, leads to a condition known as hyperbilirubinemia. This condition is identified as Crigler-Najjar syndrome, which can manifest as severe jaundice and neurological deficits, potentially necessitating a liver transplant in severe cases[165,166]. In summary, the conjugation of UDPGA plays a significant role in the elimination of a wide range of toxic endogenous and xenobiotic compounds from our bodies.

UDPGA in glycosylation

Protein glycosylation, as discussed earlier, is a critical post-translational modification that significantly impacts protein stability, folding, and functionality. UDPGA plays a pivotal role in glycosylation as one of its essential precursors. It serves as a crucial building block in the formation of hyaluronic acid, a non-sulfated proteoglycan. Additionally, it serves as a fundamental component in the synthesis of sulfated proteoglycans like chondroitin sulfate, heparin sulfate, and keratan sulfate[77,81].

Transport of UDPGA inside organelles

SLC35D1 is a known transporter responsible for transporting multiple nucleotide-sugars, such as UDPGA, GlcNAc, and GalNAc[167-169]. SLC35D2 is also predicted to facilitate the transport of UDP-sugars to the Golgi apparatus, primarily based on its sequence similarity with SLC35D1[170]. The SLC35 family, comprising 17 enzymes, that act as nucleotide-sugar transporters, exhibits a degree of redundancy. While many transporters have unknown substrates, Figure 1.6 displays some transporters with known substrates. This means that a single transporter can transport multiple types of nucleotide sugars, and conversely, for a given nucleotide sugar, there are likely multiple transporters involved[171,172]. Generally, nucleotide sugar transporters function as antiporters, a mechanism also observed in SLC35D1[173]. These antiporters move sugars in and out of the ER and Golgi lumen in exchange for other nucleotide sugars. The transport process is typically competitive, meaning that high concentrations of one nucleotide sugar can inhibit the transport of another nucleotide sugar[174]. In addition to SLC35D1, SLC35B1, and SLC35A5 have also been reported to have UDPGA transport activity[175,176].

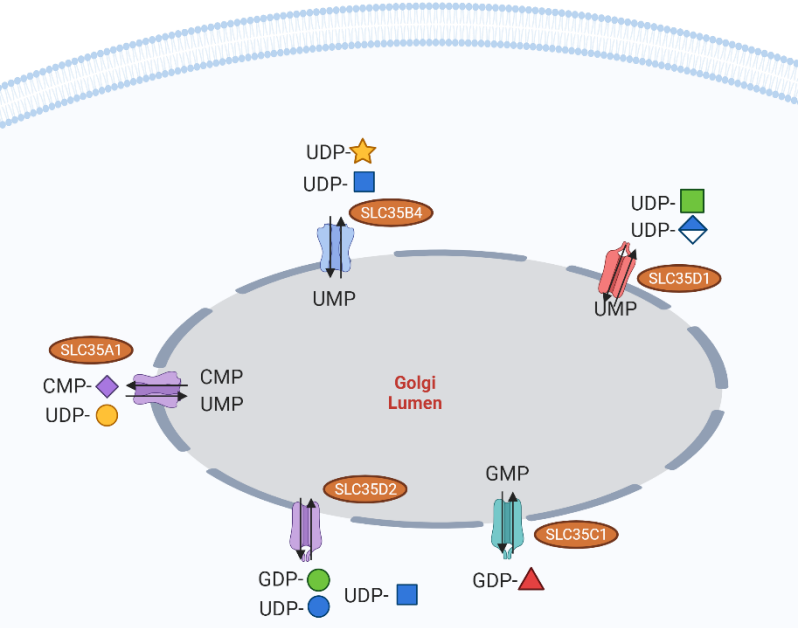

Figure 1.6: Transporters belonging to the SLC35 family located on the Golgi membrane surface, which have been researched and possess identified substrates. This figure is made using Biorender.

Chemoresistance in cancer

Overview of chemoresistance in cancer

Depending on the cancer type and stage, chemotherapy remains the first line of treatment for many cancers[177-179]. Despite significant advancement in the field of cancer biology, resistance to chemotherapeutic compounds remains an important challenge. Chemoresistance accounts for a large portion of cancer relapses and poor patient survival[180]. For example, chemo-resistance to paclitaxel and carboplatin in breast cancer is associated with poor patient survival[181-183].

Chemoresistance is mainly classified as intrinsic or acquired. When resistance-promoting elements are already present in tumor cells before treatment with chemotherapy, it is referred to as intrinsic resistance. On the other hand, when resistance arises due to mutations or adaptations such as gene amplifications or loss in response to chemo-treatment, it is categorized as acquired resistance[184]. Cancer tumors frequently exhibit heterogeneity and harbor multiple driver mutations. Thus, when subjected to chemotherapy, they have the ability to increase compensatory signaling pathways[185]. One approach employed to address chemotherapy resistance involves administering a combination of drugs, including targeted therapies. Examining the molecular underpinnings is critical in our efforts to combat chemo-resistance[180,186].

Molecular mechanism of chemoresistance

Tumor cells utilize a wide range of mechanisms to evade the effects of chemotherapy. These mechanisms include changes in drug influx and efflux, modifications in drug targets resulting in drug inactivation, epigenetic alterations, variations involving the activation and deactivation of oncogenes and tumor suppressors, increased DNA repair processes, induction of epithelial-mesenchymal transition (EMT), interactions within the tumor microenvironment, and numerous others[186,187].

Alterations in drug influx and efflux

Although the mechanisms for the cellular import of several chemotherapeutic drugs remain unclear, anti-folate chemotherapeutics like

methotrexate and pralatrexate are known to enter cells through the reduced folate carrier (RFC)[188,189]. As a result, the expression of RFC is linked to drug accumulation and its sensitivity[189]. Conversely, inactivating mutations and reduced RFC expression found in tumors are associated with drug resistance to anti-folate chemotherapeutics[190,191]. This suggests that tumor cells can exploit drug influx and import mechanisms within cells to develop resistance to chemotherapy.

Drug efflux is an energy-dependent process facilitated by efflux pumps. In eukaryotes, multiple families of proteins participate in this process, including Multidrug resistance protein (MDR), Multidrug resistance-associated proteins (MRPs), and peptide transporters (PEPTs)[192]. MDRs and MRPs are a part of a superfamily of transporters called the ATP-binding cassette (ABC) transporters[193]. One of the extensively researched members of the MDRs is MDR1, also known as p-glycoprotein. It plays a critical role in the elimination of a diverse spectrum of drugs, comprising chemotherapeutic compounds. Furthermore, it exhibits significant upregulation, in both established cancer cell lines and patient tumor samples[194,195]. Similarly, the multidrug resistance protein 1 (MRP1), encoded by ABCC1, is another notorious transporter frequently upregulated, often multiplefold, in cancer cells[196]. While some members of this family have been extensively studied, it is believed that there may be a considerable degree of redundancy within the ABC transporter family, at least in plant ABC transporters, and a comprehensive exploration of these transporters could potentially lead to the discovery of novel drug targets[197].

Oncogenes and tumor suppressors

Overexpression of several growth factor receptors, such as EFGR and FGFR, can modulate the chemo-resistance[198,199]. EGFR overexpression results in PI3K/AKT activation in non-small cell lung cancers (NSCLCs)[200]. This has been postulated as a potential mechanism contributing to the development of chemotherapy resistance. Since, in breast cancer, the process through which PI3K/AKT activation leads to chemoresistance is well-documented. Activation of the PI3K/AKT pathway leads to the generation of reactive oxygen species (ROS). Ordinarily, ROS induction triggers apoptosis. However, the activation of AKT also initiates the activation of nuclear factor erythroid 2-related factor 2 (Nrf2), which subsequently promotes cell survival[201].

The tumor suppressor protein 53 (TP53), referred to as the guardian of the genome, is a tumor suppressor gene that is frequently lost or mutated in over 50% of tumors[202]. TP53 serves as a regulator of the cell cycle, controlling cell cycle checkpoints. In the presence of DNA damage, TP53 activates the expression of DNA repair genes and, when necessary, initiates apoptosis if the DNA damage is beyond repair. Consequently, the loss of functional TP53 is associated with chemoresistance, allowing cancer cells to continue dividing despite substantial DNA damage[203,204]. Mutant TP53 exhibits oncogenic gain-of-function (GOF) characteristics, including increased tumor progression, and is associated with resistance to drugs in the absence of wild-type TP53. These effects are observed even in cells that do not have functional wild-type TP53[205].

Downregulation of apoptosis

Cancer cells enhance the expression of anti-apoptotic proteins to promote their survival in the presence of chemotherapy drugs[180]. When a cell is targeted for apoptosis through the intrinsic pathway, the outer mitochondrial membrane becomes permeable, leading to the release of proteins from the BCL2 protein family. It's important to note that the BCL2 family includes both pro-apoptotic and anti-apoptotic proteins, with BCL2 itself having anti-apoptotic functions[206]. Preclinical studies have shown promising outcomes for Navitoclax (also known as ABT-263), a BCL2 inhibitor, in both hematologic malignancies and solid tumors[207,208]. Currently, clinical trials are underway to assess its effectiveness[209]. However, it's worth noting that the expression of MCL1, another anti-apoptotic member of the BCL2 family, plays a critical role in determining Navitoclax's efficacy and can counteract the effects of BCL2 inhibition[210]. Consequently, ongoing research is focused on the development of selective MCL1 inhibitors[211].

Cancer cells employ numerous mechanisms to resist chemotherapy. Among these, cancer stem cells, known for their self-renewal capacity, play a role in promoting chemo-resistance, in contrast to terminally differentiated cells[212,213]. Tumor heterogeneity is another significant factor contributing to treatment failure and the development of acquired resistance in tumors[214,215]. Additionally, alterations in the tumor microenvironment have been recognized as a crucial component influencing chemo-resistance[216,217].

Glucuronidation and chemoresistance

UGTs (UDP-glucuronosyltransferases) play a crucial role in the process of glucuronidation which consist of conjugating insoluble lipophilic drugs with glucuronic acid using UDPGA, facilitating their removal from cells. Consequently, the overexpression of UGTs can contribute to chemo-resistance in tumor cells. While several organs, including the liver, kidney, and colon, are known for drug metabolism and exhibit high inherent expression of various UGT enzymes[218,219], it's noteworthy that UGTs have also been found to be overexpressed in a diverse range of cancers originating from non-metabolizing tissues such as lung, prostate, and gastric cancers[220-223]. UGT overexpression cooperates with ABC transporters, in the expulsion of chemotherapy compounds from cells[224,225].

The role of UGT enzymes in cancer is twofold. UGT substrates encompass not only drugs but also carcinogens and environmental pollutants. While a reduction in UGT activity can lead to increased drug retention, it also diminishes the cell's ability to eliminate carcinogens, potentially promoting carcinogenesis. Low expression of UGT in breast is associated with the risk of cancer development because lipophilic hormones such as estrogen is dependent on UGTs for its removal[226]. In stomach cancer, changes in UGT expression are complex, with some UGTs decreasing in expression while others increase[227]. Thus, in general, lower UGT activity is associated with cancer development, whereas higher activity is linked to its role in chemo-resistance.

UDPGA, a substrate of glucuronidation pathway, is also responsible in synthesis of sulfated and non-sulphate glycosominoglycans that are attached to the proteoglycans including Hyaluronic acid (HA), HSPGs and CSPGs. Hyaluronic acid plays roles in cancer proliferation, migration and invasion. HA mainly interacts with two receptors CD44 and receptor for HA-mediated motility (RHAMM). CD44 is a well-established anti-cancer target, and the inhibition of CD44 with antibodies has demonstrated a notable reduction in the malignancy of various tumor types[228]. Similarly, Overexpression of RHAMM is frequently associated with the progression of cancer[229]. HA binds directly to both CD44 and RHAMM, inducing conformational changes in these receptors and activating them. This activation initiates downstream signaling cascades, including the PI3K/AKT and Ras activation pathways, which have also been implicated and contribute to chemo-resistance[229,230]. Sulfated proteoglycans, too, play a crucial role in interacting with numerous ligands and receptors within the extracellular space and are associated with cancer progression and angiogenesis[231]. For the reasons mentioned, it can be speculated that cancer cells may benefit from upregulating UDPGA production. This not only assists cancer cells in eliminating toxic chemotherapeutic compounds but also contributes to the production of proteoglycans, which, in turn, facilitate cancer progression.

Scope and rationale for the thesis project

Our laboratory has recently showcased an alternative approach to targeting cellular metabolism, a hallmark in cancer. This approach involves inducing the

buildup of endogenous toxic metabolites by disrupting the activity of a vital detoxification enzyme within metabolic pathways that are upregulated in cancer as compared to normal cells. Over the past few years, as we have delved into this approach, we have made some key observations regarding the toxic metabolite strategy and the identification of genes responsible for cellular detoxification functions. Leveraging this knowledge, along with publicly available omics data, I aimed to systematically discover novel pathways and detoxifying enzymes for the purpose of targeting cancer cells.

Through our data mining efforts, we identified a potential detoxifying enzyme, UXS1, in the sugar-nucleotide pathway, which exhibited specific upregulation in cancer cells. Thus, the objective of this thesis was to explore whether the sugar-nucleotide pathway generates a toxic metabolite that triggers a detoxification demand via UXS1 and whether UXS1 could be a viable target for selective cancer therapy. Given that this sugar-nucleotide pathway is upregulated in certain cancer types, particularly in chemo-resistant cells, we also aimed to determine whether UXS1 might serve as a more effective target for chemo-resistant cells. The results of these studies are summarized in Ch. II of the thesis.

CHAPTER II:

Disruption of sugar nucleotide clearance is a therapeutic vulnerability of cancer cells

Significant portions of this chapter are from:

Doshi MB, Lee N, Tseyang T, Ponomarova O, Goel HL, Spears M, Li R, Zhu LJ, Ashwood C, Simin K, Jang C, Mercurio AM, Walhout AJM, Spinelli JB, Kim D. **Disruption of sugar nucleotide clearance is a therapeutic vulnerability of cancer cells.** Nature. 2023 Oct 25. doi: 10.1038/s41586-023-06676-3. Epub ahead of print. PMID: 37880368.

Abstract

Identifying metabolic steps that are specifically required for the survival of cancer cells but dispensable in normal cells remains a challenge[232]. Here, we report a therapeutic vulnerability in a sugar nucleotide biosynthetic pathway that can be exploited in cancer cells with limited impact on normal cells. A systematic examination of conditionally essential metabolic enzymes revealed that UXS1, a Golgi enzyme that converts one sugar nucleotide (UDP-glucuronic acid; UDPGA) to another (UDP-xylose), is essential only in cells that express high levels of its immediate upstream enzyme UGDH. This conditional relationship exists because UXS1 is required to prevent excess accumulation of UDPGA produced by UGDH. UXS1 functions not only to clear UDPGA, but limits UDPGA production through negative feedback on UGDH. Excess UDPGA disrupts Golgi morphology and function, which impedes the trafficking of surface receptors such as EGFR to the plasma membrane and diminishes cell signaling capacity. UGDH expression is elevated in several cancers, including lung adenocarcinoma, and is further enhanced during chemo-resistant selection. As a result, these cancer cells are selectively dependent on UXS1 for UDPGA detoxification, revealing a potential Achilles' heel for UGDH-high tumors.

Results

Altered metabolism is a hallmark of cancer and can support cancer functions such as rapid proliferation and survival under various stress states[232]. Recently, it is emerging that certain metabolic activities play important detoxifying roles by preventing the accumulation of toxic metabolic intermediates[46,48,49]. Importantly, a 'kitchen sink' model has been observed where a detoxifying enzyme is only required in cells with high metabolic production of the toxic metabolite, much as a drain is only needed when the faucet is turned on[40].

Identifying UXS1 as a candidate detoxifier

We wondered whether candidate detoxifying enzymes might be identified on this basis, i.e., whether it is required for cell survival only in the cells where its substrate is produced at high levels (Figure 2.1a). First, based on the notion that the detoxifying enzyme would be required in some cells but not others, we utilized the DEPMAP database of cancer cell line dependency[233] to identify metabolic enzymes with differential essentiality: they are required for the survival of some cancer lines but not others. This was determined by a standard deviation metric (formula: $\sqrt{\{\Sigma(x-\bar{x})^2/(n-1)}$) based data mining of gene dependency scores for all metabolic genes (determined via CRISPR/Cas9 pooled screen[233] across 572

different cancer cell lines across 25 solid tumor lineages (Methods). The selenium detoxifying enzyme 'SEPHS2'[3] was near the top of this list, supporting the notion that detoxifying enzymes can have varying essentiality across lines (Figure 2.1b).

Following the kitchen sink model, we wondered whether these enzymes' essentiality (as determined in the Cancer Dependency Map[234] in each cell line) correlates with the expression level of an upstream enzyme(s) producing the putatively toxic metabolite. Indeed, we found that for one of these variably essential enzymes, UXS1 (Figure 2.1c), the immediate upstream enzyme UGDH was the gene whose expression correlated the most with whether a cell required UXS1 or not (Figure 2.1d-f). This raised the possibility that the product of UGDH - UDP-glucuronic acid (UDPGA) - is a toxic metabolite so that only the cells expressing high UGDH and thus producing high UDPGA would be dependent on UXS1 for detoxification.

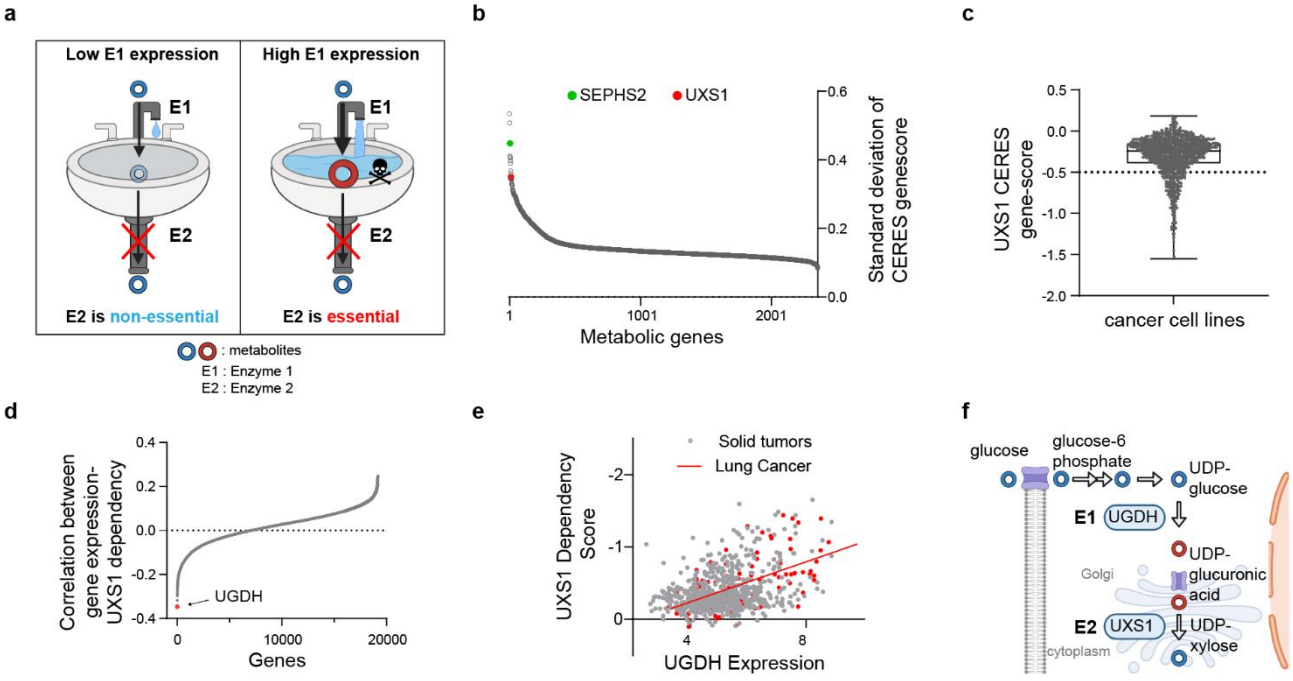

Figure 2.1 Identification of UXS1 as a potential 'detoxifying enzyme'.

(a) Strategy for identification of toxic metabolite clearing enzymes. Our approach was to identify novel detoxifier enzymes by finding scenarios where E2 is only essential in cells where E1 is highly expressed, suggesting that E2 is needed to get rid of E1's product. **(b)** Ranked list of the standard deviation of CERES gene-scores of all metabolic genes across 572 solid cancer cell lines, identifying UXS1 as one of the top enzymes having variable dependency. **(c)** UXS1 gene-score across cancer cell lines using pan-cancer dependency dataset[233] showing that only a subset of cancer cell lines (gene-scores below -0.5) is dependent on UXS1 for survival. A lower gene score means that a gene is more likely to be essential in a given cell line. A score of 0 is equivalent to a non-essential gene, whereas a score of -1 corresponds to the median of all common essential genes. **(d)** Correlation between gene expression of all genes (17386) with UXS1 dependency across 572 solid tumor cancer cell lines, showing UGDH as the top hit. **(e)** Correlation between UXS1 dependency and UGDH mRNA expression [$\log_2$(transcripts per million+1)] in cell-lines (gray) using pan-cancer genetic dependency dataset and gene expression dataset from CCLE, spearman coefficient =-0.41, R^2 = 0.17. The 122 lung cancer cell lines are highlighted in red, spearman coefficient = -0.61, R^2 = 0.37. **(f)** Simplified diagram illustrating the metabolic pathway for UDPGA production. **(a)** and **(f)** were created using Biorender (https://biorender.com/).

To confirm the UGDH expression-dependent requirement of UXS1 suggested by our data mining, we lentivirally transduced CRISPR-Cas9 knock-out (KO) of UXS1 in 19 cancer cell lines of different tissue origin with varying levels of UGDH mRNA expression. Loss of UXS1 was detrimental only to cell lines expressing high UGDH (Figure 2.2a-c). Furthermore, in these sensitive lines, which included the lung adenocarcinoma line A549 and the colorectal adenocarcinoma line DLD1, overexpression of UXS1 with CRISPR-resistant silent mutations against UXS1-g2 fully rescued against the toxicity from UXS1-g2 but not from UXS1-g1, verifying that the toxicity from UXS1 KO is on-target (Figure 2.2d-

h). We generated a UXS1 doxycycline(dox)-inducible KO (iKO) line (Figure 2.3a, b) which revealed that UXS1 loss leads to cell cycle defects and cell death consistent with apoptosis (Figure 2.3c-g). Thus, UXS1 disruption selectively kills only those cancer cells with high expression levels of UGDH.

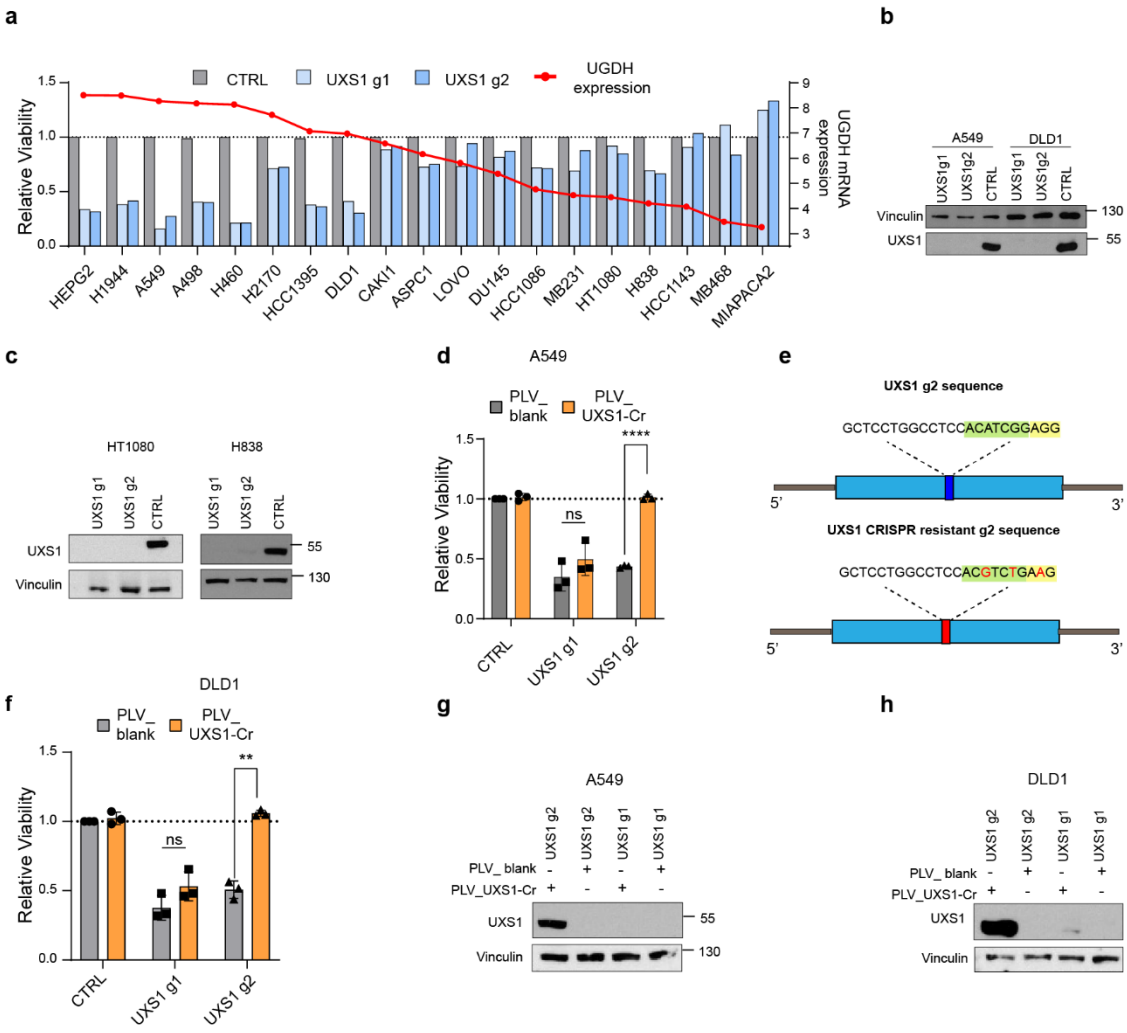

Figure 2.2 UXS1 is essential for cell survival in a manner that correlates with each cell line's expression of the upstream enzyme UGDH.

(a) Relative viability of various cell lines following transduction with CRISPR/Cas9 with guides against UXS1 (light and dark blue bars) or CTRL (gray bars = 1.0) for 10 days (left Y axis). Cells are arranged in decreasing order of UGDH mRNA expression levels [log_2(transcripts per million+1), overlaid as red line and dots; right Y axis], showing that UGDH high cancer cells are dependent on UXS1. **(b)** Immunoblots showing KO of UXS1 in A549 and DLD1 cell lines 9 days post-transduction. **(c)** UXS1 immunoblots showing KO of UXS1 in HT1080 and H838 cell lines 9 days post transduction. **(d)** Relative viability of A549 cells either overexpressing blank vector or g2-resistant UXS1 then subjected to UXS1 KO with g1 or g2, demonstrating that UXS1 KO toxicity is on target (CTRL = 1.0). **(e)** Schematic of UXS1 g2 and UXS1 CRISPR resistant g2 sequence, demonstrating the strategy of using 1 silent mutation in the PAM sequence (yellow highlight) and 2 silent mutations in the seed sequence (green highlight) to prevent CRISPR/cas9 targeting. **(f)** Relative viability of DLD1 cells either overexpressing blank vector or g2-resistant UXS1 then subjected to UXS1 KO with g1 or g2, demonstrating that UXS1 KO toxicity is on target (CTRL = 1.0). **(g)** Immunoblot of UXS1 levels in A549 and **(h)** DLD1 cells overexpressing blank or UXS1-g2 resistant vectors when subjected to CRISPR/Cas9 mediated KO of UXS1. For (**b)**, (**c), (d),** and **(f-h)**, n=3 or more biological replicates and for **(a)** n=2 biological replicates. Data are shown as mean ± s.d. P values were calculated using a two-tailed Student's t-test (n.s. not significant ($p>0.05$) **$p<0.01$, ****$p<0.0001$).

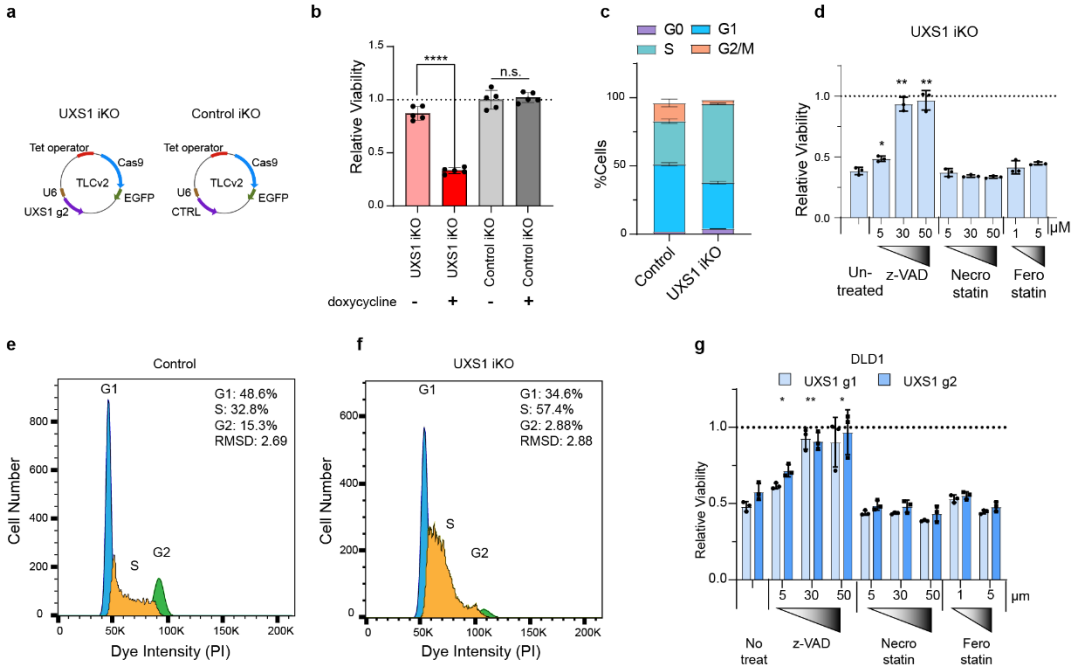

Figure 2.3 UXS1 loss leads to cell cycle defects and apoptosis.

(a) TLCv2 system[235]; LentiCRISPR v2 was modified into an all-in-one dox inducible system. The addition of doxycycline induces Cas9-2A-eGFP. The U6 promoter drives constitutive sgRNA expression. UXS1 iKO and control iKO was prepared by cloning UXS1-g2 and CTRL (non-targeting guide) into the TLCv2 system, respectively **(b)** Relative viability of UXS1 iKO and control iKO cells with and without doxycycline induction (control iKO without doxycycline = 1.0). Induction consisted of 100ng/ml doxycycline treatment for 48 hours; cells were cultured for 4 more days before measuring viability. **(c)** Cell cycle distribution in dox-inducible UXS1 iKO A549 cells, with or without induction for 5 days. **(d)** Relative viability of UXS1 iKO cells subjected to KO then treated with z-vad, Necrostain, or Ferrostatin at the indicated concentrations (Untreated = 1.0). **(e)** Representative cell cycle profiles for control iKO cells and **(f)** UXS1 iKO cells 5 days after doxycycline induction. The cell cycle phases were determined by fitting a univariate cell cycle model using the Watson pragmatic algorithm. **(g)** Relative viability of DLD1 cells subjected to UXS1 KO then treated with z-vad, Necrostain, or Ferrostatin at the indicated concentrations (Untreated = 1.0). For (**b**), and **(c-g)**, n=3 or more biological replicates. Data are shown as mean ± s.d. P values were calculated using a two-tailed Student's t-test (*p<0.05, **p<0.01, ***p<0.001, ****p<0.00001). **(a)** was created using Biorender (https://biorender.com/)

UXS1 prevents toxic UDPGA accumulation

We considered two potential mechanisms for UXS1 toxicity: 1) that accumulation of its substrate may be toxic, as suggested by the kitchen sink model, or 2) that loss of downstream product may be detrimental. To this end, we considered the known biological functions of this pathway. UGDH produces the sugar nucleotide UDP-glucuronic acid (UDPGA), the substrate of UXS1[236]. UDPGA is used in glycosylation reactions which add glucuronic acid to proteoglycans and glycoproteins in the Golgi apparatus[237]. It is also a key substrate for reactions performed by UDP-glucuronosyltransferases (UGTs) to conjugate glucuronic acid to xenobiotics (such as chemotherapeutic compounds), aiding in their deactivation and secretion, a process referred to as 'glucuronidation'[238]. UXS1 converts UDPGA to UDP-xylose, another sugar nucleotide precursor for glycosylation used in proteoglycans (Figure 2.1f)[237,239]. Thus, excessive UDPGA could introduce aberrant changes in the Golgi or the glucuronidation system; alternatively, the loss of xylose sugar modifications could be detrimental to cells.

To determine whether overabundance of UDPGA or loss of xylose modifications is the cause for toxicity, we first measured intracellular levels of UDPGA by LC-MS following UXS1 ablation. As expected, UXS1 disruption, but not UGDH loss, caused about 70-fold accumulation of UDPGA in a time-dependent manner, while several other UDP-sugars were not substantially impacted (Figure 2.4a). Using U-13C glucose labeling, we confirmed that UXS1 KO resulted in the

complete ablation of UDP-xylose formation (Figure 2.5b, c). Next, to test the kitchen-sink model (Figure 2.5a), we disrupted UGDH to prevent UDPGA production (Figure 2.4d), which completely protected both A549 and DLD1 cells against the toxic effects of UXS1 loss (Figure 2.5b-e). Similarly, 4MU, a drug that depletes UDPGA by consuming it for 4MU glucuronidation12-14, also rescued these cells from UXS1 loss toxicity (Figure 2.5f). We examined cell lines expressing low, medium, or high UGDH levels (CAKI1/ASPC1/A549) and found corresponding increasing degrees of UDPGA accumulation following UXS1 KO, which correlated with increasing toxicity (Figure 2.6a and 2.2a). Glucose is an upstream input for UDPGA biosynthesis, and we find that glucose levels directly modulate sensitivity to UXS1 KO, further supporting UDPGA accumulation as the culprit for toxicity (Figure 2.6b). Directly treating UDPGA can also induce toxicity but at high concentrations, likely due to its low cell permeability (Figure 2.6c). Finally, we are able to sensitize otherwise insensitive, low UGDH-expressing cells to UXS1 loss toxicity by overexpressing UGDH (Figure 2.7a-d). Taken together, along with the ‘kitchen sink’ rescue, we provide multiple lines of evidence that cells expressing high UGDH depend on UXS1 expressly to prevent the toxic overaccumulation of UDPGA.

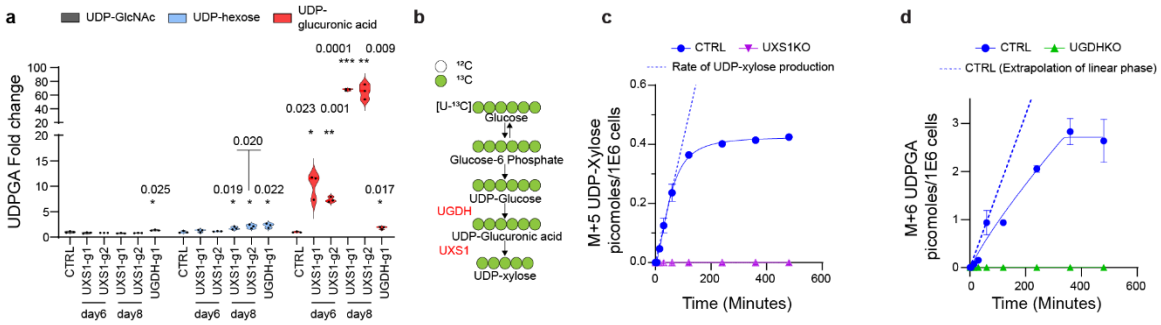

Figure 2.4 UXS1 ablation leads to UDPGA accumulation.

(a) LC-MS quantification of UDP-GlcNAc (gray), UDP-hexose (blue), and UDPGA (red) in A549 cells subjected to CTRL or UXS1 KO at 6 and 8 days of transduction. UDP-hexose includes UDP-glucose, UDP-mannose, and UDP-galactose, which cannot be resolved due to similar MS^2 spectra. **(b)** Schematic of ^{13}C labeling using U-^{13}C glucose to trace UDPGA and UDP-xylose labeling. **(c)** Production of M+5 UDP-xylose in picomoles/1E6 cells of control and UXS1 KO cells, quantified from UDP xylose standard curves. **(d)** Production of M+6 UDPGA in picomoles/1E6 cells of control and UGDH KO cells, quantified from UDPGA standard curves. For (**a), (c),** and (**d)**, n=3 or more biological replicates. Data are shown as mean ± s.d. p values were calculated using two-tailed Student's t-test (*p<0.05, **p<0.01, ***p<0.001, ****p<0.0001).

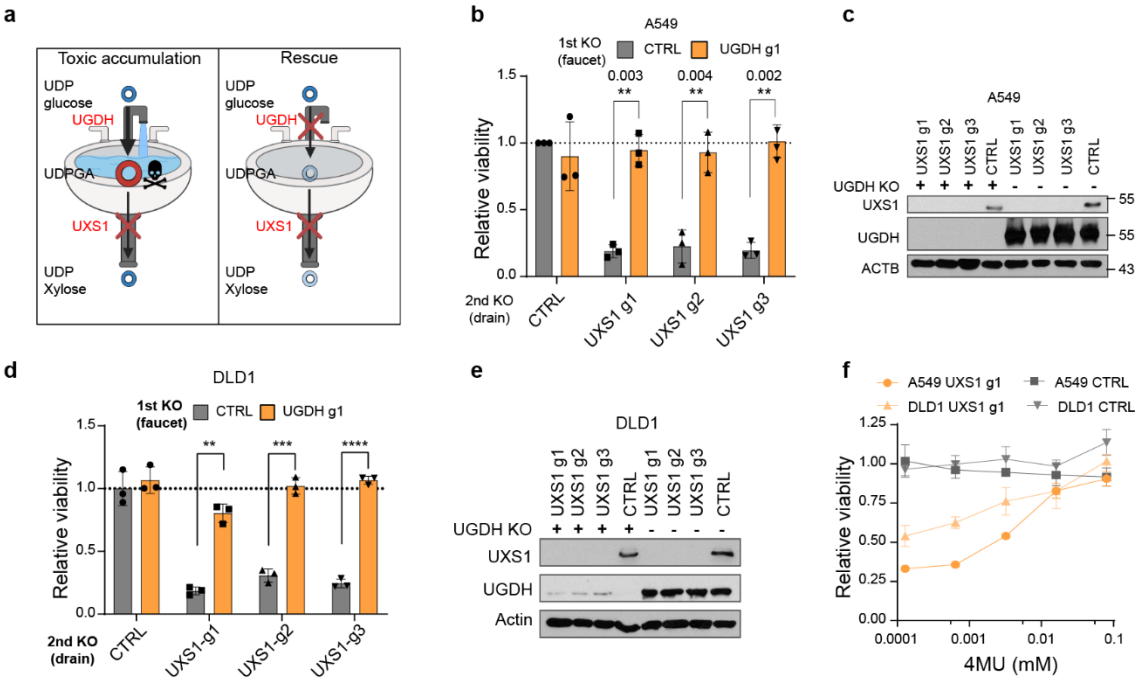

Figure 2.5 UXS1 KO toxicity can be rescued by preventing UDPGA accumulation.

(a) Theoretic toxic-metabolite accumulation model: cancer cells expressing high UGDH (faucet 'on') results in toxic accumulation of UDPGA when UXS1 (drain) is knocked out. However, preemptive UGDH KO ('faucet closed') can prevent accumulation of UDPGA in cells and prevent UXS1 KO toxicity. **(b)** Relative viability of A549 cells subjected to preemptive CTRL (gray) or UGDH (faucet; orange) KO, followed by CTRL or UXS1 (drain) KO. Values are relative to cells subjected to CTRL KO then CTRL KO (=1.0). **(c)** Immunoblot of UXS1 and UGDH protein levels under the KO combinations shown in **(b)**. **(d)** Relative viability of DLD1 cells subjected to preemptive CTRL (gray) or UGDH (faucet; orange) KO, followed by CTRL or UXS1 (drain) KO. Values are relative to cells subjected to CTRL KO then CTRL KO (=1.0). **(e)** Immunoblot of UXS1 and UGDH protein levels under the KO combinations shown in **(d)**. **(f)** Viability of A549 and DLD1 cells with CTRL KO (gray) and UXS1 KO (orange), treated with indicated concentrations of 4MU, showing dose-dependent rescue effect of this UDPGA-depleting agent. Values are relative to blank vector overexpressing, CTRL KO cells (=1.0). For b-f, n=3 biological replicates. Data are shown as mean ± s.d. p values were calculated using two-tailed Student's t-test (n.s.: not significant, *p<0.05, **p<0.01, ***p<0.001, ****p<0.0001).

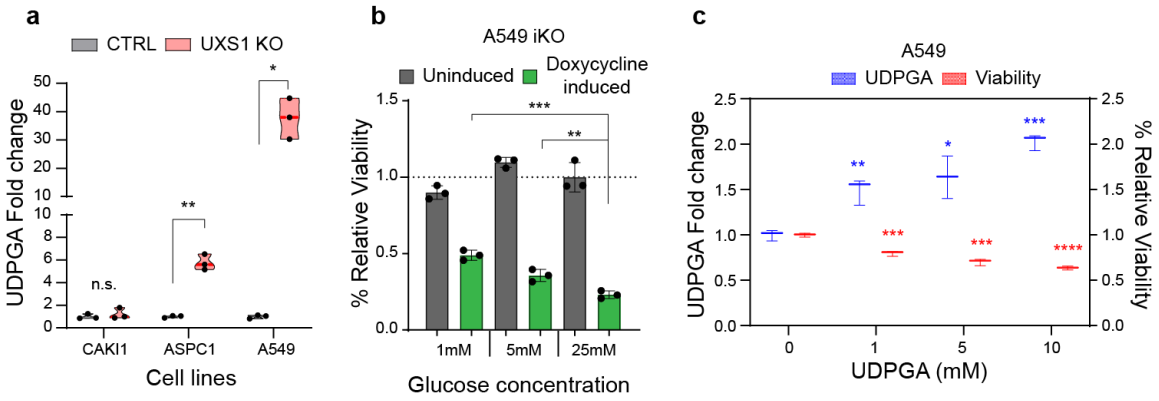

Figure 2.6 UXS1 KO toxicity correlates with UDPGA accumulation.

(a) GC-MS quantification of UDPGA in cell-lines subjected to CTRL (gray) or UXS1 KO (pink) at 8 days of transduction. **(b)** Relative viability of A549 UXS1 iKO cells grown in media containing increasing glucose concentrations. Values are relative to uninduced cells grown in media containing 25 mM glucose (=1.0). **(c)** GC-MS quantification of UDPGA (blue; left Y axis) and relative viability (red; right Y axis) of A549 cells treated with increasing concentrations of UDPGA, showing dose-dependent increase in UDPGA and accompanying decrease in viability. For a-c, n=3 biological replicates. Data are shown as mean ± s.d. p values were calculated using two-tailed Student's t-test (n.s.: not significant, *p<0.05, **p<0.01, ***p<0.001, ****p<0.0001).

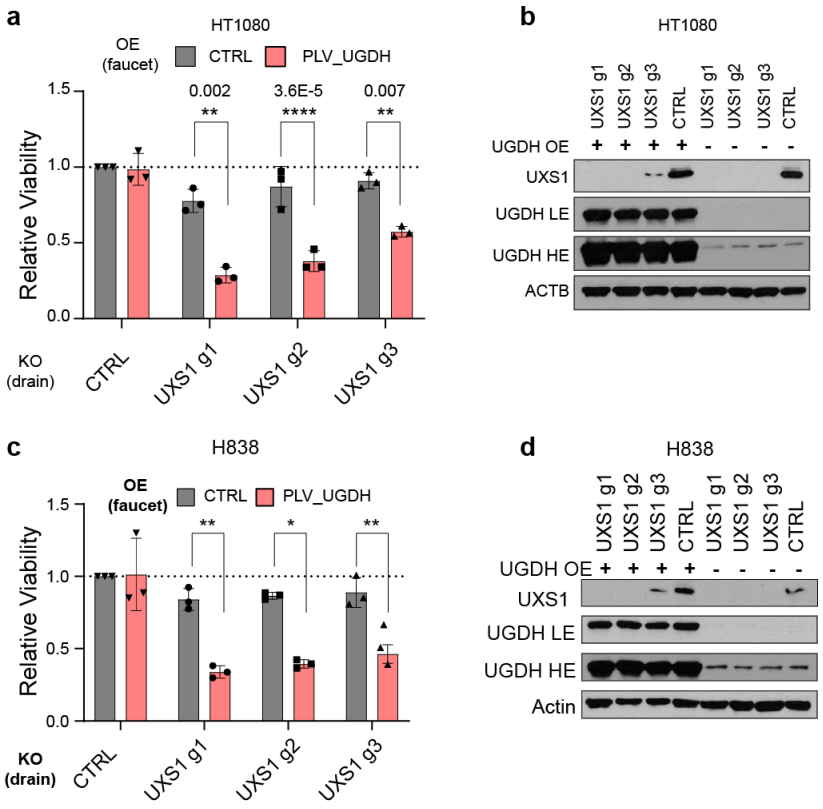

Figure 2.7 UGDH overexpression can sensitize cells to UXS1 KO toxicity.

(a) Viability of HT1080 cells overexpressing either blank vector (gray) or UGDH (red) then subjected to CTRL or UXS1 KO. Values are relative to blank vector overexpressing, CTRL KO cells (=1.0). **(b)** Immunoblot of UXS1 and UGDH protein levels under the OE/KO combinations shown in **(a);** LE indicates low exposure, HE indicates high exposure. **(c)** Viability of H838 cells overexpressing either blank vector (gray) or UGDH (red) then subjected to CTRL or UXS1 KO. Values are relative to blank vector overexpressing, CTRL KO cells (=1.0). **(d)** Immunoblot of UXS1 and UGDH protein levels under the OE/KO combinations shown in (**c)**; LE indicates low exposure, HE indicates high exposure. For a-d, n=3 biological replicates. Data are shown as mean ± s.d. p values were calculated using two-tailed Student's t-test (n.s.: not significant, *p<0.05, **p<0.01, ***p<0.001, ****p<0.0001).

To further investigate the potential impacts of losing UDP-xylose production upon UXS1 KO, we examined sulfated glycosaminoglycans, glycosylation moieties on proteoglycans which require xylose as well as glucuronic acid residues for their production[240]. UXS1 KO cells had decreased levels of total sulfated GAGs, indicating a consequence of loss of UDP-xylose production (Figure 2.8a, b). Also as expected, UGDH KO or UGDH/UXS1 double KO also resulted in a similar degree of loss of sulfated GAGs. As the latter two conditions are nontoxic, this supported that loss of sulfated GAGs are not responsible for the toxicity of UXS1 KO. We additionally examined hyaluronic acids, the predominant non-sulfated proteoglycans, which require glucuronic acid but not xylose residues in their production[240]. UGDH KO or UGDH/UXS1 double KO, the two conditions that preclude UDPGA production, resulted in loss of HAs, whereas UXS1 KO, which loses UDP-xylose but gains UDPGA, did not result in significant changes (Figure 2.8c, d). This argued against changes in HAs mediating the toxicity of UXS1 loss. However, we cannot rule out that changes to proteoglycans caused by UXS1 loss could impact other aspects of tumor biology, which future efforts should explore. Proteoglycans are key components of the extracellular matrix that interact with cell surface proteins and their dysregulation may impact various aspects such as cell adhesion and migration, and cancer cell stemness[241,242].

Intriguingly, in UXS1 KO cells, along with a loss of UDP-xylose production, the rate of production of UDPGA was dramatically increased, implying increased activity of UGDH (Figure 2.9a-f). This is in line with previous reports that indicate

that UDP-xylose can allosterically inhibit UGDH as a negative feedback loop[243-245] . Thus, these results support the model that the observed accumulation of UDPGA in UXS1 KO cells is the combination of lost clearance of UDPGA by UXS1 and higher activity of UGDH (Figure 2.9g). This explains why loss of UXS1, which turns over UDPGA at a relatively low rate (Figure 2.4c), results in such a massive increase in UDPGA (Fig.2.4a).

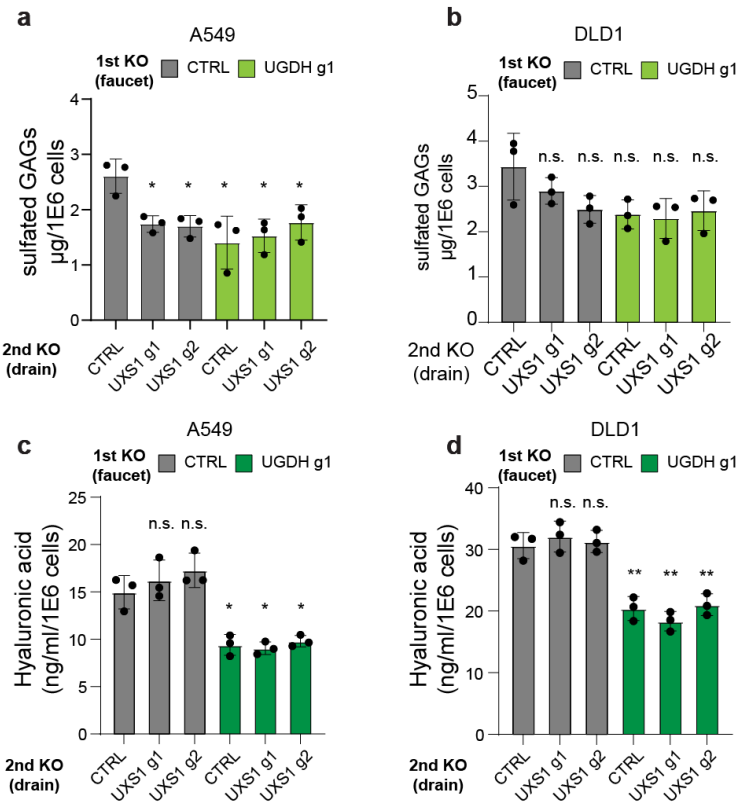

Figure 2.8 Downstream proteoglycan impact of UXS1 loss.

(a) Sulfated glycosaminoglycans (sGAG) levels quantified using DMMB assay (Methods) from UGDH KO, UXS1 KO, and UGDH-UXS1 DKO A549 cells and in **(b)** DLD1 cells. **(c)** Hyaluronic acid levels quantified via competitive ELISA (Methods) from the conditioned media obtained from UGDH KO, UXS1 KO, and UGDH-UXS1 DKO A549 cells and in **(d)** DLD1 cells. For a-d, n=3 biological

replicates. Data are shown as mean ± s.d. p values were calculated using two-tailed Student's t-test (n.s.: not significant ,*p<0.05, **p<0.01).

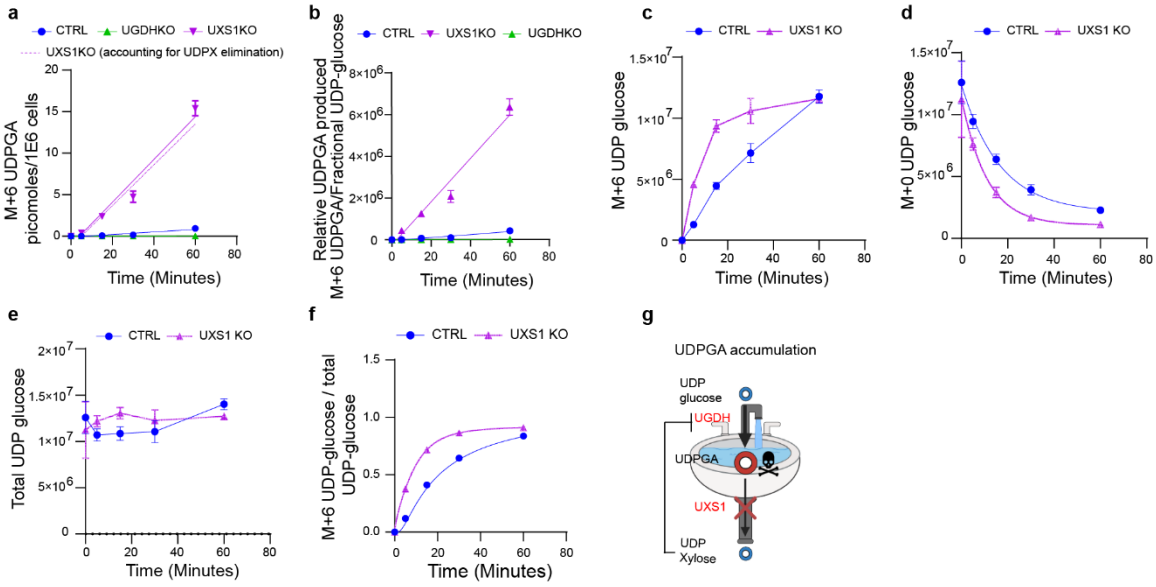

Figure 2.9 Activity of UGDH increases upon UXS1 KO due to lack of feedback inhibition from UDP-xylose.

(a) Production of M+6 UDPGA in picomoles/1E6 cells of control, UGDH KO, and UXS1 KO cells, quantified from UDPGA standard curves. Dotted purple line indicates UDPGA labeling in UXS1 KO cells, minus the normal labeling rate of UDP-xylose production calculated from panel c, representing UDPGA production not accounted for by loss of clearance via UXS1. **(b)** Relative UDPGA produced [M+6 UDPGA / (M+6 UDP-glucose/ total UDP-glucose)] in control, UGDH KO, and UXS1 KO A549 cells (n=3 per group). **(c)** Labelled UDP-glucose (M+6) in control and UXS1 KO A549 cells (<1h) (n=3 per group). **(d)** Unlabelled UDP-glucose (M+0) in control and UXS1 KO A549 cells (<1h) (n=3 per group). **(e)** Total UDP-glucose (M+6 + M+0) in control and UXS1 KO A549 cells (<1h) (n=3 per group). **(f)** Fractional labeling of UDP-glucose [M+6 UDP-glucose/ total UDP-glucose] of control and UXS1 KO cells (<1h) (n=3 per group). **(g)** Refined model depicting the negative feedback loop between UDP-xylose and UGDH. For a-f, n=3 biological replicates. Data are shown as mean ± s.d.

Excess UDPGA disrupts Golgi function

To try to understand why UDPGA accumulation upon UXS1 loss may be toxic to cells, we performed next-generation sequencing of mRNA from cancer cells subjected to UXS1 KO. Gene set enrichment analysis indicated an induction of various Golgi function-related genes, and a depletion of cell cycle and DNA repair/damage response genes following UXS1 KO in cancer cells (Figure 2.10a-c). Looking closely at the Golgi-related genes, we observed induction of various Golgi posttranslational modification genes such as N-linked glycosyltransferases and Golgi trafficking genes such as COP-I vesicular transport genes. Included in the signature was ARF4, a known Golgi stress response gene[136,246], and we verified that ARF4 protein levels are induced upon UXS1 KO (Figure 2.10d).

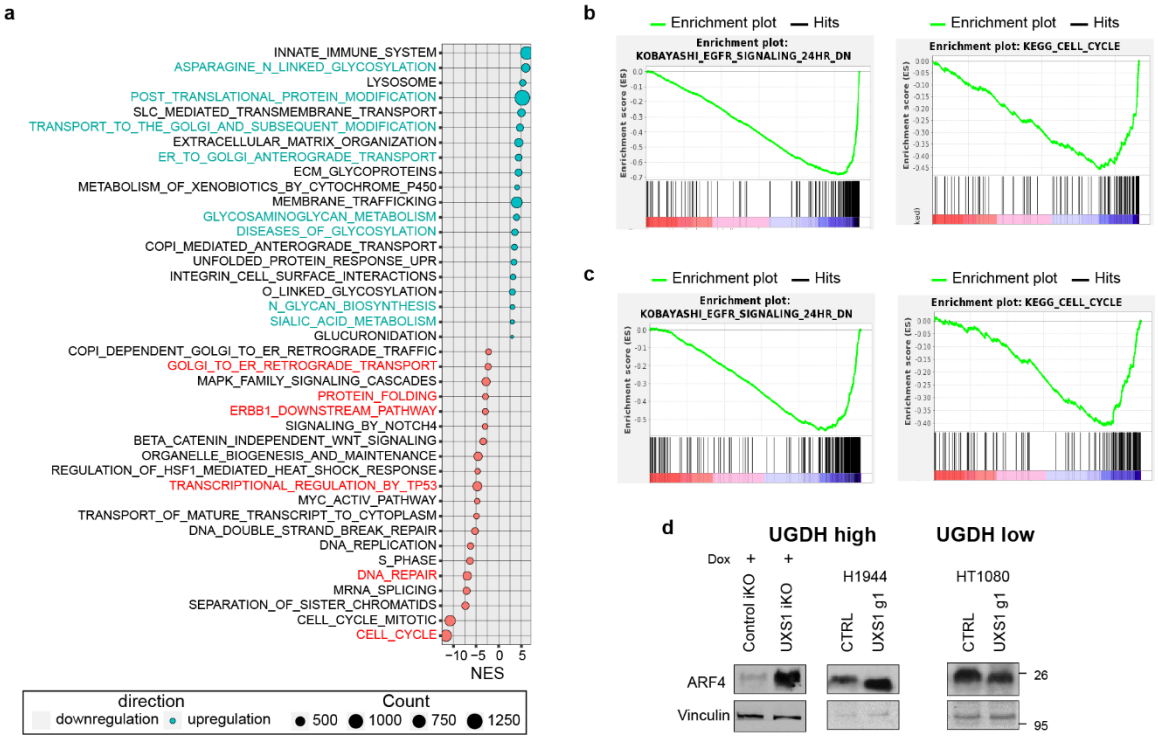

Figure 2.10: Transcriptomic analysis of UXS1 KO cells.

(a) Dot plot of differentially expressed pathways identified by GSEA pathway analysis of RNAseq data from UXS1 KO A549 cells compared to CTRL KO. **(b)** GSEA enrichment plot showing that EGFR signaling and Cell Cycle genesets are highly depleted in UXS1 KO A549 cells compared to CTRL KO. **(c)** Same findings in another UXS1 sensitive cell line (H460). Cell Cycle genes are the most depleted geneset for 'C2; canonical pathways' (as shown in Figure 3A), while EGFR Signaling genes are the most depleted geneset for the 'C2; chemical and genetic perturbations' ontology scheme. **(d)** ARF4 immunoblots in UGDH high (UXS1 (A549) iKO and H1944) and low (HT1080) cells, 7 days post UXS1 KO, showing that ARF4 is only induced only in UGDH high cells following UXS1 ablation. For a and d, n=3 biological replicates.

Overall, this transcriptional response suggested that the toxicity of UXS1 loss/UDPGA accumulation specifically involves the Golgi, which was congruent with UDPGA being a glycosylation precursor and UXS1 being a Golgi resident

enzyme. Surprisingly, the loss of UXS1 dramatically altered the morphology of the Golgi apparatus. Instead of being confined to a single region, loss of UXS1 resulted in an aberrant dispersal of the cis-, trans-, and medial components of the Golgi apparatus to multiple regions throughout the cell body, as indicated by immunolabeling and verified by electron microscopy (Figure 2.11a-h). Meanwhile, the endoplasmic reticulum (ER) appeared intact, and cells did not show signs of ER stress (Figure 2.12a-c). Importantly, the UDPGA-depleting 4MU or preemptive UGDH KO rescued the normal Golgi morphology in UXS1 KO cells, demonstrating that the Golgi transformation occurred due to UDPGA accumulation (Figure 2.11f, and i). To determine whether UXS1 KO alters Golgi glycosylation processes, we analyzed the N-linked (Figure 2.13a) and O-linked (Figure 2.13f) glycosylation profiles of A549 cells upon UXS1 loss. While these analyses show relative abundances of each species and thus do not inform of gross intracellular glycosylation level of each condition, they demonstrate that there are overall changes in glycosylation patterns upon UXS1 loss. While the relative abundance of oligomannose and paucimannose glycans decreased, sialylated and rare complex glycans with poly lac-nac extensions increased upon UXS1 loss (Figure 2.13b-e). These results indicate that the accumulation of UDPGA following the loss of UXS1 alters both the structure and function of the Golgi apparatus. Interestingly, the majority of UDPGA accumulation occurs in the cytosol (Figure 2.14a, b), and overexpression the Golgi UDPGA transporter SLC35D1[169] does not impact UXS1

KO toxicity (Figure 2.15a and, b), suggesting that excess UDPGA impacts the Golgi from the cytosolic side

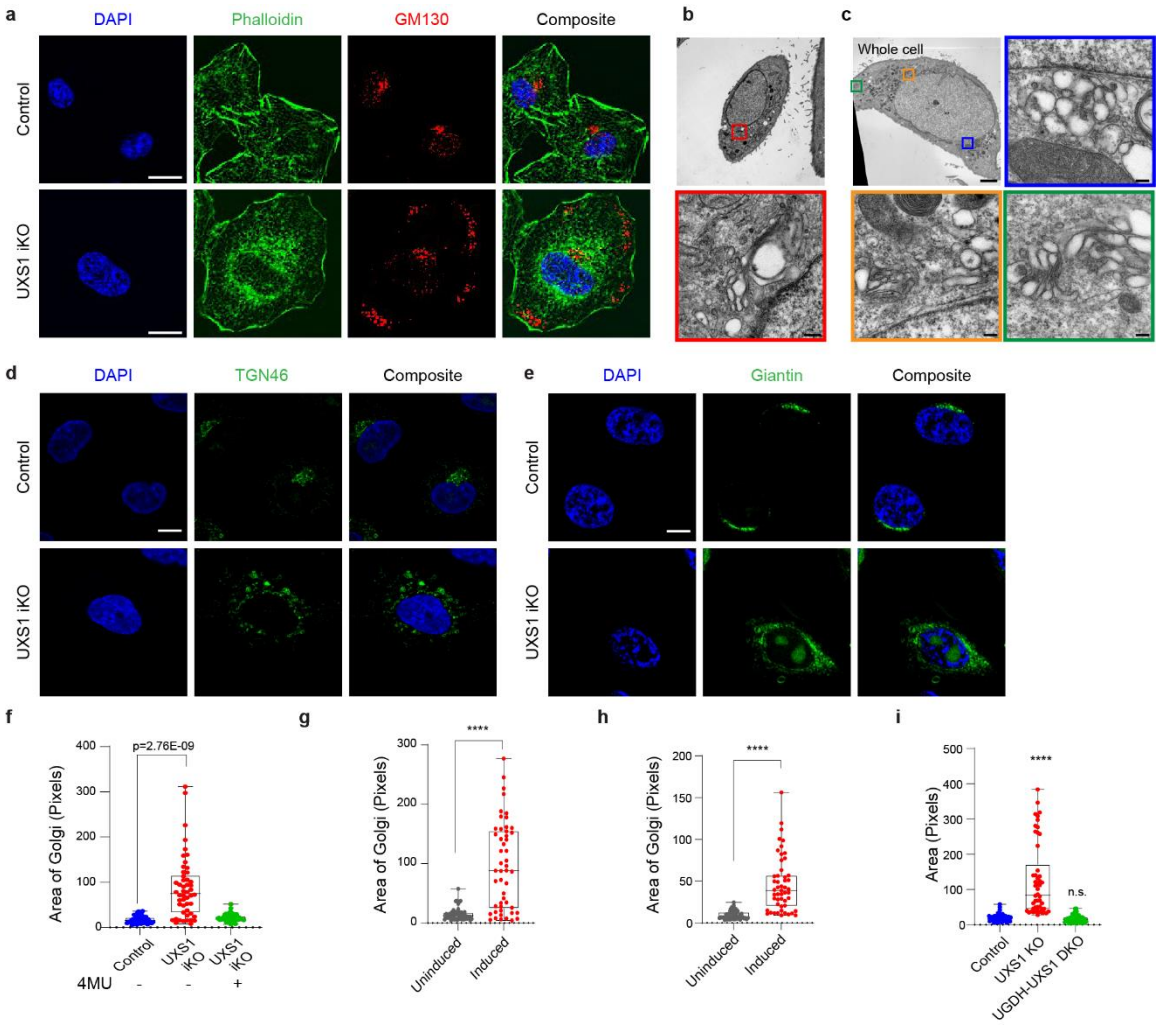

Figure 2.11 UXS1 KO disrupts Golgi structure.

(a) Immunofluorescent images of UXS1 iKO or control iKO cells, 7 days post-induction, immunostained for Phalloidin (actin, green), GM130 (Golgi, red), and DAPI (nucleus, blue); scale bar=20μm. **(b)** Representative transmission electron microscope images of A549 control and **(c)** A549 UXS1 KO cells. The colored boxes in the whole cell images indicate locations where golgi structures are found, and the zoomed version of each is shown alongside, with the corresponding colored outline. Scale bar: Whole cell images=5μm, zoomed images=0.2μm. **(d)** Immunofluorescent images of UXS1 iKO or control iKO cells, 7 days post doxycycline induction, immunostained with Giantin (medial-golgi, green), **(e)**

TGN46 (trans-golgi, green) scale bar=20 μm. **(f)** Dot plot of total Golgi area per cell, labeled using GM130, from control, induced, and induced + 4MU (15 μM) UXS1 iKO cells, 7 days post-induction. Each dot represents a different cell, n=50 cells per condition. **(g)** Dot plot of total golgi area per cell from uninduced and induced UXS1 iKO cells at 7 days postinduction, as labeled with Giantin or **(h)** TGN-46 (n=50 cells for each stain). **(i)** Dot plot of total golgi area per cell, labeled using GM130, from control, UXS1 KO, and UGDH-UXS1 DKO (A549) cells, 7 days post UXS1 transduction; n=50 cells. For data in **(f)**, **(g)**, **(h)**, and **(i)**, box plot shows median (centre) with interquartile range of 25% to 75%, minima and maxima, Two-tailed unpaired Student's t-test (n.s.: not significant, *p<0.05, ***p<0.001, ****p<0.0001).

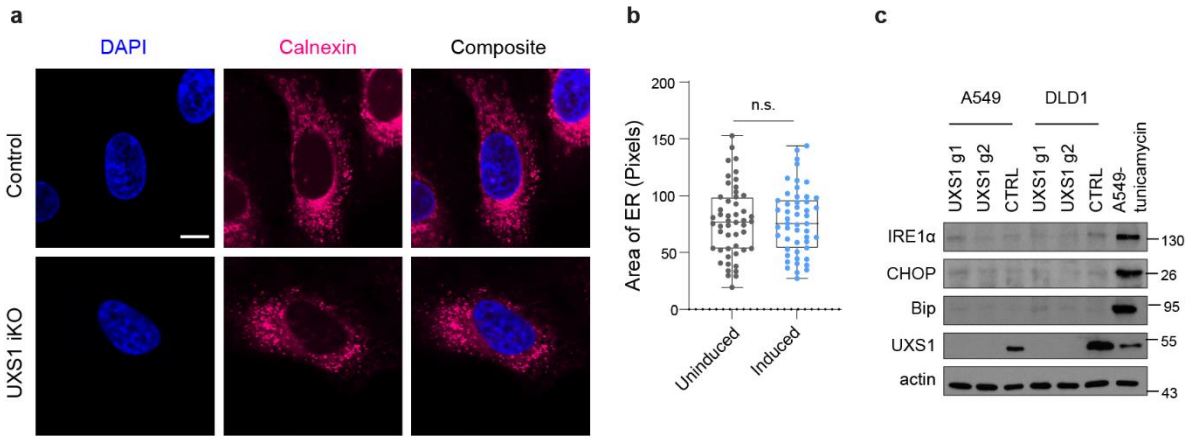

Figure 2.12 UXS1 ablation does not cause ER stress.

(a) Immunofluorescent images of UXS1 iKO or control iKO cells, 7 days post doxycycline induction, immunostained with**)** Calnexin (ER, red); scale bar=20 μm. **(b)** Dot plot of total golgi area per cell from uninduced and induced UXS1 iKO cells at 7 days postinduction, as labeled with Calnexin (n=50 cells). **(c)** Immunoblot for ER stress markers IRE1α, CHOP, and BiP in A549 and DLD1 UXS1 KO cells 7 days post transduction. Tunicamycin treated cells are positive control for ER stress. In **(b)** box plot shows median (centre) with interquartile range of 25% to 75%, minima and maxima, Two-tailed unpaired Student's t-test (n.s.: not significant, *p<0.05, ***p<0.001, ****p<0.0001).

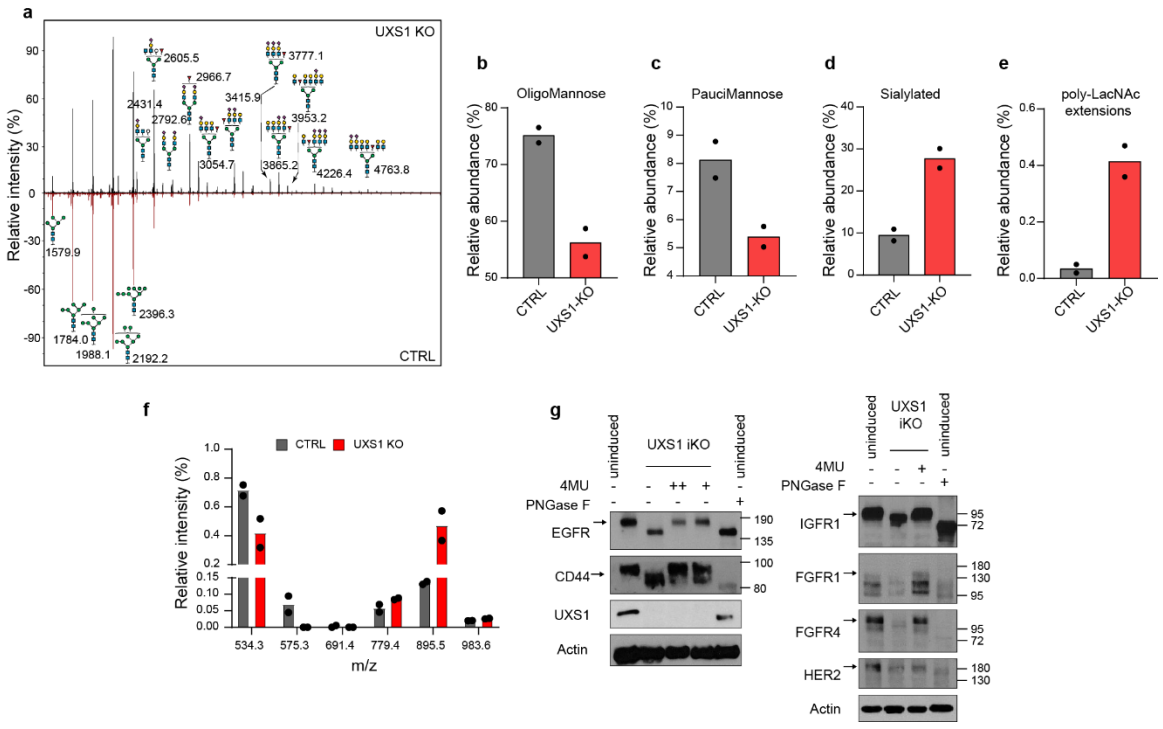

Figure: 2.13 UDPGA accumulation causes aberrant glycosylation.

(a) Representative mass spectrometry N-glycan profiles of A549 cells subjected to CTRL or UXS1 KO, at 7 post-transduction, with annotated mass peaks. Values are relative to the total N glycans detected. **(b)** Changes in Oligomannose glycans **(c)** Paucimannose glycans **(d)** Sialylated glycans and **(e)** glycans with poly-LacNac extensions in A549 cells subjected to CTRL or UXS1 KO. **(f)** O-glycan profiling analysis performed on A549 cells subjected to CTRL or UXS1 KO at 7d post-transduction. **(g)** Immunoblots for EGFR, CD44, IGFR1, FGFR1, FGFR4, and HER2 glycoproteins in uninduced, induced, or induced plus 4MU UXS1 iKO cells. + indicates 15μM and ++ indicates 80μM 4MU. Cell lysates were harvested from n=2 biological replicates for each condition for glycan profiling. p values were calculated using two-tailed Student's t-test. (n.s.: not significant, *p<0.05, **p<0.005, ***p<0.001****p<0.0001).

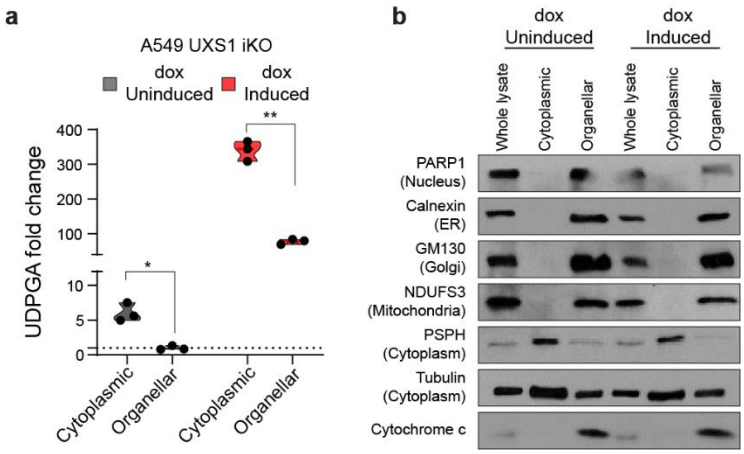

Figure 2.14 UDPGA accumulates in cytoplasm upon UXS1 loss.

(a) GC-MS UDPGA quantitation of cytoplasmic and organellar fractions of either induced or uninduced A549 UXS1 iKO cells. **(b)** Immunoblots of proteins located in nucleus (PARP1), ER (Calnexin), Golgi (GM130), mitochondria (NDUFS3), and cytoplasm (PSPH and tubulin) in cytosolic and organellar fractions. Cytochrome c is used as a control for intact organelles (mitochondria). For **(a)** and **(b)**, n=3 biological replicates. Data are shown as mean ± s.d. p values were calculated using two-tailed Student's t-test (n.s.: not significant, *p<0.05, **p<0.005, ***p<0.001****p<0.0001).

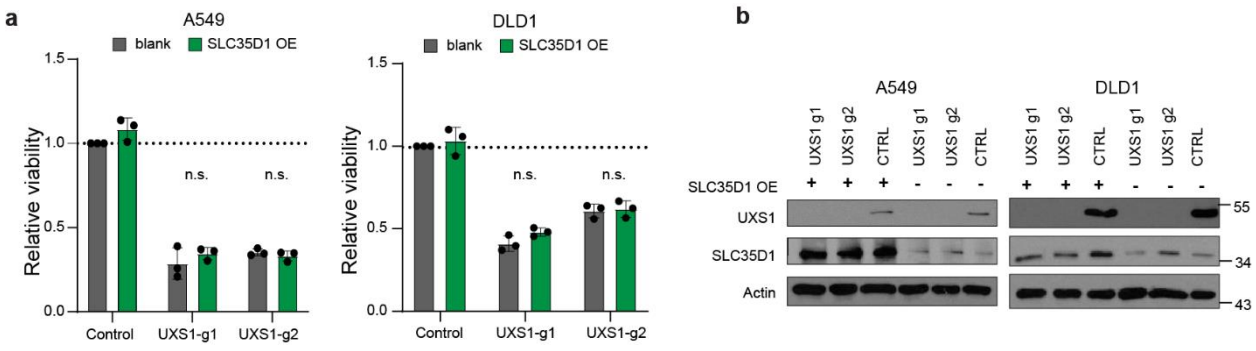

Figure 2.15 SLC35D1 OE does not exacerbate UXS1 KO toxicity.

(a) Viability of A549 and DLD1 cells overexpressing either blank vector (gray) or SLC35D1 (dark green) then subjected to CTRL or UXS1 KO. Values are relative

to blank vector overexpressing, CTRL KO cells (=1.0). **(b)** Immunoblot of UXS1 and SLC35D1 protein levels under the OE/KO combinations shown in **(a)**. For **(a)** and **(b)**, n=3 biological replicates. Data are shown as mean ± s.d. p values were calculated using two-tailed Student's t-test (n.s.: not significant, *p<0.05, **p<0.01).

The Golgi apparatus is the gateway for the terminal glycomodifications and trafficking for cell surface proteins such as growth factor receptors and other surface markers that play essential roles in cancer biology[247,248]. Therefore, we examined whether cell surface proteins have changes in mobility which are commonly associated with glycosylation defects[249-251]. We examined various cell surface receptors (EGFR, CD44, FGFR1, FGFR4, IGF1R) which are key upstream components of signaling cascades[252-255]. We found that loss of UXS1 caused increased gel migration in all of these receptors, suggesting their defective glycosylation[249-251], as is seen by treating cells with the glycosidase PNGase[249] (Figure 2.13g). In most cases protein levels were also significantly decreased, which may be due to degradation, misfolding and/or decreased stability known to occur for mis-glycosylated proteins[256-258]. These results suggested that the Golgi dysfunction caused by UXS1 loss has a far-reaching consequence of preventing the proper maturation of essential cell surface glycoproteins.

Among these, EGFR is an upstream oncogenic signaling component that is required for the proliferation and survival of cancers such as Non-Small Cell Lung Carcinoma (NSCLC) and glioblastoma[255], and our RNA sequencing of UXS1 KO

cells suggested a profile of impaired EGFR signaling (Figure 2.10b, c). Therefore, we looked more closely at EGFR as an example surface protein that is impaired due to UDPGA-induced Golgi dysfunction. Immunolabeling of EGFR strikingly showed that it is absent at the plasma membrane following KO of UXS1, with decreased overall levels (Figure 2.16a-c). We next examined the ability of UXS1 iKO cells to respond to EGF mitogen. Cells lacking UXS1 could not properly respond to EGF, not undergoing autophosphorylation of EGF, which is the canonical initial step in the EGFR signaling cascade (Figure 2.16e). Furthermore, the cells lacked the characteristic phosphorylation of Akt and ERK, which is a standard downstream manifestation of EGFR activation. While these results demonstrate effects on EGFR and its downstream signaling, the general effects of UXS1 KO across cell various surface receptors (Figure 2.13g) suggest that cancer cells have in effect been ‘silenced’ in their ability to respond to various extracellular cues. Thus, while EGFR loss is likely to be highly detrimental to the cancer cells, it is unlikely to be the sole culprit, and we propose that death may occur from a global deregulation of cell surface proteins.

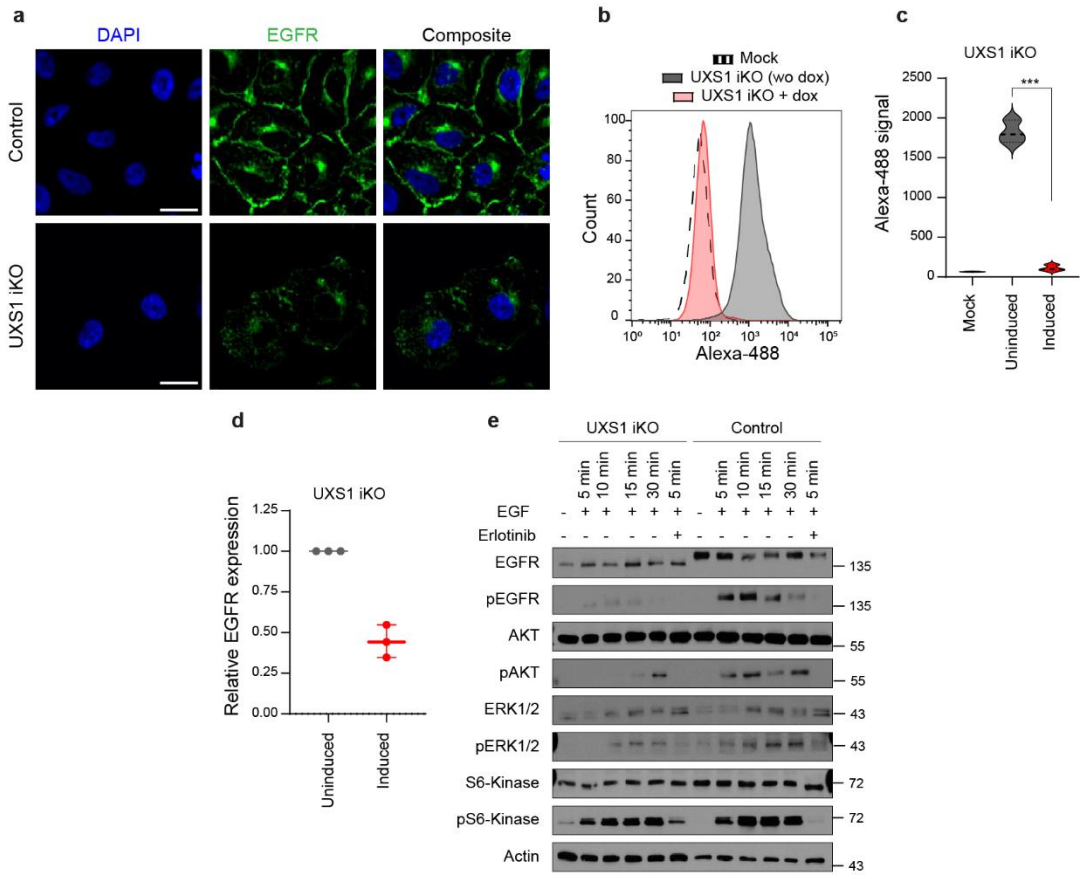

Figure 2.16 Excess UDPGA causes Golgi trafficking defects that leads to EGFR inactivation.

(a) Immunofluorescent images of uninduced or induced UXS1 iKO cells, immunostained for EGFR (green) and DAPI (blue). Scale bar = 40μm. **(b)** FACS-based fluorescence histogram showing doxycycline induced and non-induced UXS1 iKO cells labeled with FITC conjugated EGFR antibody showing surface EGFR binding. **(c)** Quantitation of cell surface EGFR labeling via 3 independent flow cytometry experiments. **(d)** Quantification of relative actin-normalized EGFR expression (immunoblots from 3 independent experiments) in induced compared to uninduced UXS1 iKO A549 cells, 5d postinduction. In each experiment, the uninduced EGFR = 1.0. **(e)** Immunoblotting of EGFR and downstream signaling components from induced UXS1 iKO cells or induced CTRL iKO cells, following serum starvation then EGF stimulation. pAkt = phospho (S473) Akt; pERK1/2 = phospho ERK1/2(T202/Y204); pS6-kinase = phospho-S6 kinase(T389)

phopshoantibodies. EGFR blotting was run on 4-15% gradient gel to show maximal shift of the protein, while the rest of the probes are run in 10% to allow probing for multiple epitopes. For **(a-e)**, n=3 biological replicates. Data are shown as mean ± s.d. . p values were calculated using two-tailed Student's t-test (n.s.: not significant, *p<0.05, ***p<0.001, ****p<0.0001).

We also considered the downregulation of cell cycle genes that were observed in the RNA-SEQ. Golgi fragmentation occurs during mitosis, thus a mitotic block could indirectly account for the golgi-related pathologies that we observed. However, propidium iodide based fluorescence-activated cell sorting (FACS) cell cycle analyses of UXS1 iKO cells indicate that the S phase population is increased while G2 population (which includes M phase cells) is decreased (Extended Fig.2b, c). We did not observe any accumulation of M phase as marked by phospho-Histone-H3 (Figure 2.17a). We find that serum starvation- induced block of cell cycle progression block does not enhance and instead slightly decreases Golgi dispersion upon UXS1 iKO (Figure 2.17b). Overall, it is unlikely that UXS1 KO causes the Golgi dispersion phenotype via cell cycle defects. Rather, the downregulation of various cell cycle genes may be a consequence of the 'silencing' of mitogenic surface receptors such as EGFR, which can drive cell cycle progression[255].

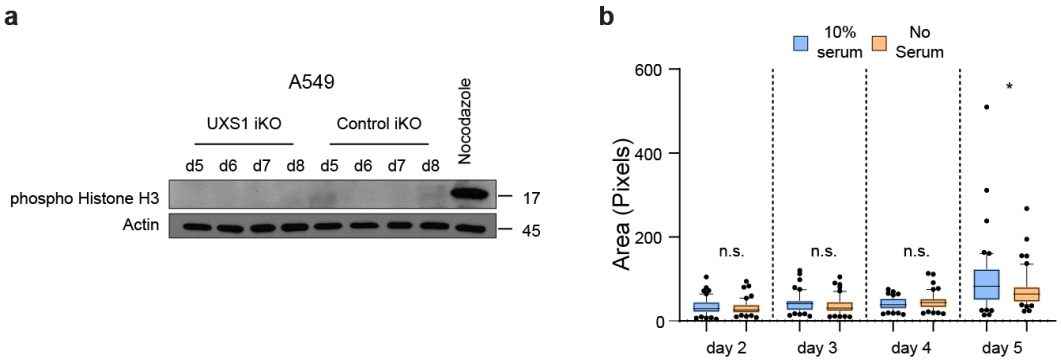

Figure 2.17 UXS1 KO led Golgi dispersion is independent of cell cycle defects.

(a) Immunoblots of phospho-histone H3 and actin from A549 UXS1 iKO and control iKO cells at indicated timepoints post doxycycline induction. Nocodazole-treated cells are used as a positive control for enrichment for cells in M phase. **(b)** Dot plot of total Golgi area per cell, from A549 UXS1 iKO cells induced via doxycycline, then labeled using GM130 at indicated days post-induction. No serum (orange) cells were serum starved for 12 hours before labeling, which results in G0 cell cycle arrest and synchronization. For **(a-b)**, n=3 biological replicates. . In **(b)** box plot shows median (centre) with interquartile range of 25% to 75%, minima and maxima. Data are shown as mean ± s.d. p values were calculated using two-tailed Student's t-test (n.s.: not significant, *p<0.05).

UXS1 as a cancer-selective target

We next set out to examine the consequences of UXS1 loss in the *in vivo* context of a tumor. To examine effects of disruption of UXS1 in an already formed tumor, we utilized dox-inducible UXS1 KO in three subcutaneous xenograft models (A549 and H460, both UGDH-high, non-small cell lung cancer lines; and HT1080, a UGDH-low fibrosarcoma line), where dox was administered on timepoints where

average tumor sizes were at least 200mm^3 (Figure 2.18a-c). For both UGDH-high lines, induction of UXS1 loss resulted in a significant stunting of tumor growth (and regression in H460), and extended median survival by 27 days for A549, and 50 days for H460 (Figure 2.19a, b, d, and e, Figure 2.20b, c). We observed ~40-fold accumulation of UDPGA (Figure 2.20e) and induction of ARF4, a Golgi stress marker (Figure 2.20f) in A549 iKO tumors. On the other hand, despite efficient induced KO (Figure 2.20a, d), UXS1 loss in the UGDH-low HT1080 tumors had no effect on tumor growth and overall survival (Figure 2.19c, f). Collectively, these experiments demonstrate a therapeutic potential for targeting UXS1 that depends on the high-UGDH status of the tumor.

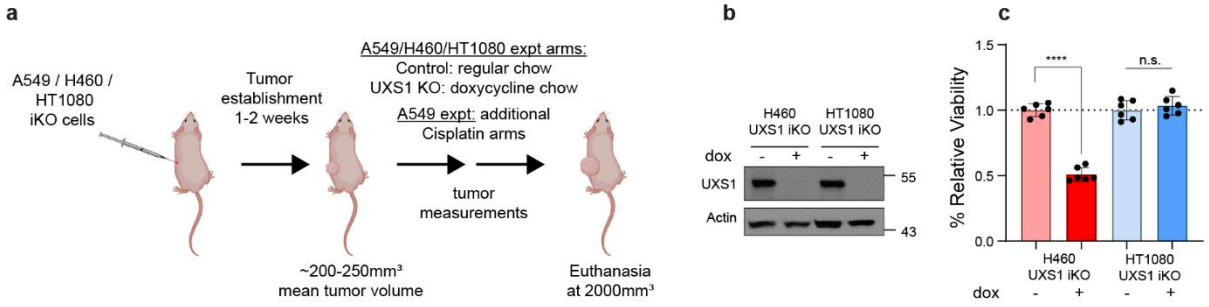

Figure 2.18 Xenograft experiment design and characterization of H460 and HT1080 dox-inducible UXS1 iKO cells.

(a) Schematic of in-vivo xenograft experiments. A549/H460/HT1080 UXS1 iKO cells were injected subcutaneously into 6 weeks old nude female mice and allowed for tumors to establish. Once the mean tumor was 200-250mm^3, the mice were divided into groups for control (uninduced) and dox chow induction of UXS1 KO. A549 xenograft experiment had additional cisplatin arms. The animals were euthanized when individual tumor volume reached 2000mm^3. **(b)** Immunoblots for UXS1 and actin of H460 and HT1080 UXS1 iKO cells in culture with and without doxycycline induction. **(c)** Relative viability of H460 UXS1 iKO and HT1080 UXS1

iKO cells with and without doxycycline induction (without doxycycline = 1.0). Induction consisted of 100ng/ml doxycycline treatment for 48 hours; cells were cultured for 4 more days before measuring viability. For **(b)** and **(c)**, n=3 biological replicates. Data are shown as mean ± s.d. p values were calculated using two-tailed Student's t-test (n.s.: not significant, *p<0.05).

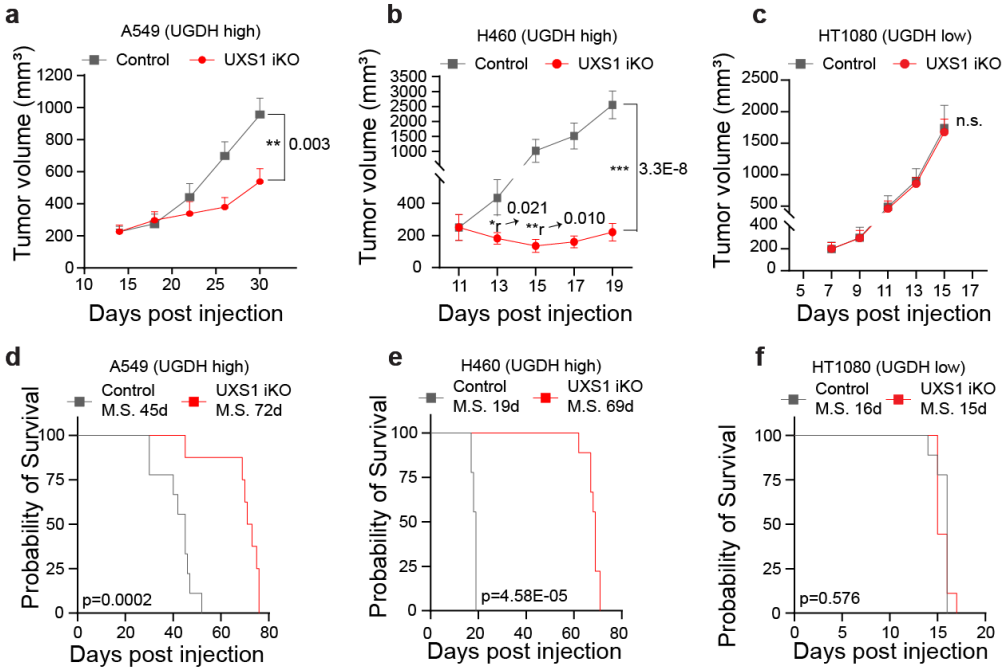

Figure 2.19 Loss of UXS1 results in in-vivo tumor regression and increase in survival benefit.

(a) Mean volumes (±s.e.m.) of A549, **(b)** H460, and **(c)** HT1080 subcutaneous xenograft tumors, UXS1 iKO induced when mean tumor volume reached 200-250mm^3 (red, n=12 per line except n=11 for A549) or left uninduced (gray, n=12 per line) (Methods). **(d-f)** Kaplan-Meier survival analysis for the groups shown in **a-c** (M.S. = median survival). (**a-c)**, Two-tailed unpaired Student's t-test. *r and **r denotes significant regression compared to starting tumor volume. **h**, Wilcoxon matched-pairs signed rank test. **d-f**, Mantel–Cox test for survival.

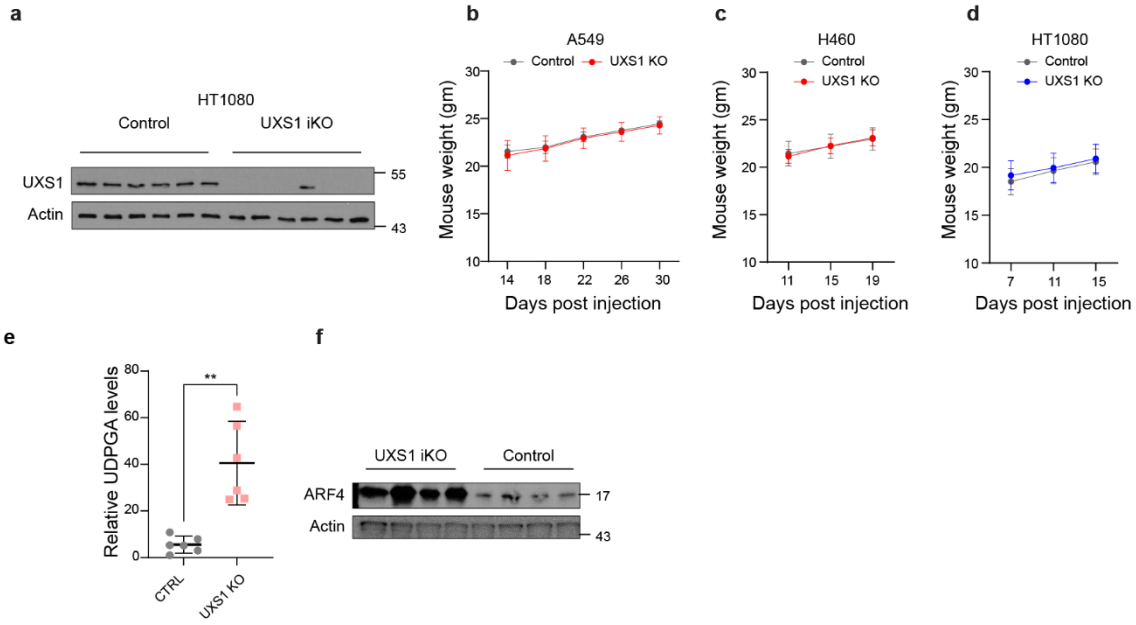

Figure 2.20 Additional details of xenograft experiments.

(a) Immunoblot for UXS1 and actin in six individual tumors each from the control and UXS1 iKO group of HT1080 UXS1 iKO xenograft experiment. **(b)** Weight of mice in grams from xenograft experiments of A549, **(c)** H460, and **(d)** HT1080 from control and UXS1 iKO arms of the experiment. **(e)** LC-MS Quantification of UDPGA from endpoint tumors from another A549 iKO cohort where tumors were allowed to form for 17 days, induced for KO, then euthanized at 19 days postinduction. **(f)** Immunoblot for ARF4 and actin from four individual tumors in panel **(e)**. For **(a)**, **(e)**, and **(f)**, n=3 biological replicates. Data are shown as mean ± s.d. . p values were calculated using a two-tailed Student's t-test (n.s.: not significant, **p<0.005).

For UXS1 to be an ideal cancer target, it should demonstrate cancer cell-selective toxicity. Recently, UGDH itself was examined in cancer contexts: it was elevated in some subtypes of lung and breast cancers which correlated with poor prognosis[259-261], suggesting UGDH as a cancer target[262,263]. In our kitchen sink

model, UGDH is not a cancer target *per se* but a biomarker and functional determinant for which cells will require UDPGA detoxification via UXS1. Importantly, comparing tumors and adjacent normal tissues, we observed that UGDH is elevated in lung and breast cancers compared to normal tissues, suggesting that UXS1 targeting would hurt cancer cells but not normal cells (Figure 2.21a-d). RNA-SEQ database comparison of UGDH transcript abundance across tumor types and normal organs also indicates that UGDH may be elevated in multiple tumors relative to normal tissues (Figure 2.22a). The variability of UGDH expression across the solid tumor lines (Figure 2.1e) and tumors (Figure 2.22a) suggest that the applicability of targeting UXS1 may depend both on the cancer type and on a patient-by-patient basis. We confirmed overall low protein levels of UGDH expression across various patient normal liver, kidney, and colon tissues, suggesting that targeting UXS1 would not cause toxic UDPGA accumulation in organs (Figure 2.22b). Finally, we compared UGDH expression and UXS1 essentiality across a panel of noncancer (primary or immortalized) cells. Normal cells express lower levels of the 'faucet' UGDH than the UXS1 KO sensitive cancer cells, and they are also insensitive to the KO of UXS1 as predicted (Figure 2.23a-d). Collectively, these findings suggest a therapeutic window for UXS1 targeting, and we note that partial loss of UXS1 via RNAi is still effective (Figure 2.24a-c). Nonetheless, UXS1 KO mice are embryonic lethal[264], which may indicate importance for UXS1 detoxification or downstream proteoglycan function (UDP-xylose) in a developmental and/or organismal context. Thus, as some important

normal cells may depend on UXS1, examination of patient toxicity will be an important concern in future therapies targeting UXS1.

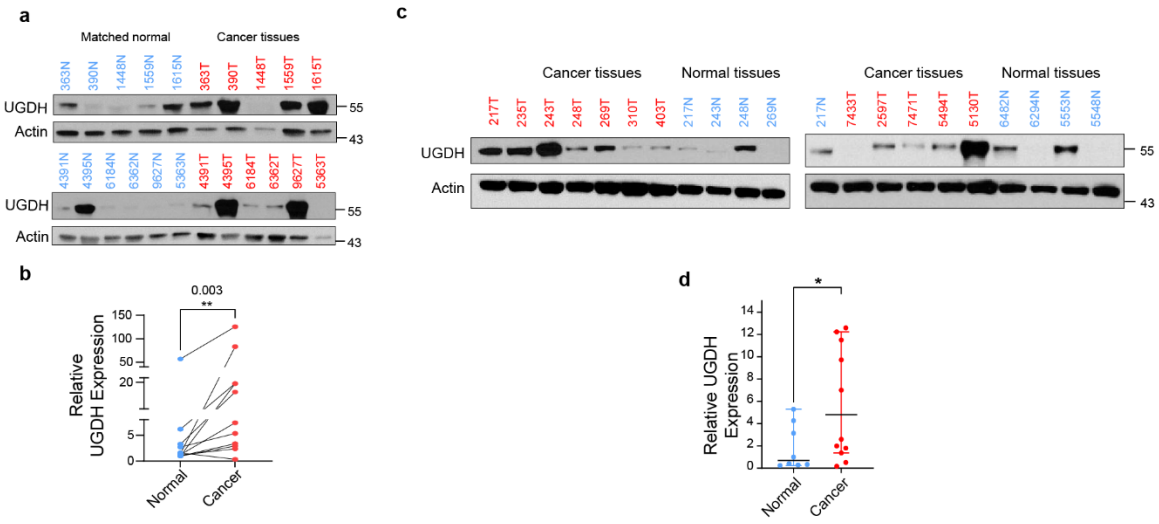

Figure 2.21 UGDH protein expression in lung and breast patient tumor samples.

(a) Immunoblots for UGDH and actin from 11 lung cancer patient tissue samples and patient-matched normal lung tissues; cancer tissues are labeled in red and normal tissues are marked in blue. **(b)** Quantification of relative, actin normalized UGDH band intensities from panel **(a)**. **(c)** Immunoblots for UGDH and actin from 11 breast cancer patient tissue samples and 8 normal breast tissues; cancer tissues are labeled in red and normal tissues are labeled in blue. Numbers indicate deidentified patient code, and tumors and normals sharing the same number are adjacent samples from the same patient. **(d)** Quantification of relative, actin normalized UGDH band intensities from panel **(c).** Data are shown as mean ± s.d. . p values were calculated using a two-tailed Student's t-test (n.s.: not significant,*p<0.05, **p<0.005).

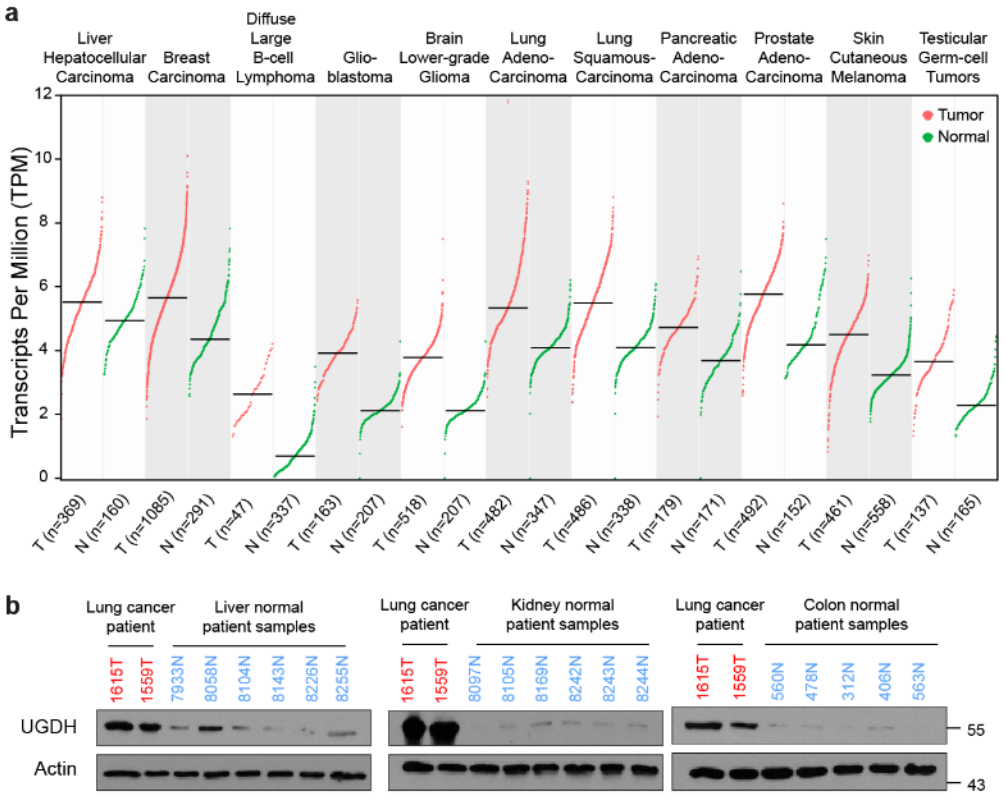

Figure 2.22 UGDH expression in cancer subsets.

(a) Expression profiles of UGDH in 11 types of normal and tumor tissues. The plot is obtained from GEPIA2[265], a web gene expression profiling tool that plots normalized mRNA-seq data from patient tumor tissues and normal tissues obtained from TCGA and GTEx. All tumor types shown have over 2-fold UGDH expression in tumors than normal tissues (q value <0.01). q values have been determined by ANOVA and adjusted for false discovery rate. The dotted line indicates mean UGDH TPM of liver normal samples, highest among other normal organs. **(b)** Immunoblots for UGDH and actin from 6 normal liver, 6 normal kidney and, 5 normal colon patient tissue samples compared with 2 representative (UGDH high) lung cancer patient samples; cancer tissues are labeled in red and normal tissues are labeled in blue.

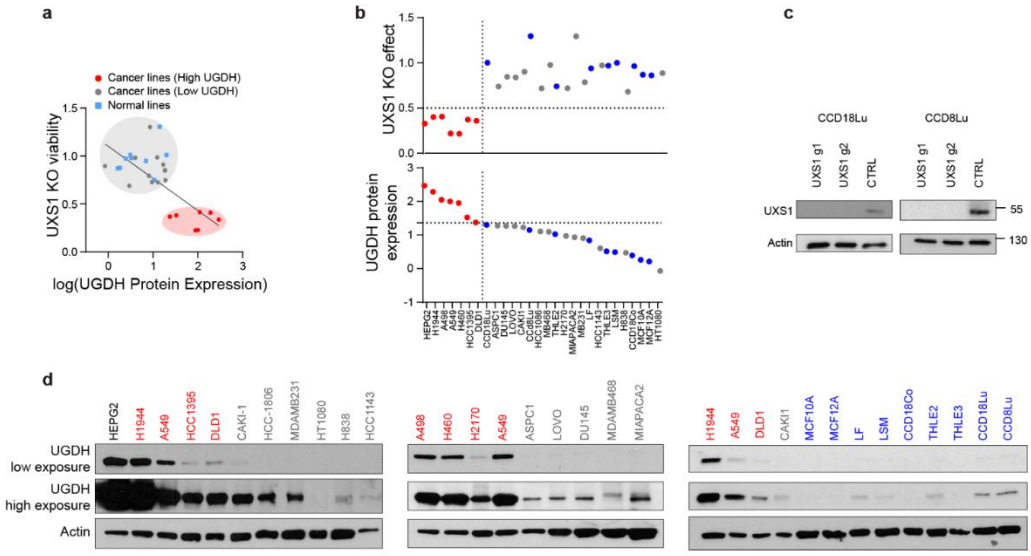

Figure 2.23 Normal cells can tolerate UXS1 loss and UGDH protein levels better predict the dependency of cancer cells on UXS1.

(a) Scatter plot of viability following UXS1 KO (y axis) against UGDH protein expression level (x axis) for 19 cancer and 9 normal cell lines of varying lineage, showing that all normal cell lines are in the UGDH-low, UXS1 KO-insensitive cluster (gray circle), in contrast to the UGDH-high, UXS1 KO-sensitive cancer lines (red circle). Immunoblots of UGDH level for each line are provided in panel (d) Linear regression trendline is shown in black for all cancer lines examined. **(b)** Top dot plot showing viability following UXS1 KO (y axis) and bottom dot plot showing corresponding UGDH protein expression level (y axis) for 19 cancer and 9 normal cell lines of varying lineage (x axis). Cancer lines are divided between High (red) and Low(gray) UGDH expressing lines based on arbitrary cut-off 1.25 units; normal lines are labeled as blue dots. **(c)** UXS1 immunoblots showing KO of UXS1 in CCD18Lu and CCD8Lu cells, 9 days post-transduction. **(d)** Immunoblots of UGDH and actin for cancer cell lines and normal cells (non-transformed primary or immortalized cells shown in panel (a) and (b); UXS1 KO sensitive cell lines are labeled in red and insensitive lines are labeled in gray and normal lines are labeled in blue.

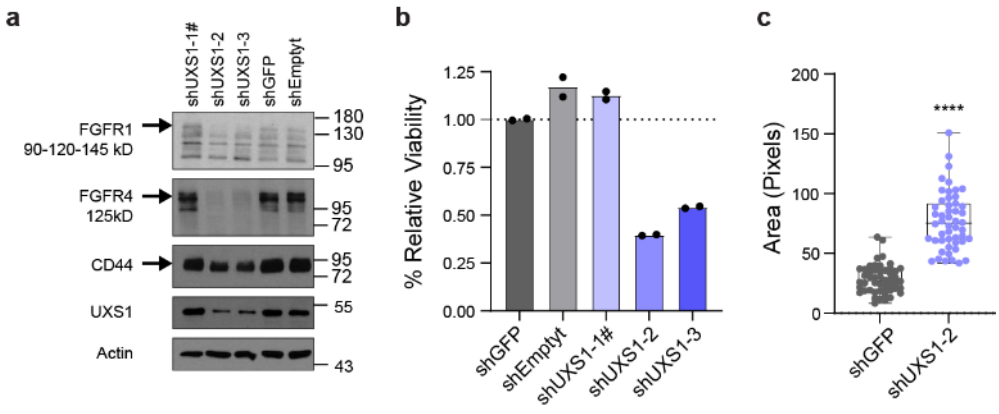

Figure 2.24 Partial UXS1 loss is toxic and causes Golgi dysfunction.

(a) Immunoblots for glycoproteins FGFR1, FGFR4, CD44 and UXS1 in A549 cells subjected to RNAi. UXS1 blots indicate that shUXS1-2 and shUXS1-3, but not shUXS1-1, result in effective knockdown of UXS1, # denotes that shUXS1-1 is a poor performing shRNA. **(b)** Relative viabilities of A549 cells subjected to RNA interference (RNAi) mediated knock-down of UXS1, showing that the two guides which effectively knock down UXS1 result in toxicity. **(c)** Dot plot of total Golgi area per cell, labeled using GM130, from A549 cells subjected to shGFP or shUXS1-2, 7 days post-transduction; n=50 cells. In (c) box plot shows the median (centre) with interquartile range of 25% to 75%, minima and maxima.

We wondered why UGDH, which imposes a detoxification burden, might be upregulated in cancer cells in the first place. Higher levels of UGDH were correlated with a worse prognosis in triple-negative breast cancer patients that received chemotherapy[266]. Proteomic studies also found that UGDH was elevated in chemo-resistant cells as compared to chemo-naïve or untreated cells in the context of lung and ovarian cancer[267,268]. This suggested one rationale for why UGDH may be elevated in cancer: its upregulation could provide an advantage in

chemoresistance, which would be in line with the known function of its product UDPGA, as a substrate for the xenobiotic clearance mechanism of glucuronidation. Indeed, examining how UGDH expression correlates with drug resistance across cancer cell lines, we found that an elevated expression of UGDH correlated with increased resistance to many drugs, including staple chemotherapeutics such as doxorubicin, paclitaxel, and gemcitabine (Figure 2.25a). We also examined whether exposure to and/or selection in chemotherapeutics itself results in induction of UGDH. We formed persister populations of lung cancer line (H2170), triple negative breast cancer line (MDAMB231), and patient derived organoids (TPN1 and TPN2) through cisplatin exposure; these displayed both robust induction of UGDH and sensitization to UXS1 KO (Figure 2.25b-g, Figure 2.26) compared to their parental counterparts. Chemotherapy in the A549 inducible xenograft model induces UGDH in tumors (Figure 2.27a, b) and synergizes with UXS1 iKO to regress tumor growth (Figure 2.27c), although we did not examine effects on overall survival. The same chemotherapy regimen does not induce UGDH in normal mouse tissues (Figure 2.27d, e), suggesting a method to increase the therapeutic window for targeting cancer cells via UXS1. These findings suggest that UXS1 targeting may be particularly damaging to chemo-resistant subpopulations of cancer cells, or to cancer cells being treated with chemotherapeutics, due to their induction of UGDH.

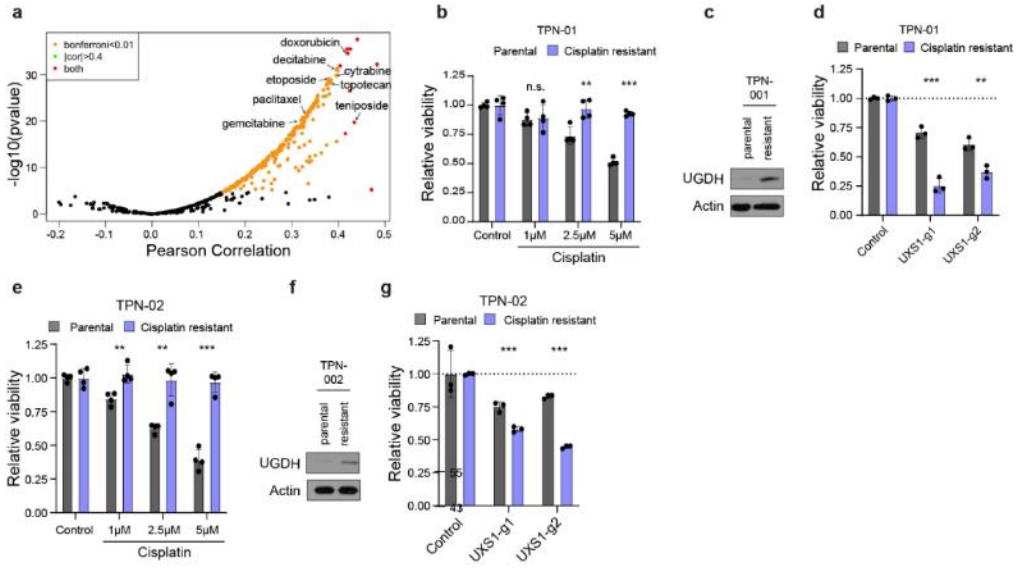

Figure 2.25 chemo-resistant PDOs induce UGDH and demonstrate increased sensitivity to UXS1 KO.

(a) Volcano plot showing spearman correlation between UGDH expression and Drug AUC (546 drugs), constructed by mining CCLE gene expression database[234] and drug AUCs (from PRISM drug sensitivity database[269]), indicating that more chemo-resistant cancer cells express higher UGDH. (b) Survival data for parental (chemo-sensitive) and chemo-resistant Patient-derived organoid (PDO) TPN-01. **(c)** Immunoblot for UGDH and actin from parental and chemo-resistant PDO TPN-01. **(d)** Relative viabilities of parental and cisplatin-resistant TPN-01 subjected to UXS1 KO, indicating that cisplatin-resistant organoids are more sensitive to UXS1 loss. Values are relative to parental cells CTRL-KO (=1.0). **(e)** Viability of parental (chemo-sensitive) and chemo-resistant Patient-derived organoid (PDO) TPN-02 subjected to varying doses of cisplatin. **(f)** Immunoblot for UGDH and actin from parental and chemo-resistant PDO TPN-02. **(g)** Relative viabilities of parental and cisplatin-resistant TPN-02 subjected to UXS1 KO, indicating that cisplatin-resistant organoids are more sensitive to UXS1 loss. Values are relative to parental cells CTRL-KO (=1.0). For **(b-g)**, n=3 biological replicates. Data are shown as mean ± s.d. . p values were calculated using a two-tailed Student's t-test (n.s.: not significant, *p<0.05, **p<0.005, ***p<0.0005).

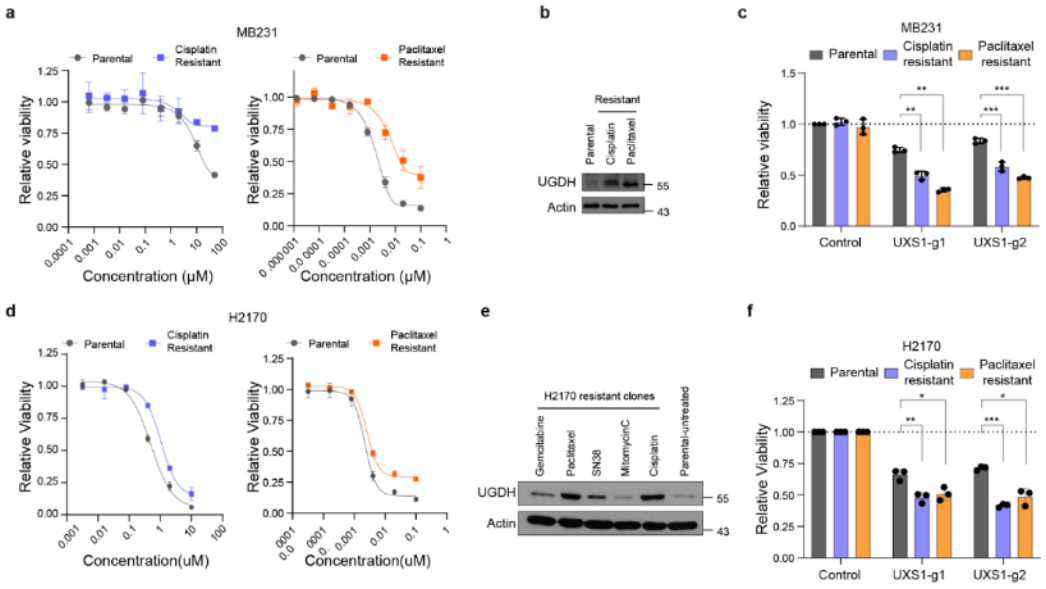

Figure 2.26 Chemo-resistant cell lines induce UGDH and show higher sensitivity to UXS1 KO.

(a) Sigmoidal drug response curves for MDAMB231 parental (gray) and cisplatin-resistant (violet) cells in response to cisplatin treatment and MDAMB231 parental (gray) and paclitaxel-resistant (orange) counterparts in response to paclitaxel. **(e)** Immunoblot for UGDH and actin from MDAMB231 parental and drug-resistant counterparts. **(f)** Relative viabilities of MDAMB231 cisplatin (violet) and paclitaxel (orange) resistant clones subjected to UXS1 KO, indicating that MDAMB231 resistant clones are more sensitive to UXS1 loss. Values are relative to CTRL-KO for each clone (=1.0). **(g)** Sigmoidal drug response curves for H2170 parental (gray) and cisplatin-resistant (violet) cells in response to Cisplatin treatment and H2170 parental (gray) and paclitaxel-resistant (orange) cells in response to paclitaxel. **(h)** Immunoblot for UGDH and actin from H2170 parental and drug-resistant clones. **(i)** Relative viabilities of H2170 cisplatin (violet) and paclitaxel (orange) resistant clones subjected to UXS1 KO, indicating that H2170 resistant clones are more sensitive to UXS1 loss. Values are relative to CTRL-KO for each clone (=1.0). For **(a-f)**, n=3 biological replicates. Data are shown as mean ± s.d. . p values were calculated using a two-tailed Student's t-test (n.s.: not significant, *p<0.05, **p<0.005, ***p<0.0005, ****p<0.00005).

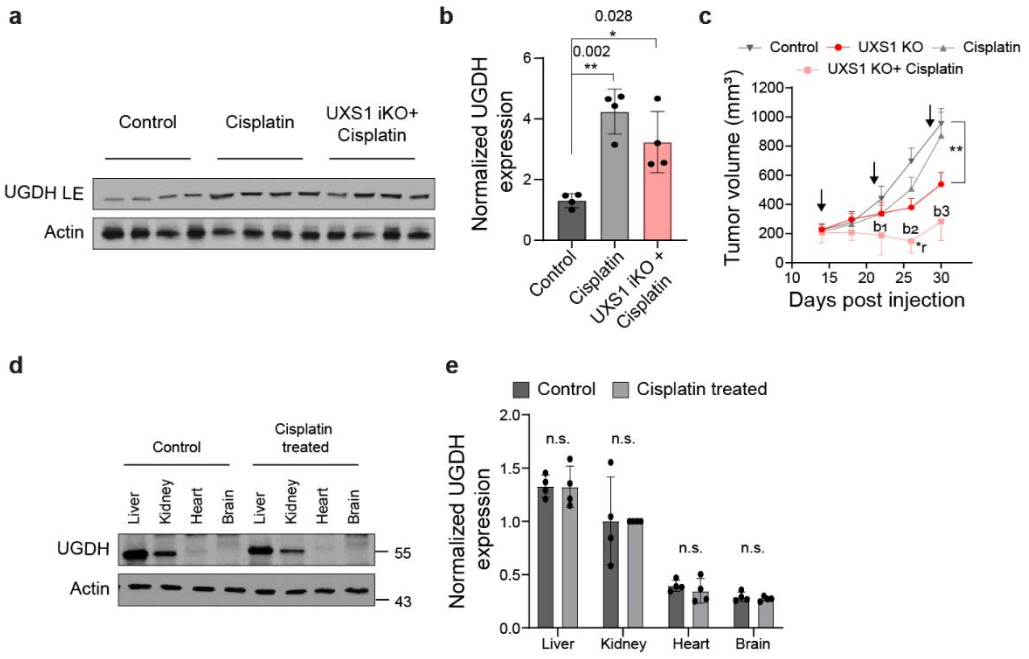

Figure 2.27 Chemotherapy induces UGDH expression in in vivo tumor xenografts but not in normal tissues.

(a) Immunoblot for UGDH and actin in four randomly selected tumors from the control, cisplatin-treated, and UXS1 iKO groups of A549 UXS1 iKO xenograft experiment in 2.19a. **(b)** Quantification of relative, actin normalized UGDH band intensities from (a). **(c)** Volume measurements showing mean (±SEM) of A549 UXS1 iKO subcutaneous xenograft tumors. Data are from same experiment shown in 2.19a, but showing two additional arms, UXS1 KO and CTRL-KO treated with cisplatin (4mg/kg iv 1x weekly, 3 weeks; indicated by arrows) at the same time as dox induction. Bliss independence scores (Methods) were calculated for UXS1+cisplatin arm denoted by b#; values less than 1 indicate synergism. b1=0.66 (d22), b2=0.47 (d26), b3=0.57 (d30). **(d)** Immunoblot for UGDH and actin from organs harvested from control and cisplatin-treated mice (representative pair shown) treated with the same regimen of cisplatin as in Figure 4n (4mg/kg iv 1x weekly, 3 weeks). **(e)** Quantitation of relative, actin normalized UGDH band intensities from control and cisplatin-treated mice (n=4 each) with the same regimen. Data are shown as mean ± s.d. . p values were calculated using a two-tailed Student's t-test (n.s.: not significant, *p<0.05, **p<0.005, ***p<0.0005).

Discussion

The sugar nucleotide UDPGA is a multifunctional metabolite that is a currency for glycosylation and a substrate that cells conjugate to various xenobiotics to aid in their expulsion from cells[270-272]. Here, we find that UDPGA clearance by UXS1 is critically required for Golgi homeostasis in some cells. Importantly, this is a conditional requirement: only cells that express elevated levels of the enzyme UGDH, which produces UDPGA, have this detoxification requirement.

We demonstrate that this has a vital cancer therapy implication, as many types of cancers have elevated UGDH relative to normal cells. Only in these types of cancer cells, UXS1 disruption can result in aberrant Golgi morphology and glycosylation defects leading to death. The upregulation of UGDH in cancer cells may occur in some cancers from the selective advantage in drug clearance, as we show that the development of resistant subpopulations of cancer cells to xenobiotic, cancer cell-killing compounds is accompanied by elevated UGDH expression. This introduces a targetable liability in the form of a requirement for UDPGA detoxification via UXS1.

Our findings also reveal an unexpected link between a sugar nucleotide metabolic pathway and the modulation of signal transduction processes. We show that impairment of UXS1 and accumulation of UDPGA, by impairing the Golgi

maturation of cell-surface proteins such as growth factor receptors, acts to ‘silence’ a cancer cell so it cannot respond to extracellular cues. Thus, in addition to killing cancer cells outright via toxic UDPGA levels, we envision nuanced cancer therapy strategies using such mechanisms to ‘silence’ cancer cell activities such as hyperproliferation and metastasis. That deregulation of sugar nucleotide metabolism can subdue the sensitivity of cells to extracellular cues is a concept that may be broadly relevant to cell biology and in multiple health contexts beyond cancer therapy.

Materials and Methods

Materials

Details of all the chemicals, DNA constructs, guide sequences, antibodies, and other materials are provided in Supplementary Table S1. All requests for information, reagents, and resources should be directed to the Corresponding Author, Dohoon Kim (dohoon.kim@umassmed.edu)

Cell lines and cell culture

All cell lines were cultured at 37°C under 5% CO_2 and 20% O_2. The cell lines used in this paper are listed in Supplementary Table S2, along with information about their media, supplements, and sources. Most cancer lines used (except otherwise mentioned in Supplementary Table S2) were cultured in Dulbecco’s Modified Eagle

Medium (DMEM, Gibco #11995073) supplemented with 10% fetal bovine serum (Sigma #F2442), 100 units/ml Penicillin-Streptomycin (Gibco #15140122), and 2mM L-glutamine (Gibco #25030081).

Datamining analysis

A list of genes encoding metabolic enzymes and transporters (which we refer to as MetGene) was curated from the Kyoto Encyclopedia of Genes and Genomes (KEGG). First, we tried to identify which of the genes in MetGenes have differential essentiality, i.e., their CRISPR/Cas9 KO of that gene is lethal to some of the cancer cell lines but not to others. These genes were identified by mining a pan-cancer dependency dataset[234] (Post-Chronos_ Combined Achilles and Sanger SCORE Chronos data using Harmonia) from Broad Institute. The standard deviation (formula: $\sqrt{\{\Sigma(x-\bar{x})^2/(n-1)}$; where x: mean of essentiality of a gene across cell lines, n: the number of total cell lines) of the essentiality of each MetGene across the different cell lines from all solid cancer cell lines (572) from 25 different lineages were determined, high standard deviation values indicating high differential essentiality.

For each MetGene hit, we next set to identify genes whose mRNA expression level (transcript per million) predicts how essential the MetGene was in a given cell line. To this end, we determined Pearson Correlation values for all genes (17386) with a given MetGene across all 572 cells, cross-referencing gene essentiality values with RNAseq values from the CCLE{Barretina, 2012 #151} RNA sequence dataset.

Figure 1c shows the Pearson correlation between the dependency of UXS1 and the expression of all the genes in solid cancer lines.

CRISPR/Cas9-mediated genome editing

Guide RNA sequences were obtained from a published guide sequence library[273] and cloned into the lentiCRISPR v2 (pLCv2) construct[274]. Lentivirus was produced in HEK293T cells by co-transfecting plasmid pLentiCRISPR v2 containing guide sequence of interest with the Delta-Vpr packaging plasmids and VSV-G envelope plasmid using X-tremeGENE 9 transfection reagent (Roche). Lentivirus containing media was harvested 48 hours after transfection, and virus titer was determined. Target cells were infected with lentivirus in the presence of 10 ug/ml polybrene with a multiplicity of infection (MOI) less than 1 to avoid the non-specific toxicity of Cas9. Infected cells were selected with media containing puromycin (1-2 ug/ml) for 4-5 days to ensure a full selection of cells.

Cell viability assay

Cell viability was measured using CellTiter-Glo 2.0 (Promega) reagent according to manufacturer instructions for 96 well plates. The plates were read using the Synergy HT Multi-Detection Microplate Reader.

Relative viability measurements post CRISPR-Cas9 mediated gene KO

Cells were plated to 6-well plate and infected with lentiviruses containing CTRL (non-targeting guide) or guides containing the gene of interest. Infected cells were

selected with media containing puromycin (1-2 ug/ml) for 4 days. At 5 days post infection, fully selected cells were counted and plated to 96-well plates (each condition with 3-6 technical replicates). CTRL and KO cells (typically 500-1000 cells/well; depending on the growth rate of cell-line) were plated at equal seeding density to 96-well plates with media containing puromycin (0.5-1 ug/ml; to ensure selection pressure) for comparable baseline CTG values across conditions. To determine relative viability, CTG measurements were taken at two-time points. The baseline (first) time point was measured the day after cells were plated in 96 well plates, and the second time point was typically taken five days after baseline measurement. The fold changes in viable cells were calculated for each condition (day 5 CTG/ baseline CTG). These fold changes were then normalized to that of the same cells with non-targeting control guide (CTRL) to obtain relative viability following KO of our gene of interest (UXS1).

For double knock-out (DKO) experiments, cells were plated to 6-well plates and infected with lentiviruses containing pLCv2 CTRL or guides targeting either UGDH/SLC35D1 and selected with puromycin (1-2 ug/ml). Upon complete selection (5-6 days) the cells were infected with pMD154 lentivirus containing CTRL guides or guides targeting UXS1 to induce UXS1 KO. Cells were selected with hygromycin (500 ug/ml) for 5 days and double KO cells were plated to 96-well plates with media containing hygromycin (typically 500-1000 cells/well; depending on the growth rate of cell-line) in 6 technical replicates. To determine relative viability, CTG measurements were taken at two-time points. The baseline (first)

time point was measured the day after cells were plated in 96 well plates, and the second time point was typically taken five days after baseline measurement. The fold changes in viable cells were calculated for each condition (day 5 CTG/ baseline CTG). These fold changes were then normalized to that of the same cells with non-targeting control guide (CTRL).

CRISPR resistant UXS1 molecular cloning and rescue experiment

A CRISPR-resistant version of UXS1-g1 (CR UXS1) was designed by introducing three silent mutations: 1 mutation in the Protospacer Adjacent Motif (PAM) sequence and two mutations in the seed sequence (GCTCCTGGCCTCCAC**G**TC**T**GA**A**G). It was synthesized by GenScript with the addition of NotI and HPAI restriction sites. CR UXS1 was digested with NotI and HPAI and ligated into the expression vector pLV-EF1a-IRES-Blast. Lentiviruses were produced as described above, containing blank pLV vector or pLV-CR UXS1.

To confirm whether preventing targeting of UXS1 with UXS1-g1 rescues the toxic effect of UXS1 g1, we assessed the effect of UXS1 KO in cells expressing pLV-Blank or pLV-CR UXS1. We first transduced cells with lentivirus containing pLV-Blank or pLV-CR UXS1 and selected cells with blasticidin for six days. At seven days post first infection, we infected pLV-Blank and pLV-CR UXS1 cells with lentivirus containing pLCV2 CTRL (or UXS1-g1 or UXS1-g2) and selected cells with puromycin for five days. 6 days post-second infection, cells were counted and plated to 96 well plates at identical cell density (500 cells/well). We measured

baseline seeding density by performing a CTG measurement at day seven post-second infection. Subsequently, we measured viability 12 days post the second infection to determine relative cell growth over five days.

Cell cycle analysis

Cells were grown to sub-confluency. Cells were trypsinized, fixed in pre-chilled 70% ethanol in PBS, and stored at -20°C overnight. The following day cells were centrifuged and incubated with 50ug/ml of propidium iodide with 0.1 mg/ml RNAse A in PBS containing 0.05% TritonX-100 for 45 minutes. Cells were then centrifuged and resuspended in PBS and were analyzed on a Biorad ZE5 cell analyzer where at least 10,000 events were assessed. Data was collected with Everest software (version 2.0) and were analyzed for cell cycle distribution using a univariate model (Watson pragmatic) in FlowJo (v10.8.1).

Immunoblots

Cell lysates were harvested using RIPA buffer (Boston Bioproducts) with protease inhibitors (cOmplete, Roche) and phosphatase inhibitors (Cell signaling technology). Harvested proteins were denatured in 6x Laemmli buffer (Boston Bioproducts) and boiled at 90°C for 5 minutes. Samples were loaded at equal concentrations and analyzed by standard SDS-PAGE western blotting techniques. Protein levels were detected using HRP-conjugated secondary antibodies and chemiluminescent substrates (Pierce ECL or Pico PLUS), and exposed via

traditional film or Biorad ChemiDoc imaging system. We found that not boiling the samples before gel electrophoresis was necessary to detect UXS1 protein.

Cell death rescue experiments

Cells were infected with lentiviruses containing CTRL (non-targeting guide) or UXS1-g1 in 6 well format. Infected cells were selected with puromycin (2µg/ml) for three days. Four days post-infection, the selected cells were plated to two separate 96 well plates in 3 technical replicate wells at seeding density ~500 cells/well. Alternately, UXS1 iKO cells were induced with doxycycline treatment for 48 hours and 5 days after induction, cells were plated to two separate 96 well plates in 3 technical replicate wells at seeding density ~500 cells/well. Baseline CTG measurements were taken at 24 hours after seeding from one set of 96 well plates. Cells in other plates were either untreated or treated with Z-VAD-FMK or Necrostatin orFerrostatin-1 at indicated concentrations. Cell viability was then measured five days after drug treatment (day 9 post-infection/induction). Relative viability was then determined by calculating fold change in viability (day9/baseline CTG) for UXS1-g1 and CTRL.

Sulfated Glycosaminoglycan (sGAG) and Hyaluronic acid (HA) quantification

A549 cells were infected with lentiviruses (pLentiCRISPR V2-based) containing CTRL (non-targeting guide) or UGDH-g1 and selected using puromycin (2µg/ml). 6 days after selection these cells were infected with lentiviruses (pMD154 based) which express only the guides (CTRL, UXS1-g1, or UXS1-g2) two induce double

knock-out (as mentioned in methods above). These cells were selected with Hygromycin (500µg/ml) for 5 days. On day 6 $0.5X10^6$ cells were plated in 6 well plate for each condition in media without phenol red. Conditioned media (CM) were collected 48 hours after seeding the cells and cells plated in technical replicate plates were counted for each condition for normalization. CM samples were centrifuged at 1000xg to remove any cell debris.

For HA quantification, Supernatants were used for quantification using a Competitive-ELISA detection method (Biomatik, catalog# EKF57990) in which HAs in our sample competes for sites on the biotinylated detection antibody, along with the use of a standard to verify the results. Manufacturer protocols were followed.

For sGAG quantification, Cells were digested with papain using tissue digestion kit (AMSbio; catalog# 280560-TDK) to remove protein portion of the proteoglycans per manufacturer protocol. The digested samples were assayed for sGAGs using sulfated Glycosaminoglycan quantification kit (AMSbio; catalog# 280560-N), that uses 1, 9-dimethylmethylene blue (DMMB) dye that binds to sulfated glycosaminoglycans and the shift in absorption spectrum due to this binding can be measured at 520nm. Manufacturer protocol was followed. Chondroitin Sulfate (Bovine Trachea) was used as a standard.

Metabolomics: UDPGA quantification by LC-MS/MS

A549 cells were infected with lentiviruses containing either CTRL or UGDH-g1 or UXS1 g1in biological triplicates. Cells were selected with Puromycin for five days.

Cells at indicated time-points were washed thrice with ice-cold PBS and extracted on dry ice on 1ml 80% methanol containing 500nM internal standards (Metabolomics Amino Acid Mix Standard; Cambridge Isotope Laboratories). Cell extracts were collected using a cell scraper and transferred to a microcentrifuge tube. Samples were vortexed for 15 minutes at 4°C and centrifuged at 18000 x g for 10 minutes at 4°C. Supernatants were transferred to a new microcentrifuge tube and stored at -80°C until analysis. These samples were then dry evaporated using vacuum centrifugation. Polar metabolite profiling was performed on dried polar extracts at the Whitehead metabolite profiling core facility. It was performed on a QExactive orbitrap mass spectrometer equipped with an ion Max source and a HESI II probe coupled with a Dionex Ultimate 3000 HPLC system containing SeQuant® ZIC®- pHILIC analytical column. Relative quantitation of polar metabolites, including UDPGA, was performed with XCalibur QuanBrowser 2.2 and TraceFinder 4.1 (both Thermo Fischer Scientific) using a 5ppm mass tolerance and referencing an in-house library of chemical standards.

Transcriptomic analysis

A549 cells were infected in 6 well plates in biological triplicate (n=3) with lentivirus containing pLCV2 CTRL or UXS1-g1. Cells were selected for five days, and cell pellets were harvested seven days post-infection (timepoint was chosen such that UXS1 KO cells do not start undergoing a significant level of cell death). Total RNA was isolated using the Qiagen RNAeasy kit per manufacturer extraction protocol. BGI Americas Corporation performed sample quality control, cDNA library

preparation, and sequencing. The pair end sequencing was performed on the DNBseq platform (BGI Americas Corporation) with ~20 million reads per sample. The reads were aligned and mapped to the human genome and were normalized to the transcripts per million (TPM) for each sample.

The differentially expressed transcripts obtained through RNA-seq between control and UXS1 KO conditions were compared to curated gene sets from online pathway databases, publications in PubMed, and knowledge of domain experts using the GSEA tool. The results from GSEA are evaluated based on the Normalized enrichment score (NES). Since GSEA accounts for differences in gene set size and in correlations between gene sets and the expression dataset, the NES can be used to compare analysis results across gene sets.

Generation of doxycycline Inducible UXS1 KO system

To generate a doxycycline-inducible CRISPR/Cas9 mediated UXS1 knockout system, we cloned UXS1-g2 into TLCv2 plasmid[235] to prepare an all-in-one inducible system. U6 promoter in this plasmid drives constitutive expression of UXS1-g2, and the addition of doxycycline induces Cas9-2A-eGFP. A549 cells were infected with lentiviruses containing the plasmid mentioned above, and the cells were selected with Puromycin (2 ug/ml) for five days. The selected cells were then diluted to 0.3 cells per 150µl for single-cell sorting and plated in 96 well plates (150µl/well). Total twelve clones were screened for eGFP expression and loss of UXS1 by immunoblotting, and TLCv2 “Clone 6” (referred to as UXS1 iKO)

displayed homogeneous eGFP expression along with UXS1 loss upon doxycycline induction and was hence selected for future experiments. Similarly, H460 and HT1080 cells were infected with the lentiviruses containing the plasmid mentioned above, and single cell clones were isolated that displayed homogeneous eGFP expression along with UXS1 loss upon doxycycline induction. These are referred as ‘H460 UXS1 iKO’ and ‘HT1080 UXS1 iKO’ respectively.

Doxycycline treatment

Doxycycline was prepared as a 100mg/ml stock solution, and aliquots were stored at -80°C. Cells were treated with 100ng/ml doxycycline in DMEM with 10% FBS (regular growth media) for 48 hours. Cells were changed into fresh media after 48 hours of doxycycline induction.

[U-^{13}C]-glucose labeling experiments

A549 cells were transduced with lentivirus containing pLCv2 UGDH-g1. Cells were completely selected with Puromycin for 5 days, were changed into fresh media and seeded for the experiment in 10cm dishes at 70% confluency. UXS1 iKO and control iKO cells were induced with doxycycline (100ng/ml) in separate 10cm dishes. Cells were changed into fresh media after 48 hours. 5 days post induction, cells were seeded for the experiment in 10cm dishes at 70% confluency. For regular media 4.5g/ L glucose (C# G8270, Sigma) was added in glucose-free DMEM (C# 11966025, ThermoFisher) supplemented with 10% FBS, 1% P/S, 1mM Pyruvate. Labeling media was identical except using [U-^{13}C] Glucose (CLM-1396,

Cambridge Isotope Laboratories) in place of glucose. 1 day after seeding, the cells were changed into fresh regular media. 2 hours after the regular media change, the cells were changed into labeling media containing [U-^{13}C] Glucose and the metabolites were isolated from the cells at indicated timepoints.

To isolate metabolites, medium was removed, cells were washed 2 times with ice cold 1X PBS, and plates were covered in a total of 3ml of LC-MS grade 80:20 methanol:Water. Plates were scraped on dry ice and lysates were collected into 15ml conical tubes. Lysates were vortexed for 10 minutes at 4℃ and centrifuged at 16,000 x g for 10 minutes at 4℃. Supernatants were dried down in a benchtop Vacuum Concentrator. Dried pellets were stored at -80℃ until they were run on LC-MS.

A QExactive Plus quadrupole orbitrap mass spectrometer (Thermo Fisher Scientific) equipped with an Ion Max source and a HESI II probe coupled to a Vanquish Horizon UHPLC System (Thermo Fisher Scientific) was used to perform LC-MS experiments. Prior to operation, the instrument underwent mass calibration for positive and negative ion mode using Calmix (Thermo Fisher Scientific) every 7 days. Dried samples were re-suspended in 200 uL of HPLC water and 2 uL of re-suspended polar metabolite samples were injected into a SeQuant ZIC-pHILIC 5µm 150 x 2.1 mm analytical column equipped with a 2.1 x 20 mm guard column (MilliporeSigma). The column oven was held at 25°C and the autosampler tray was held at 4°C. Buffer A was comprised of 20 mM ammonium carbonate, 0.1% ammonium hydroxide. Buffer B was comprised of 100% acetonitrile. The

chromatographic gradient was run at a flow rate of 0.150 mL/min as follows: 0-20 min: linear gradient from 80-20% B; 20-20.5 min: linear gradient from 20-80% B; 20.5- 28 min: hold at 80% B. The mass spectrometer was operated in full-scan, polarity switching mode, and targeted selected ion monitoring (tSIM), negative mode, for UDP-xylose (m/z: 535.0371) and 13C5-UDP-xylose (m/z: 540.0539). The spray voltage set to 4.0 kV, the heated capillary at 350°C, and the HESI probe at 350°C. The sheath gas flow was 10 units, the auxiliary gas flow was 2 units, and the sweep gas flow was 1 unit. MS data was collected in a range of m/z = 55–825. The resolution was set at 70,000, the AGC target at 1x106, and the maximum injection time at 20 msec. Rate of production of UDPGA and UDP-xylose (Fig.2 c, e and k) is quantified based on respective standard curves and depicted in picomoles per million cells.

Immunocytochemistry

Cells were plated on poly-D-lysine (PDL) coated coverslips kept in 12-well tissue culture plates. On day seven post lentiviral infection, the coverslips were rinsed once with PBS and fixed with 4% paraformaldehyde in PBS for 15 minutes at room temperature. The coverslips were then rinsed three times with PBS, and the cells were permeabilized with 0.2% TritonX-100 v/v in PBS for 15 mins at room temperature. Coverslips were washed three times and blocked in 4% horse serum for 1 hour at room temperature. The coverslips were incubated in the primary antibody at 4°C overnight, rinsed three times with PBS, and then incubated with secondary antibody for 45 minutes at room temperature in the dark along with

Phalloidin-iFluor488 (Abcam). Coverslips were then washed three times with PBS and mounted on the slides using ProLong Gold Antifade mountant containing DAPI. Images were acquired on the Nikon Eclipse Ti2 confocal microscope. Raw images were opened in ImageJ and processed similarly for all experimental conditions. Golgi area measurement was carried out using ImageJ (1.53q). Identical thresholding was performed on the golgi-stained images. Stained Golgi pixel area per cell was calculated using ‘measure’ function in imageJ.

Transmission Electron Microscopy (TEM)

Cell cultures of A549 control and UXS1 KO (day7 post infection) in plates were processed and analyzed at the University of Massachusetts Medical School Electron Microscopy core facility according to standard procedures. Samples were fixed by adding equal volume 2.5% glutaraldehyde/1.6% paraformaldehyde in 0.1 M Sodium Cacodylate buffer pH 7. to the culture plates after half the media was removed. The cell cultures were allowed to stabilize in this solution for 10 min, then all the media/glutaraldehyde was removed and fresh 2.5% glutaraldehyde/1.6% paraformaldehyde in the same buffer was added and the cells were allowed to fix for 60 min. at room temperature. After this primary fixation, the cells were rinsed three times in fresh fixation buffer for 10 min. each time and were secondarily fix with 1.0% osmium tetroxide in ddH2O for 1hr at room temperature. The cell cultures were then washed again three times in ddH2O and then scraped into pellets. The cells were dehydrated through a graded series of ethanol (10% to 100%; 3 changes). Samples were then infiltrated first with two

changes of 100% Propylene Oxide and then with a 50%/50% propylene oxide / SPI-Pon 812 resin mixture. The following day five changes of fresh 100% SPI-Pon 812 resin were performed before the samples were polymerized at 68℃ in embedding molds. The samples were then trimmed for TEM. 70nm thin sections were placed on gold support grids and contrasted with Lead citrate and Uranyl acetate. Sections were examined using the CM10 with 80Kv accelerating voltage and images were captured using a Gatan TEM CCD camera.

Subcellular Fractionation

Cells cultured in 10 cm plates were harvested at 80% confluency. Cells were trypsinized and washed with ice cold PBS twice. 2x106 cells were resuspended in 400µl of ice cold digitonin buffer (150mM NaCl, 50mM HEPES pH 7.4, 50µg/ml digitonin (Sigma)) containing protease inhibitors at room temperature for 10 mins. This has been shown to disrupt plasma membrane via cholesterol interaction, while preserving organellar membrane integrity, allowing organellar metabolite measurements[275,276]. The cells were then centrifuged at 2000xg to pellet the cells. The supernatant was collected as the ‘cytosolic’ fraction. 400µl of RIPA buffer containing protease inhibitors were added to the cell pellet and was incubated at 4℃ for 10 mins to disrupt organellar membranes. This was then subjected to centrifugation at 7000xg for 10 mins and the supernatant was collected as the ‘organellar’ fraction. 200µl of each of the ‘cytosolic’ and ‘organellar’ fraction was saved for running immunoblots and 800µl of methanol (Millipore Sigma) was added

to the rest of 200µl fractions to extract the metabolites. Metabolite samples were stored at -80℃ until analysis.

Quantification of UDPGA using GC-MS

600 µl of cell extracts were dried in a vacuum evaporator (Thermo SPD111V). Dry residues were derivatized using 50 µl of N-methyl-N-(trimethylsilyl) trifluoroacetamide (MilliporeSigma) and 20 µl of pyridine (MilliporeSigma) for 3 hours at 37℃ and allowed to complete at room temperature for another 5 hours. Split mode with 1:5 ratio was used to inject 1 µl of the sample into the Agilent 5977B gas-chromatograph interfaced with an Agilent 7890B mass selective detector. The capillary column was Agilent HP-5MS UI (30 m × 0.25 mm internal diameter × 0.25 µm film thickness). Helium was supplied as a carrier gas at a constant flow of 1 ml/min. The oven temperature conditions were as follows: started at 80 ℃, held for 1 min, increased at 7 ℃/min to 285 ℃. The inlet, ion source and transfer line were heated to 230, 280 and 250 ℃, respectively. The mass detector performed 3 scans per second in the range from 30 to 500 m/z, electron impact ionization energy 70 eV. UDPGA was detected as three fragments matching the spectra and retention time of the reference compound. Corresponding peaks eluted at 17, 24.5 and 25.8 minutes and were quantified using ions m/z 217, 217 and 299, respectively. The most abundant among the three correlated ions/fragments (m/z 299 at minutes 25.8) was used for quantification. Peak integration and

quantification of peak areas were done using MassHunter software (Agilent v.10.1).

N-glycan and O-glycan profiling and composition analysis

For glycan profiling and composition analyses, protein extracts (120 µg) were lyophilized, reduced in a 25 mM dithiothreitol solution (Sigma-Aldrich, St. Louis, MO) at 50 °C for 90 min, and then alkylated with a 65 mM iodoacetamide solution for 90 min at room temperature in the dark. Samples were dialyzed against 50 mM ammonium bicarbonate for 24 hours at 4°C, lyophilized, and incubated with 1 mL of 50 µg/mL TPCK-treated trypsin (Sigma-Aldrich) at 37°C overnight. The digested peptides were then purified using a Sep-Pak C18 (200-mg) cartridge (Waters Corp., Milford, MA), lyophilized, and incubated with 2 µL (500 units/µL) of PNGase-F (New England Biolabs, Ipswich, MA) in 200 µL of 50 mM ammonium bicarbonate at 37°C for 4 hours. The mixture was further incubated with 3 µL of PNGase-F at 37°C overnight. O-glycans were released from O-glycopeptides by reductive β-elimination, 1 M NaOH with 50 mM $NaBH_4$ held at 50°C for 18 hours. The released N-glycans and O-glycans were purified over a Sep-Pak C18 (200-mg) cartridge. The flow-through and wash fraction containing the released glycans were collected, pooled, and lyophilized.

Purified glycans were then permethylated by incubation with 1 mL of a NaOH: dimethyl sulfoxide slurry solution and 500 µL of methyl iodide (Sigma-Aldrich) for 30 min with vigorous shaking. One mL of chloroform and 3 mL of Milli-Q water were

then added, and the mixture was briefly vortexed to wash the chloroform fraction. The wash step was repeated three times. The chloroform fraction was dried, dissolved in 200 mL of 50% methanol, and loaded into a Sep-Pak C18 (200-mg) cartridge. The eluted fraction was lyophilized and dissolved in 10 µL of 75% methanol from which 1 µL was mixed with 1 µL 2,5-dihydroxybenzoic acid (Sigma-Aldrich; 5 mg/mL in 50% acetonitrile with 0.1% trifluoroacetic acid) and spotted on a matrix-assisted laser desorption/ionization polished steel target plate (Bruker Daltonics, Bremen, Germany).

Mass spectrometry data were acquired on an UltraFlextreme matrix-assisted laser desorption/ionization–time-of-flight mass spectrometer (Bruker Daltonics). Reflective, positive mode was used, and data was recorded between m/z 500 and 6000. The mass spectrometry glycan profiles were acquired by aggregating at least 10,000 laser shots. Mass peaks were manually annotated and assigned to a particular N and O-glycan composition when a match was found.

EGF stimulation of UXS1 iKO cells

UXS1 iKO and control iKO cells were induced with doxycycline (100ng/ml) in separate wells of 6 well plates. Cells were changed into fresh media after 48 hours. 6 days post induction, cells were serum starved overnight using DMEM media without serum. The next day cells were stimulated with 100ng/ml of EGF, and protein lysates were harvested 5min, 10min, 15 min, and 30min after EGF stimulation. As a negative control, UXS1 and control iKO cells were also pre-

treated with 5μM Erlotinib for 30 mins and harvested 5 mins after EGF stimulation. Harvested proteins were denatured in 6x Laemmli buffer (Boston Bioproducts) and boiled at 90°C for 5 minutes. Samples were loaded at equal concentrations and analyzed by standard SDS-PAGE western blotting techniques as described before in this section.

EGFR surface quantitation

The evaluation of EGFR surface expression on UXS1 iKO cells was performed by flow cytometry. Cells were washed with ice cold FACS buffer (10% FBS, 0.1% NaN3 in PBS). $1x10^6$ cells were incubated with 10μl of Human EGFR Fluorescein-conjugated Antibody (R&D systems) in dark for 30 minutes at room temperature. Cells were then centrifuged (300xg) and washed three times with ice-cold FACS buffer to remove any unbound antibody. Cells were resuspended in 400ul of FACS buffer and immediately analyzed on a Biorad ZE5 cell analyzer where at least 10,000 events were assessed and plotted using FlowJo (v10.8.1).

Inducible UXS1 KO Xenograft models

The research project has been reviewed by the institutional Animal Care and Use Committee (IACUC) at the University of Massachusetts Medical School and complied with all ethical regulations. To establish inducible UXS1 KO xenograft models, 2.5 X 10^6 A549 UXS1 iKO or H460 UXS1 iKO or HT1080 UXS1 iKO cells were injected subcutaneously into the right flank of female athymic nude mice in a total of 100ul of PBS at six weeks of age. In each of the three experiments, tumors

were allowed to grow until the mean tumor volume of each group was 200-250mm^3(A549: 14 days, H460: 11 days, HT1080: 7 days), upon which point mice were divided into two groups in a manner that each group had comparable average tumor volumes, and dox induction started in one of the groups via doxycycline chow (TD.01306) to induce Cas9 expression for UXS1 KO. There were 12 animals for every condition except one animal was excluded from the study due to no visible tumor in A549 xenograft experiment.

The A549 xenograft experiment had total four arms. 1. Control 2. Cisplatin 3. UXS1 KO 4. UXS1 KO+ Cisplatin. The UXS1 KO arms (3 and 4) were put on Doxycycline containing diet as described and the first two arms were continued on regular control diet (Prolab® 5P76) upon randomization. The cisplatin arms (2 and 4) were administered 4 mg/kg cisplatin via intravenous (i.v.) tail vein injections once a week for a total of three weeks, first injection being on same day as the dox induction (14 days). H460 and HT1080 xenograft experiments had two arms each. Similarly, UXS1 KO arm were put on Doxycycline containing diet (TD.01306) and the control arm were continued on regular control diet (Prolab® 5P76).

Tumors were measured every 2-3 days using a vernier caliper and the tumor volume was calculated using the formula 4/3π X (length x width x depth)/2. Mice were monitored regularly for appearance and body weight throughout the experiment. The endpoint for survival data calculation was set to the tumor size of 2000mm^3 and mice were euthanized as soon as possible upon reaching the limits

as defined in our IACUC protocol. Upon reaching the endpoint, animals were euthanized, and the tumors were isolated, and snap-frozen for further analysis.

Processing of human breast and lung tissues for UGDH protein quantification

All human breast and lung normal and cancer tissues were obtained from de-identified patients with informed consent from the University of Massachusetts Medical School Biorepository and Tissue bank using procedures conducted under an Institutional Review Board (IRB) approved protocol. All tissue samples were snap-frozen in liquid nitrogen immediately after surgical removal and stored at -80°C. The frozen tissues were homogenized in RIPA buffer (Boston Bioproducts) containing protease inhibitors (cOmplete, Roche) and phosphatase inhibitors (Cell signaling technology). Supernatants containing proteins were collected after centrifugation at 13000 x g at 4°C for 10 minutes. Protein samples were normalized using the Pierce BCA assay kit (Thermofisher Scientific). Samples were analyzed by standard SDS-PAGE western blotting techniques. Protein levels were detected using HRP-conjugated secondary antibodies and chemiluminescent substrates (Pierce ECL or Pico PLUS).

Induction of chemo-resistance in H2170 and MDAMB231 cells

Resistant versions of the H2170 and MDAMB231 cell lines were derived from parental cells by continuous exposure to increasing concentrations of the chemo-drugs. H2170 cells were exposed to (Gemcitabine, starting dose: 4nM end dose:

12μM; SN38, start dose: 5nM end dose: 10nM; Paclitaxel, starting dose: 0.004nM end dose: 0.012nM; Mitomycin C, starting dose: 30nM end dose: 60nM; Cisplatin starting dose: 360nM end dose 600nM) and MDAMB231 cells were exposed to (Cisplatin, starting dose: 1.5μM end dose: 3μM ;Paclitaxel, starting dose: 0.1nM end dose: 0.4nM). Dose-response studies of chemotherapeutics were carried out over 72 hours to assess IC50 values. H2170 and MDAMB231 cells were grown in chemo-drugs for 2 and 3 months respectively. IC50 concentrations were reassessed in each cell line. CRISPR/Cas9 KO experiments using these lines were performed in the absence of chemotherapeutics.

Patient derived Organoids

Deidentified tumor tissues of freshly resected biopsies from patients with TNBC were obtained from UMass Cancer Center Tumor Bank. These tumors were digested using gentleMACS Dissociator and tumor dissociation kit (Miltenyi Biotech). The digested tumors were washed using 1x phosphate-buffered saline, and partially digested tumor pieces were embedded into reduced growth factor basement membrane extract (BME) (R&D systems). For passaging, the organoids were dissociated using TrypLE™ Express Enzyme (Gibco) and cultured in organoid media. The organoid media is described here[277]. The drug-resistant organoids were derived from parental organoids by culturing them in cisplatin (starting dose 10nM, final dose 1uM) for 4 weeks.

Lentiviral infection in Organoids

The organoids were dissociated from the plate by adding TrypLE™ Express and disrupting the BME droplets with P1000 pipette. They were incubated in TrypLE™ Express at 37℃ for 15 mins. After dissociation cells were centrifuged at 350xg at room temperature for 5 mins and resuspended in 1ml of organoid media. After counting, equal numbers of cells were distributed in separate eppendorf tubes and centrifuged at 300xg to collect cell pellets. 250ul of pre-titered lentiviral supernatants were added to each condition to ensure equal transduced units/ml along with 1µl of polybrene (2.5µg/ml). These cell/lentivirus mixes were transferred to separate wells of ultra-low attachment 48 well plates (Sciencell). The cells were spin-infected by centrifuging at 600xg at room temperature for 60 mins. The cells were then incubated for 6 hours in cell culture incubator at 37℃. They were transferred to eppendorf tubes and centrifuged (350xg) at room temperature for 5 mins. Supernatants were discarded and the cells were re-suspended in BME (R&D systems). Infected organoid cells were then seeded in BME droplets in 48 well plates. Infected cells were selected with Puromycin (0.5µg/ml) 24 hours after seeding into BME droplets. Cell viability was measured seven days post infection using CellTiter-Glo® 3D (Promega) reagent according to manufacturer instructions.

RNA interference mediated knock-down (KD) of UXS1

We obtained TRC lentiviruses for UXS1 shRNAs from Umass Chan Medical school RNAi core. A549 cells were transduced in 6-well plates with the TRC lentiviruses for either shGFP, shEmpty_vector or shUXS1 in the presence of 10 ug/ml

polybrene with a multiplicity of infection (MOI) less than 1. Infected cells were selected with media containing puromycin (2 ug/ml) for 4 days. Upon complete selection, the cells were plated to 96-well plates. To determine relative viability, CTG measurements were taken at two time points. The baseline (first) time point was measured the day after cells were plated in 96 well plates, and the second time point was taken five days after baseline measurement. The fold changes in viable cells were calculated for each condition (day 5 CTG/ baseline CTG). These fold changes were then normalized to that of the same cells with shGFP to obtain relative viability following KD of our gene of interest (UXS1).

Statistics and Reproducibility

For all experiments showing relative viability; each condition was measured in at least three technical replicates within each experiment, and each datapoints shown (each n) is from an independent experiment (e.g. n=3 indicates 3 independent experiments). Unless otherwise indicated, each experiment was repeated at least three times (represented by individual points in graphs). LC-MS metabolites quantitation, labeling experiments, transcriptomic analysis, FACS analysis were performed in biological triplicates, and n=3 would indicate 3 biological replicates. Technical replicates are never represented as n's. Data are presented as mean ± standard deviation. Statistics were calculated using a two-tailed Student's t-test. $P<0.05$ was considered statically significant, and data marked with statical significance as follows: *$p<0.05$, **$p<0.01$, ***$p<0.001$, ****$p<0.0001$, NS: not

significant (unless otherwise mentioned). Statistics and graphs were prepared using Microsoft Excel and Graphpad Prism.

Bliss independence values (Fig 4n) were calculated using standard formula of Ec = Ea + Eb - Ea × Eb. A bliss independence score that equals 1.0 indicates additive effect, greater than 1.0 indicates antagonistic effect, and less than 1.0 indicates a synergistic effect.

Acknowledgments

We would like to thank Melanie Walker, Richard Cummings, Chao Gao, Keith Reddig, and Michael Pacold for expert advice, helpful discussion, and other assistance. We thank David Sabatini, Scot Wolfe, Wen Xue, Michael Green, and Michael Lee for materials, including vectors and cell lines. This work was supported by the Suh Kyungbae Foundation (SUHF) Young Investigator Award and National Institutes of Health (NIH) grant R01CA269711 to D.K.; Mogam Fellowship to N.L. The electron microscopy work was supported by Award Numbers S10OD025113-01, and S10OD021580, from the National Center For Research Resources. O.P. and A.J.M.W. were supported by the NIH grants GM122502 and DK068429. C.J. was funded by Edward Mallinckrodt, Jr. Foundation Award and NIH grant R01AA029124. H.L.G. was supported by NIH grant R50CA221780 and A.M.M. by National Institutes of Health grant R01CA218805. J.B.S. was funded by the Worcester Foundation Grant and the Smith Family Foundation Grant.

Data Availability Statement

The transcriptomic data included in this study has been deposited to GEO (accession number: GSE240344). Source data for all figures are provided in the online version of the manuscript. Uncropped westerns are provided in the Supplementary section. Additional raw data and materials that support the findings of the study are available from the corresponding author upon request.

Competing interests

M.B.D. and D.K. are listed as authors on a patent application filed by the University of Massachusetts Chan Medical School on targeting UXS1 in cancer therapy. All other authors declare no competing interests.

CHAPTER III:

DISCUSSION

Summary of major findings of the thesis

This study uncovers a targetable metabolic vulnerability within the sugar nucleotide pathway. We found an inherently toxic endogenous metabolite, UDPGA, necessitating the need for detoxification. This dependence on UXS1, the UDPGA processing enzyme, is observed in cancer cells that upregulate the enzyme UGDH, responsible for producing the toxic metabolite. Elimination of UDPGA from cells is essential for preserving Golgi structure and function. Notably, UXS1 can be targeted, leading to the accumulation of UDPGA, specifically in cancer cells that upregulate the sugar nucleotide pathway via UGDH, thereby offering a potential biomarker for patient selection. Additionally, this approach holds promise in targeting chemo-resistant cells, making them more susceptible to UXS1-based cancer therapy.

Through our endeavors to identify endogenous toxic metabolites and their associated detoxifying enzymes within the human metabolome, we have observed that cancer cell lines with elevated UGDH expression exhibit an increased dependence on UXS1 for their viability. This dependence is particularly pronounced in lung cancer cell lines, which have a tendency of high UGDH expression. Furthermore, our investigations have revealed that the depletion of UXS1 results in cell cycle aberrations, characterized by an increased percentage of cells arrested in the 'S' phase, ultimately culminating in apoptosis. We discovered that disrupting UXS1 in cell lines leads to increased activity of UGDH, resulting in a significant time-dependent accumulation of UDPGA. Importantly, we

demonstrate the complete rescue of the toxicity associated with UXS1 loss by reducing intracellular UDPGA levels through two distinct strategies: firstly, by treating cells with 4-methylumbelliferone (4MU), a known drug that reduces intracellular UDPGA by forming 4MU-glucuronides; and secondly, by preemptively knocking out UGDH, thereby halting UDPGA production before UXS1 disruption. This indicates that the toxicity from UXS1 loss is induced by excess of UDPGA, and not due to the lack of UDP-xylose, the product of UXS1 that functions as a glycosylation precursor used in glycosaminoglycans. Additionally, the observed increase in UDPGA accumulation and toxicity due to UXS1 loss both displayed a correlation with the expression levels of UGDH within the cells. Consequently, all the aforementioned findings collectively indicate a toxic gain of function resulting from the loss of UXS1, due to accumulation of UDPGA.

Moreover, our study offers novel insights into the intrinsic toxicity of UDPGA. Transcriptomic profiling unveiled the upregulation of Golgi-related pathways, including protein trafficking, glycosylation, and glycosaminoglycan metabolism upon loss of UXS1. This result suggests that UXS1 ablation induces Golgi stress, which is supported by the observed accumulation of ADP-Ribosylation Factor 4 (ARF4), a Golgi stress induced protein. We observed that the buildup of UDPGA leads to the dispersion of the Golgi apparatus. We found further evidence for Golgi abnormalities such as causing aberrant protein glycosylation and the improper trafficking of vital glycoproteins in cancer cells (Figure 3.1). As an example of an altered glycoprotein, we illustrate how the incorrect maturation and trafficking of

EGFR results in reduced signaling through EGFR. Disrupted Golgi function may lead to the widespread deregulation of cell surface glycoproteins, which play a pivotal role in the signaling processes within mammalian cells.

We recapitulated the correlation between elevated UGDH expression and UXS1 dependency *in vivo* via subcutaneous xenograft models of lung adenocarcinoma. We demonstrate that we could leverage the elevated UGDH expression in several cancer subtypes, which exhibit significantly higher UGDH levels compared to normal tissues, as a biomarker for UXS1 targeting. Our findings in patient-derived organoid (PDO) models confirm the notion that chemotherapy treatment induces UGDH expression. Furthermore, our *in vivo* experiments substantiate that UXS1 knockout synergizes with chemotherapy treatments that induce UGDH expression. In all, our findings explore the therapeutic potential of UXS1 to target cancer and provide a means to exploit sugar nucleotide metabolism.

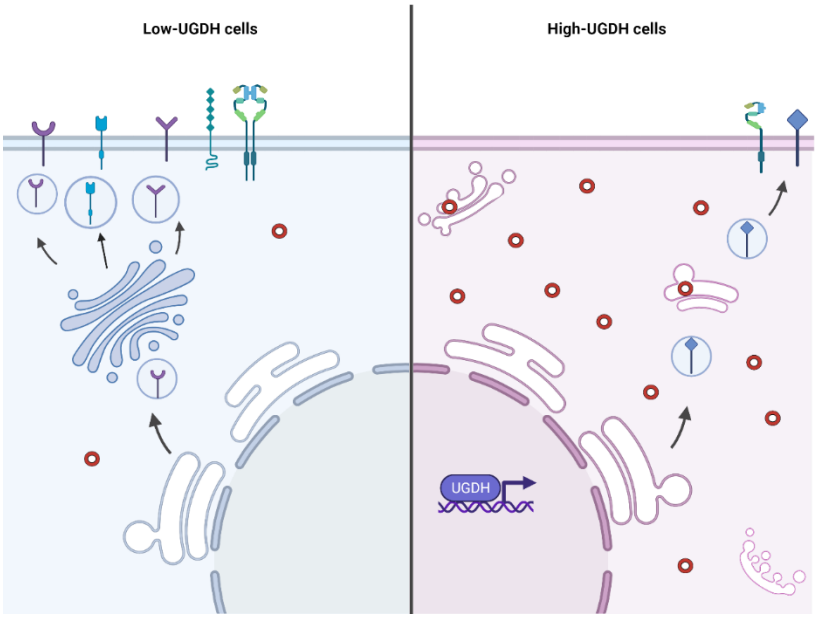

Figure 3.1: A model depicting UDPGA toxicity in UGDH-high cells following UXS1 KO. In cells with elevated UGDH levels, UXS1 KO leads to an excess of UDPGA, resulting in dysfunction of Golgi structure and function. This figure is made using biorender.

UGDH-UXS1 forms a kitchen sink model

Over the last few years, our laboratory has established a novel approach to targeting cancer metabolism by inducing toxic accumulation of naturally occurring toxic metabolites. We have observed that many toxic metabolites present within the linear metabolic pathway follow a 'kitchen-sink' model (as discussed in Chapter I). Briefly, in this model, upstream metabolic enzymes function as a faucet, while detoxifying enzymes, responsible for converting the potentially toxic byproducts of

the faucet enzyme, serve as a drain, preventing the overflow of the system (Figure 1.1). Our laboratory has elucidated several instances of reprogrammed metabolic pathways in cancer cells, which involve endogenous toxic metabolites and follow "kitchen-sink" dynamics. The detoxifying enzymes within these pathways emerge as promising candidates for cancer therapy. GLDC, which plays a role in clearing mitochondrial glycine, SEPHS2, responsible for selenide clearance, and KDSR, involved in clearing 3KDS from cells, are examples of detoxifying enzymes that have emerged as promising targets for cancer therapy.

Our objective was to systematically identify additional instances of toxic metabolites and explore their potential for selectively targeting cancer cells. The Broad Institute has released a wealth of omics data in recent years, including a dependency dataset that assigns a score to each gene based on its importance in specific cell lines for its survival, spanning several hundred cell lines. We utilized the dependency dataset to identify metabolic genes that exhibit the highest variability in their dependency scores across different cell lines. This approach was informed by our knowledge that detoxifying enzymes tend to be selectively dependent, showing greater dependence in cell lines where genes responsible for producing the toxic metabolite are overexpressed or upregulated. In this process, we identified a selectively dependent enzyme, UXS1. When we correlated the dependency scores of UXS1 with the expression of all the genes in the genome across hundreds of cancer cell lines, UGDH, a direct upstream enzyme, scored as the top hit with the lowest negative correlation (Figure 2.1d). This finding suggested

that UXS1 plays a crucial role in detoxifying the product of UGDH. We find that UXS1 is indeed required in clearing UDPGA from the cells that express high levels of UGDH, thus following the ‘kitchen-sink’ mechanics.

The abovementioned relationship between UGDH-UXS1 is tissue lineage-independent. As demonstrated, cancer cell lines with high UGDH levels from several different lineages are dependent on UXS1 (Figure 2.2a). Moreover, cell lines insensitive to UXS1 KO toxicity can be sensitized by overexpressing UGDH (Figure 2.7). Additionally, we observed that UXS1 dependence can be more accurately associated with UGDH protein expression even more so than its mRNA expression. For instance, despite having higher UGDH mRNA levels in the expression dataset, H2170 cells exhibited only mild dependence on UXS1 due to their lower UGDH protein levels (Figure 2.2a, 2.23d). Thus, overall, our study indicates that UGDH protein expression can be utilized as a biomarker for the UXS1-based therapy.

Implications of proteoglycan alterations downstream of UGDH or UXS1

The sequential products of UGDH and UXS1 are the sugar nucleotides UDP-glucuronic acid and UDP-xylose (Figure 2.1f). These act as glucuronic acid and xylose sugar donors in glycosylation. Both glucuronic acid and xylose units are required components in sulfated glycosaminoglycans, negatively charged

polysaccharides that are attached to core proteins to form secreted proteoglycans forming extracellular material such as in connective tissue or one of several transmembrane surface proteoglycans[240,241,278]. Meanwhile, glucuronic acid but not xylose units are required to produce hyaluronic acid, the predominant species of non-sulfated glycosaminoglycans, which is a key component of biological lubricant and structural fluids (e.g., synovial fluid) (31294035).

We observed that UGDH KO or UGDH/UXS1 double KO, but not UXS1 KO, resulted in a significant decrease in total hyaluronic acid levels (Figure 2.8c, d). This is consistent with glucuronic acid (but not xylose) being required in hyaluronic acids. As UXS1 KO does not decrease HA species, this argues against the loss of HA, contributing to the toxicity of UXS1 loss.

Meanwhile, UGDH KO, UXS1 KO, or double UGDH/UXS1 KO all result in a significant drop in total sulfated proteoglycans in A549 cells (with an insignificant trend for loss in DLD1). This is consistent with their downstream product, UDP-xylose, being a component of sulfated glycosaminoglycans (Figure 2.8a, b). UXS1 KO is toxic, while UGDH or UGDH/UXS1 double KO is not (Figure 2.5b-e); the fact that all three of these lower proteoglycans to similar extents but only UXS1 KO is toxic supports that loss of sulfated glycosaminoglycans does not contribute to the toxicity of UXS1.

The fact that UXS1 KO toxicity is rescued by conditions that remove UDPGA - preemptive KO of UGDH or clearing UDPGA via 4MU– further supports that the

upstream UDPGA accumulation rather than downstream impacts in proteoglycans cause the acute toxicity of UXS1 loss.

It is important to note that our results do not rule out the possibility that the effects on proteoglycans resulting from UGDH or UXS1 loss could impact other aspects of the cancer cell aside from viability. Proteoglycans, either as secreted components or as cell surface proteins, are involved in both structural and signaling mechanisms and can play important roles in diverse processes such as cell adhesion, migration, and differentiation[240,279]. As such, they may play various roles in cancer and tumor progression, such as in invasion, migration, chemoresistance, epithelial-mesenchymal transition, and stemness[241,242,280]. Indeed, it was recently shown that targeting UGDH can decrease cancer cell migration and metastasis, and epithelial-mesenchymal transition[261,262]. Thus, future investigations should investigate the additional impacts of targeting UXS1 in such cancer properties, which may involve its impacts on proteoglycans.

The UDP-xylose and UGDH feedback mechanism

An interesting consideration is that xylose units are relatively rare compared to other units, such as glucuronic acid, and are required in small amounts in some sulfated glycosaminoglycans but not present in most glycosylated proteins[52]. Thus, it appears that UXS1 is not needed for a high rate of conversion of UDPGA to UDP-xylose, raising the possibility that some proteoglycans could act as a sink for

excess UDPGA not converted to UDP-xylose. However, we do not see any increases in hyaluronic acid or sulfated proteoglycans, arguing against this possibility.

An important detail in the relationship between UGDH and UXS1 is that normally, the UDP-xylose produced by UXS1 appears to limit the activity of UGDH in a negative feedback loop. It was shown that UDP-xylose is an allosteric feedback inhibitor of UGDH in various species ranging from plants to humans[243,244,281]. Supporting the presence of a negative feedback loop, UXS1 KO, which eliminates UDP-xylose production, results in substantially increased production of UDPGA (Figure 2.4a), more than can be accounted for by the loss of UDPGA clearance from UXS1 (Figure 2.9a). UXS1 KO is in effect, blocking the 'drain' for UDPGA removal, but at the same time, amplifying the 'faucet' (UGDH activity). This adds an important detail to the UGDH/UXS1 kitchen sink relationship that explains how such a massive accumulation can occur when only moderately active enzyme is lost (Fig. 2.9g).

UDPGA accumulation and cell death

Glucose serves as the primary precursor for the biosynthesis of various sugar nucleotides, including UDP-glucuronic acid (UDPGA). The conversion of glucose to UDP-glucose involves four consecutive enzymatic reactions, catalyzed

by three key enzymes: hexokinase (HK), phosphoglucomutase (PGM), and UDP-glucose phosphorylase (UGP2)[282]. Subsequently, UDP-glucose dehydrogenase facilitates the NAD+-dependent oxidation of UDP-glucose, yielding UDPGA. All the above mentioned reactions take place within the cytoplasm[58].

UDPGA generated can be employed within the cytoplasm for the synthesis of hyaluronic acid or transported to various organelles, including the ER and Golgi apparatus. In the ER, UDPGA serves as a substrate for UDP-glucuronosyltransferases (UGTs), participating in glucuronidation processes. Inside the Golgi apparatus, UDPGA undergoes conversion into UDP-Xyl by the enzyme UXS1. UDP-Xyl is then transported back to the cytoplasm, where it exerts feedback inhibition on cytoplasmic UGDH, limiting its activity and restricting further UDPGA production[52].

One of the key questions we sought to address was the intracellular localization of UDPGA accumulation. Our study involved digitonin-based subcellular fractionation experiments that allow for subsequent metabolic measurements to determine the localization of UDPGA accumulation within the cells. Digitonin, a detergent that precipitates cholesterol, exploits the higher cholesterol concentration within plasma membranes compared to organellar membranes, specifically permeabilizing the plasma membrane but leaving organelles intact, allowing fractionation of organelles from the cellular milieu. Our findings revealed a significant accumulation of UDPGA within the cytoplasm of UXS1 knockout cells, as opposed to its localization in organelles or the nucleus of

these cells (Figure 2.14). Notably, the overexpression of SLC35D1, a well-established Golgi transporter for UDPGA[169], did not exacerbate any toxicity resulting from UXS1 ablation (Figure 2.15). However, SLC35D1 is not the exclusive UDPGA transporter; within the SLC35 family of transporters, several orphan members have undefined substrates, and there are multiple transporters within the SLC35 family with substrate redundancy[283]. Thus, while we cannot rule out transport of UDPGA via other SLC35 members, our results support the notion that the transport of UDPGA into the Golgi or other organelles is possibly dispensable for the manifestation of its anti-proliferative effects upon its intracellular accumulation.

We illustrate that the accumulation of UDPGA leads to Golgi dysfunction, resulting in impaired glycosylation of vital cell surface glycoproteins and ultimately leading to reduced cell signaling. Nonetheless, additional research is required to precisely elucidate the mechanisms through which excess UDPGA causes aberrations in Golgi structure and function.

There are various possibilities by which UDPGA accumulation could exert toxicity to cancer cells, including excess glucuronidation, increase in hyaluronic acid levels, and competitive transport of sugar nucleotide into Golgi apparatus, among others. While glucuronidation, a phase II metabolic reaction, is primarily associated with detoxifying non-soluble xenobiotic molecules by increasing their polarity, it can also lead to the formation of toxic and reactive metabolites. Notably, acidic metabolites undergoing glucuronidation from ester hydrolysis can give rise

to acyl glucuronides[284]. Acyl glucuronides are electrophilic and reactive, making them prone to forming covalent bonds with macromolecules such as proteins and DNA. In some cases, this interaction can lead to the formation of protein adducts associated with adverse drug reactions[285]. However, it is noteworthy that our investigation did not reveal an exacerbation of toxicity in control and UXS1 knockout (KO) cells following treatment with a panel of drugs known to form acyl glucuronides (data not shown). This observation suggests that the contribution of acyl glucuronides to UXS1 loss-induced toxicity is less likely.

Hyaluronic acid (HA), a non-sulfated polymer composed of UDPGA and GalNAc, undergoes rapid turnover within the extracellular matrix (ECM) of cells. The metabolism of hyaluronan is intricately regulated in cells, and alterations are associated with developmental defects and genetic disorders[286]. We sought to investigate whether the accumulation of excess UDPGA in UXS1 KO cells led to alterations in HA levels. However, our quantification of HA levels revealed no significant differences between control and UXS1 KO cells. Furthermore, prior knockout of enzymes (HAS1, HAS2, and HAS3) responsible for hyaluronic acid formation did not impact the toxicity resulting from UXS1 KO (data not shown). This indicates that UXS1 KO-induced toxicity is unlikely to be attributed to increased HA levels.

Considering that many transporters within the SLC35 family responsible for sugar nucleotide transport into the Golgi apparatus function as antiporters and exhibit significant redundancy, it is reasonable to hypothesize that an excess of

UDPGA cytoplasmic pools may disrupt the balance of sugar nucleotide transport to the Golgi apparatus. SLC35D1 is an antiporter responsible for transporting UDPGA, UDP-GalNAc, and UDP-GlcNAC from the cytoplasm into the ER or Golgi lumen[173,287]. This antiporter exchanges either the corresponding nucleoside monophosphates (UMPs) or, as reported, can facilitate the efflux of UDP-GalNAc and UDP-GlcNAc in exchange for UDPGA influx[168,173,288]. Typically, when a specific transporter facilitates the transport of multiple substrates, it can lead to competitive interactions with elevated concentrations of one substrate inhibiting the transport of the other substrate. Berninsone et al. demonstrated competitive transport of UDPGA, UDP-GalNAc, and UDP-Gal by SQV-7, a paralog of SLC35D2, in Caenorhabditis elegans[174]. One possibility is that an excess of UDPGA in the cytoplasm could potentially lead to either excess or inadequate levels of other sugar nucleotides inside Golgi apparatus, consequently resulting in either decreased glycosylation events or mis-corporation events, overall dysregulating Golgi function.

UXS1 as a cancer therapeutic target

In this study, we provide compelling data that support UXS1 as a promising novel candidate for cancer therapy, as discussed in Chapter II, with UGDH protein expression serving as a distinctive biomarker. Furthermore, we offer mechanistic insights into the anti-proliferative effects induced by UXS1 loss in cancer cells.

Nevertheless, further exploration is needed to firmly establish UXS1 as a viable targetable enzyme for cancer treatment.

We have validated the therapeutic potential of targeting UXS1 through *in vivo* experiments. Our findings indicate that UXS1 knockout in two distinct subcutaneous lung xenograft models not only induced tumor regression but also substantially improved survival in both models. We utilized doxycycline-inducible xenograft models, enabling the injection of cells with wild-type UXS1. The knockout of UXS1 occurred in formed tumors only after tumors reached an approximate volume of 200 mm^3.

One of the limitations of our tumor model is that UXS1 disruption was limited to tumor cells, while in clinical practice, most treatments are administered systemically. Consequently, this approach does not allow us to gain insights into the potential effects of systemic UXS1 inhibition on normal tissues. To comprehensively evaluate the potential of UXS1 targeting in cancer therapies, the development of UXS1 inhibitors becomes imperative. Such inhibitors would enable us to assess UXS1 targeting within more clinically relevant models. For example, administering systemic UXS1 inhibitor treatment to mice harboring patient-derived xenograft tumors could yield valuable insights into the effects of UXS1 inhibition on normal tissues. Furthermore, this approach could better capture the heterogeneity observed in patient tumors.

We provide *in vivo* evidence that only the high UGDH tumors regress following UXS1 inhibition, accompanied by the substantial accumulation of UDPGA (Figure 2.20e). In contrast, in a subcutaneous tumor xenograft model of HT1080, which expresses lower levels of UGDH, UXS1 loss does not confer any benefit, and there is no observable survival advantage.

Analysis of publicly accessible gene expression data from GTEx and TCGA shows a substantial upregulation of UGDH in numerous cancer subtypes, including breast carcinoma, glioblastoma, lung adenocarcinoma, lung squamous carcinoma, pancreatic carcinoma, prostate adenocarcinoma, skin cutaneous melanoma, and testicular germ cell tumors[265]. Among normal tissues, hepatic cells exhibit the highest median UGDH expression. However, in several cancer lineages, including breast, lung, and prostate cancers, tumors show significantly higher median UGDH expression. This suggests that these tumors may be suitable candidates for UXS1-based therapy, as they offer a potentially adequate therapeutic window for inducing UDPGA in tumor cells without causing harm to normal cells.

Multiple lines of evidence indicate that UGDH is induced and upregulated in chemo-resistant cells in contrast to their chemo-naïve counterparts[267,268]. Our findings demonstrate a positive correlation between higher UGDH expression in cancer cell lines and increased resistance to a wide range of chemotherapeutic compounds. Additionally, elevated UGDH levels are associated with aggressive lung and breast tumors, which exhibit reduced survival rates[260,289].

Cancer cells may benefit in multiple ways from elevating UGDH expression. Firstly, elevated UGDH leads to increased synthesis of hyaluronic acid (HA) and glycosaminoglycan-containing proteoglycans, both of which play critical roles in cancer cell adhesion and migration. The glycocalyx, composed of glycoproteins, proteoglycans, and glycolipids, collectively governs receptor-ligand interactions, invasion, and migration in cancer cells[290]. Furthermore, HA, through its interaction with CD44, contributes to chemo-resistance by promoting the expression of P-glycoprotein[291,292]. Particularly, treatment with hyaluronidase synergizes with the action of various chemotherapeutic agents[293]. Secondly, UGDH overexpression also results in higher production of UDPGA, thereby increasing glucuronidation capacity, which could be utilized by cancer cells in the removal of chemotherapeutics from cells. For instance, in colon cancers, the upregulation of UGTs, along with UGDH, facilitates drug inactivation and removal from cells, contributing to intrinsic chemo-resistance[294].

In line with this, our study demonstrates that patient-derived organoids (PDOs) obtained from breast carcinoma patients, and subsequently rendered chemo-resistant through cisplatin exposure, exhibit an induction of UGDH expression and are more sensitive to UXS1 ablation. Likewise, chemo-resistant variants of lung and breast cancer cell lines, H2170 and MDAMB231, respectively, were generated by subjecting their parental cells to a panel of chemotherapeutic agents. Resistant cells derived from both cisplatin and Paclitaxel treatments, also displayed an upregulation of UGDH, rendering them more susceptible to UXS1

inhibition. In our in vivo experiment employing A549 cells, combined treatment with cisplatin and UXS1 knockout (KO) led to significant tumor regression in a synergistic manner. These findings underscore the potential of UXS1 as a viable target for chemo-resistant cells, advocating for further exploration of combination therapies.

Limitations of the study

Identifying tumor subsets amenable to UXS1-based therapy

While UGDH is elevated in multiple tumors and cell lines and generally low across normal tissues and noncancer lines (Figure 2.22), high variability can be seen in UGDH expression across both cancer lines and tumors, which will likely impact the antitumor efficacy of strategies that target UXS1. Indeed, in our analyses of the UXS1 KO effect across cancer lines, 7 lines were UGDH high / UXS1 KO sensitive, while 11 lines were UGDH low / UXS1 KO insensitive.

TCGA analyses reveal that specific cancers, including lung, liver, breast, and prostate, generally exhibit elevated UGDH expression levels compared to others. These tumor types are likely the most suitable candidates for UXS1-targeting approaches. Nonetheless, even within these tumor types, there exists variability in UGDH expression. Therefore, an optimal strategy would involve

UXS1-based therapy tailored not only to tumor types but also on a patient-specific basis, potentially through UGDH-level assessments obtained from tumor biopsies.

Variability in UGDH expression presents a potential challenge in therapy, a phenomenon commonly observed in other chemotherapeutic approaches. There may be cells with low UGDH levels that exhibit resistance to UXS1 inhibitors, leading to their survival and tumor repopulation. To counteract this scenario, a valuable strategy could involve the concurrent administration of chemotherapeutic agents in combination with UXS1-targeting agents. As discussed earlier, chemotherapeutics induces UGDH expression in various contexts, including cell lines in culture, patient-derived organoids, and xenografts. This induction can even convert UXS1-insensitive cell lines into sensitive ones. Importantly, chemotherapeutics do not induce UGDH in normal tissues, in contrast to tumors (Figure 2.27d). Therefore, a combined approach involving chemotherapy and UXS1 inhibition may enable the targeting of subpopulations that would otherwise be unresponsive to either the chemotherapeutic or UXS1 inhibitor.

Safety considerations in targeting UXS1 for cancer therapy

While our findings provide a promising basis for further investigations into UXS1 as a cancer target, there are safety concerns that should be considered while exploring UXS1 targeting agents. Firstly, our studies cannot rule out that rare but important normal cell subtypes may have high UGDH expression and thus be

sensitive to UXS1 loss due to UDPGA overaccumulation. Secondly, UXS1 loss-induced changes to proteoglycans (such as loss of sulfated proteoglycans) may have cell-extrinsic consequences that negatively impact the organism, based on the known roles of secreted proteoglycans in various biological processes[240]. Indeed, it should be noted that UXS1 KO is embryonic lethal[264], although it is unknown whether this is due to UDPGA toxicity or external proteoglycan defects during development. It is also unknown whether this negative impact of UXS1 loss is limited to the development, or whether UXS1 loss would be similarly harmful in an adult organism. Future *in vivo* experiments with UXS1 inhibitors or conditional and/or whole-body KO models of UXS1 would address these questions and guide subsequent therapeutic strategies. We note that incomplete loss of UXS1 via shRNAs still has cancer-toxic consequences observed with UXS1 KO (Figure 2.24), suggesting that partial inhibition of UXS1, which may be more tolerable, could still have anticancer effects. We are also hopeful for a therapeutic window based on the high requirement of cancer cells for UDPGA detoxification, noting that other previously established chemotherapeutics. Another strategy to consider would be the administration of proteoglycans along with UXS1 inhibitors, as proteoglycans are bioavailable and can be supplemented orally or via local injection[295,296].

New perspectives on targeting cancer metabolism and future steps

Numerous small molecule compounds, which aim to target metabolic vulnerabilities, are currently undergoing clinical trials, such as FASN inhibitors, MCT1 inhibitors, and NAMPT inhibitors[297]. However, as discussed in Chapter I, the principal challenge encountered in targeting cancer metabolism lies in the concurrent toxicity to normal cells. Given that normal cells utilize the same metabolic pathways, achieving the required therapeutic window for addressing metabolic vulnerabilities in cancer cells proves to be a formidable task.

For instance, NAMPT, an enzyme integral to NAD biosynthesis, has been recognized as a viable target in cancer cells, given its involvement in critical processes such as DNA repair, proliferation, invasion, stemness, phenotype plasticity, metastasis, angiogenesis, immune regulation, and drug resistance[298]. Nevertheless, prior clinical investigations involving potent NAMPT inhibitors were halted due to the occurrence of clinically significant thrombocytopenia resulting from the dependency of platelets on NAD synthesis[299]. It has, thus, become evident that the field of cancer metabolism necessitates the identification of metabolic targets that offer a higher therapeutic margin. Additionally, there is a growing interest in combination therapy involving chemotherapeutics and immunotherapy to mitigate host toxicity resulting from on-target effects of metabolic targeting, such as GLS1 inhibitors, mutant IDH1 inhibitors, and IDO1 inhibitors[297]. The toxic metabolite theory, as outlined in this study, while not

guaranteeing the complete absence of host toxicity, holds promise due to its requirement for elevated metabolic pathway activity or flux in the identification of novel detoxification enzymes. Furthermore, in the case of UXS1, there is potential for combining UXS1 inhibitors with chemotherapeutics and cancer immunotherapy.

UXS1 is one of the detoxifying enzymes identified through the toxic metabolite theory, representing a promising candidate for cancer therapy. Metabolic enzymes are considered druggable due to their targetable substrate binding sites, allosteric regulation sites, and catalytic sites (once their structures are elucidated). Our data mining analysis, aimed at discovering novel detoxifying enzymes, has yielded a list of potential hits. This suggests the existence of additional toxic metabolites and their corresponding detoxifying enzymes that could be explored as potential targets for cancer treatment.

One of the future steps in this study involves screening for potential UXS1 inhibitors and optimizing promising candidates. This involves the purification of recombinant UXS1 protein using a bacterial expression system, which has previously been successfully employed for UXS1 structure determination, yielding high concentrations[300]. Subsequently, the development of an enzyme assay is essential to measure UXS1 activity. UXS1 functions as a decarboxylase enzyme, generating CO2 as it converts UDP-glucose to UDPGA. Assays can be configured to detect CO2 production through either high-throughput 384 well plates equipped with CO2 sensors or calorimetric assays that identify carbonic acid, a product formed from CO2 and water. Once the activity assay is developed and optimized,

a library of compounds can be screened to identify potent UXS1 inhibitors. Further studies include characterizing the pharmacological effects of UXS1 disruption for ensuring safety and efficacy in in-vivo PDX models.

Another promising avenue for investigation involves exploring the immune response to UXS1 inhibition. Glycosylated peptides play a crucial role in antigen presentation on antigen-presenting cells, facilitating the recognition and activation of cytotoxic T cells for cancer cell elimination[301]. Recent research has demonstrated that alterations in post-translational modifications, particularly glycosylations, can lead to the formation of neoantigens on the surface of cancer cells[302]. Furthermore, there is evidence that a high burden of tumor neoantigens is correlated with the effectiveness of cancer immunotherapy. A high burden of neoantigens is also associated with the expression of immune-related genes such as PD-1, PD-L1, GZMB, and IFNG (interferon gamma) and can serve as a biomarker in lung cancer immunotherapy[303]. Given that UXS1 disruption results in altered glycosylation, it is plausible that UXS1 inhibition may lead to the formation of neoantigens. Future investigations should aim to determine whether UXS1 inhibition in UGDH-high tumors leads to neoantigen formation in lung cancer tumors and whether combining UXS1 inhibition with cancer immunotherapy holds promise as a potential therapeutic approach.

In summary, our study illustrates that an excess of a specific sugar nucleotide can lead to Golgi dysfunction and glycosylation abnormalities in vital cell surface proteins, ultimately culminating in cell death. This observation unveils

an unforeseen connection between a sugar nucleotide metabolic pathway and the regulation of signal transduction processes. This finding prompts further exploration into whether the modulation of other sugar nucleotides might induce similar defects and whether these mechanisms can be harnessed for targeting cancer cells. Crucially, it prompts the inquiry of whether the manipulation of sugar nucleotide metabolism could be utilized to impact the responsiveness to cancer immunotherapy across a broad spectrum of tumors, extending beyond merely UGDH-high tumors.

Bibliography

1 Pavlova, N. N. & Thompson, C. B. The Emerging Hallmarks of Cancer Metabolism. *Cell Metab* **23**, 27-47, doi:10.1016/j.cmet.2015.12.006 (2016).

2 Zou, W. & Green, D. R. Beggars banquet: Metabolism in the tumor immune microenvironment and cancer therapy. *Cell Metab* **35**, 1101-1113, doi:10.1016/j.cmet.2023.06.003 (2023).

3 Chen, X., Chen, S. & Yu, D. Metabolic Reprogramming of Chemoresistant Cancer Cells and the Potential Significance of Metabolic Regulation in the Reversal of Cancer Chemoresistance. *Metabolites* **10**, doi:10.3390/metabo10070289 (2020).

4 Farber, S. & Diamond, L. K. Temporary remissions in acute leukemia in children produced by folic acid antagonist, 4-aminopteroyl-glutamic acid. *N Engl J Med* **238**, 787-793, doi:10.1056/NEJM194806032382301 (1948).

5 Luengo, A., Gui, D. Y. & Vander Heiden, M. G. Targeting Metabolism for Cancer Therapy. *Cell Chem Biol* **24**, 1161-1180, doi:10.1016/j.chembiol.2017.08.028 (2017).

6 Warburg, O. On the origin of cancer cells. *Science* **123**, 309-314, doi:10.1126/science.123.3191.309 (1956).

7 Weinhouse, S. On respiratory impairment in cancer cells. *Science* **124**, 267-269, doi:10.1126/science.124.3215.267 (1956).

8 Hay, N. Reprogramming glucose metabolism in cancer: can it be exploited for cancer therapy? *Nat Rev Cancer* **16**, 635-649, doi:10.1038/nrc.2016.77 (2016).

9 Doherty, J. R. & Cleveland, J. L. Targeting lactate metabolism for cancer therapeutics. *J Clin Invest* **123**, 3685-3692, doi:10.1172/JCI69741 (2013).

10 Wick, A. N., Drury, D. R., Nakada, H. I. & Wolfe, J. B. Localization of the primary metabolic block produced by 2-deoxyglucose. *J Biol Chem* **224**, 963-969 (1957).

11 Zhang, D. *et al.* 2-Deoxy-D-glucose targeting of glucose metabolism in cancer cells as a potential therapy. *Cancer Lett* **355**, 176-183, doi:10.1016/j.canlet.2014.09.003 (2014).

12 Landau, B. R., Laszlo, J., Stengle, J. & Burk, D. Certain metabolic and pharmacologic effects in cancer patients given infusions of 2-deoxy-D-glucose. *J Natl Cancer Inst* **21**, 485-494 (1958).

13 Mergenthaler, P., Lindauer, U., Dienel, G. A. & Meisel, A. Sugar for the brain: the role of glucose in physiological and pathological brain function. *Trends Neurosci* **36**, 587-597, doi:10.1016/j.tins.2013.07.001 (2013).

14 Lieu, E. L., Nguyen, T., Rhyne, S. & Kim, J. Amino acids in cancer. *Exp Mol Med* **52**, 15-30, doi:10.1038/s12276-020-0375-3 (2020).

15 Newsholme, E. A., Crabtree, B. & Ardawi, M. S. Glutamine metabolism in lymphocytes: its biochemical, physiological and clinical importance. *Q J Exp Physiol* **70**, 473-489, doi:10.1113/expphysiol.1985.sp002935 (1985).

16 Yuneva, M., Zamboni, N., Oefner, P., Sachidanandam, R. & Lazebnik, Y. Deficiency in glutamine but not glucose induces MYC-dependent apoptosis in human cells. *J Cell Biol* **178**, 93-105, doi:10.1083/jcb.200703099 (2007).

17 Le, A. *et al.* Glucose-independent glutamine metabolism via TCA cycling for proliferation and survival in B cells. *Cell Metab* **15**, 110-121, doi:10.1016/j.cmet.2011.12.009 (2012).

18 Livingston, R. B., Venditti, J. M., Cooney, D. A. & Carter, S. K. Glutamine antagonists in chemotherapy. *Adv Pharmacol Chemother* **8**, 57-120, doi:10.1016/s1054-3589(08)60594-3 (1970).

19 O'Dwyer, P. J., Alonso, M. T. & Leyland-Jones, B. Acivicin: a new glutamine antagonist in clinical trials. *J Clin Oncol* **2**, 1064-1071, doi:10.1200/JCO.1984.2.9.1064 (1984).

20 Possemato, R. *et al.* Functional genomics reveal that the serine synthesis pathway is essential in breast cancer. *Nature* **476**, 346-350, doi:10.1038/nature10350 (2011).

21 Zhang, B. *et al.* PHGDH Defines a Metabolic Subtype in Lung Adenocarcinomas with Poor Prognosis. *Cell Rep* **19**, 2289-2303, doi:10.1016/j.celrep.2017.05.067 (2017).

22 Amelio, I., Cutruzzola, F., Antonov, A., Agostini, M. & Melino, G. Serine and glycine metabolism in cancer. *Trends Biochem Sci* **39**, 191-198, doi:10.1016/j.tibs.2014.02.004 (2014).

23 Furuya, S. *et al.* Inactivation of the 3-phosphoglycerate dehydrogenase gene in mice: changes in gene expression and associated regulatory networks resulting from serine deficiency. *Funct Integr Genomics* **8**, 235-249, doi:10.1007/s10142-007-0072-5 (2008).

24 Maddocks, O. D. K. *et al.* Modulating the therapeutic response of tumours to dietary serine and glycine starvation. *Nature* **544**, 372-376, doi:10.1038/nature22056 (2017).

25 Menendez, J. A. & Lupu, R. Oncogenic properties of the endogenous fatty acid metabolism: molecular pathology of fatty acid synthase in cancer cells. *Curr Opin Clin Nutr Metab Care* **9**, 346-357, doi:10.1097/01.mco.0000232893.21050.15 (2006).

26 Medes, G., Thomas, A. & Weinhouse, S. Metabolism of neoplastic tissue. IV. A study of lipid synthesis in neoplastic tissue slices in vitro. *Cancer Res* **13**, 27-29 (1953).

27 Snaebjornsson, M. T., Janaki-Raman, S. & Schulze, A. Greasing the Wheels of the Cancer Machine: The Role of Lipid Metabolism in Cancer. *Cell Metab* **31**, 62-76, doi:10.1016/j.cmet.2019.11.010 (2020).

28 Miska, J. & Chandel, N. S. Targeting fatty acid metabolism in glioblastoma. *J Clin Invest* **133**, doi:10.1172/JCI163448 (2023).

29 Tabata, S. *et al.* Thymidine Catabolism as a Metabolic Strategy for Cancer Survival. *Cell Rep* **19**, 1313-1321, doi:10.1016/j.celrep.2017.04.061 (2017).

30 Elledge, S. J., Zhou, Z. & Allen, J. B. Ribonucleotide reductase: regulation, regulation, regulation. *Trends Biochem Sci* **17**, 119-123, doi:10.1016/0968-0004(92)90249-9 (1992).

31 Peters, G. J. *et al.* Thymidylate synthase and drug resistance. *Eur J Cancer* **31A**, 1299-1305, doi:10.1016/0959-8049(95)00172-f (1995).

32 Robinson, A. D., Eich, M. L. & Varambally, S. Dysregulation of de novo nucleotide biosynthetic pathway enzymes in cancer and targeting opportunities. *Cancer Lett* **470**, 134-140, doi:10.1016/j.canlet.2019.11.013 (2020).

33 Chen, B. Y. *et al.* Targeting deoxycytidine kinase improves symptoms in mouse models of multiple sclerosis. *Immunology* **168**, 152-169, doi:10.1111/imm.13569 (2023).

34 Fugger, K. *et al.* Targeting the nucleotide salvage factor DNPH1 sensitizes BRCA-deficient cells to PARP inhibitors. *Science* **372**, 156-165, doi:10.1126/science.abb4542 (2021).

35 Walter, M. & Herr, P. Re-Discovery of Pyrimidine Salvage as Target in Cancer Therapy. *Cells* **11**, doi:10.3390/cells11040739 (2022).

36 Howell, N. & Sager, R. Cytoplasmic genetics of mammalian cells: conditional sensitivity to mitochondrial inhibitors and isolation of new mutant phenotypes. *Somatic Cell Genet* **5**, 833-845, doi:10.1007/BF01542645 (1979).

37 Kroll, W., Loffler, M. & Schneider, F. Energy parameters, macromolecular synthesis and cell cycle progression of in vitro grown Ehrlich ascites tumor cells after inhibition of oxidative ATP synthesis by oligomycin. *Z Naturforsch C Biosci* **38**, 604-612 (1983).

38 DeBerardinis, R. J. & Chandel, N. S. Fundamentals of cancer metabolism. *Sci Adv* **2**, e1600200, doi:10.1126/sciadv.1600200 (2016).

39 Sullivan, L. B., Gui, D. Y. & Vander Heiden, M. G. Altered metabolite levels in cancer: implications for tumour biology and cancer therapy. *Nat Rev Cancer* **16**, 680-693, doi:10.1038/nrc.2016.85 (2016).

40 Lee, N., Spears, M. E., Carlisle, A. E. & Kim, D. Endogenous toxic metabolites and implications in cancer therapy. *Oncogene* **39**, 5709-5720, doi:10.1038/s41388-020-01395-9 (2020).

41 Burgos-Barragan, G. *et al.* Mammals divert endogenous genotoxic formaldehyde into one-carbon metabolism. *Nature* **548**, 549-554, doi:10.1038/nature23481 (2017).

42 Nguyen, Y., Stirnemann, J. & Belmatoug, N. [Gaucher disease: A review]. *Rev Med Interne* **40**, 313-322, doi:10.1016/j.revmed.2018.11.012 (2019).

43 Ozen, H. Glycogen storage diseases: new perspectives. *World J Gastroenterol* **13**, 2541-2553, doi:10.3748/wjg.v13.i18.2541 (2007).

44 Zhou, X., Cui, Y. & Han, J. Methylmalonic acidemia: Current status and research priorities. *Intractable Rare Dis Res* **7**, 73-78, doi:10.5582/irdr.2018.01026 (2018).

45 Ross, K. M. *et al.* Dietary Management of the Glycogen Storage Diseases: Evolution of Treatment and Ongoing Controversies. *Adv Nutr* **11**, 439-446, doi:10.1093/advances/nmz092 (2020).

46 Kim, D. *et al.* SHMT2 drives glioma cell survival in ischaemia but imposes a dependence on glycine clearance. *Nature* **520**, 363-367, doi:10.1038/nature14363 (2015).

47 Ingold, I. *et al.* Selenium Utilization by GPX4 Is Required to Prevent Hydroperoxide-Induced Ferroptosis. *Cell* **172**, 409-422 e421, doi:10.1016/j.cell.2017.11.048 (2018).

48 Carlisle, A. E. *et al.* Selenium detoxification is required for cancer-cell survival. *Nat Metab* **2**, 603-611, doi:10.1038/s42255-020-0224-7 (2020).

49 Spears, M. E. *et al.* De novo sphingolipid biosynthesis necessitates detoxification in cancer cells. *Cell Rep* **40**, 111415, doi:10.1016/j.celrep.2022.111415 (2022).

50 Mikkola, S. Nucleotide Sugars in Chemistry and Biology. *Molecules* **25**, doi:10.3390/molecules25235755 (2020).

51 Corfield, A. P. & Berry, M. Glycan variation and evolution in the eukaryotes. *Trends Biochem Sci* **40**, 351-359, doi:10.1016/j.tibs.2015.04.004 (2015).

52 Bakker, H. *et al.* Functional UDP-xylose transport across the endoplasmic reticulum/Golgi membrane in a Chinese hamster ovary cell mutant defective in UDP-xylose Synthase. *J Biol Chem* **284**, 2576-2583, doi:10.1074/jbc.M804394200 (2009).

53 Wopereis, S., Lefeber, D. J., Morava, E. & Wevers, R. A. Mechanisms in protein O-glycan biosynthesis and clinical and molecular aspects of protein O-glycan biosynthesis defects: a review. *Clin Chem* **52**, 574-600, doi:10.1373/clinchem.2005.063040 (2006).

54 G.D. Khedkar, B. P., C.D. Khedkar, B.A. Chopade. *Nucleic Acids*. Pages 84-92 (2016).

55 Na, L., Li, R. & Chen, X. Recent progress in synthesis of carbohydrates with sugar nucleotide-dependent glycosyltransferases. *Curr Opin Chem Biol* **61**, 81-95, doi:10.1016/j.cbpa.2020.10.007 (2021).

56 Moffatt, B. A. & Ashihara, H. Purine and pyrimidine nucleotide synthesis and metabolism. *Arabidopsis Book* **1**, e0018, doi:10.1199/tab.0018 (2002).

57 Varki A, C. R., Esko J. *Essentials of Glycobiology*. Vol. Chapter 6, Monosaccharide Metabolism (Cold Spring Harbor (NY): Cold Spring Harbor Laboratory Press, 1999).

58 Zimmer, B. M., Barycki, J. J. & Simpson, M. A. Integration of Sugar Metabolism and Proteoglycan Synthesis by UDP-glucose Dehydrogenase. *J Histochem Cytochem* **69**, 13-23, doi:10.1369/0022155420947500 (2021).

59 Perepelov, A. V. *et al.* Structure of a teichoic acid-like O-polysaccharide of Escherichia coli O29. *Carbohydr Res* **341**, 2176-2180, doi:10.1016/j.carres.2006.05.016 (2006).

60 Adeva-Andany, M. M., Gonzalez-Lucan, M., Donapetry-Garcia, C., Fernandez-Fernandez, C. & Ameneiros-Rodriguez, E. Glycogen metabolism in humans. *BBA Clin* **5**, 85-100, doi:10.1016/j.bbacli.2016.02.001 (2016).

61 Cantu-Reyna, C. *et al.* Glucose-6-Phosphate dehydrogenase deficiency incidence in a Hispanic population. *J Neonatal Perinatal Med* **12**, 203-207, doi:10.3233/NPM-1831 (2019).

62 Thomas, D., Rathinavel, A. K. & Radhakrishnan, P. Altered glycosylation in cancer: A promising target for biomarkers and therapeutics. *Biochim Biophys Acta Rev Cancer* **1875**, 188464, doi:10.1016/j.bbcan.2020.188464 (2021).

63 Pietrobono, S. & Stecca, B. Aberrant Sialylation in Cancer: Biomarker and Potential Target for Therapeutic Intervention? *Cancers (Basel)* **13**, doi:10.3390/cancers13092014 (2021).

64 Reiter, W. D. & Vanzin, G. F. Molecular genetics of nucleotide sugar interconversion pathways in plants. *Plant Mol Biol* **47**, 95-113 (2001).

65 Succoio, M., Sacchettini, R., Rossi, A., Parenti, G. & Ruoppolo, M. Galactosemia: Biochemistry, Molecular Genetics, Newborn Screening, and Treatment. *Biomolecules* **12**, doi:10.3390/biom12070968 (2022).

66 Marin-Quilez, A. *et al.* GALE variants associated with syndromic manifestations, macrothrombocytopenia, bleeding, and platelet dysfunction. *Platelets* **34**, 2176699, doi:10.1080/09537104.2023.2176699 (2023).

67 Jacobson, B. & Davidson, E. A. UDP-D-glucuronic acid-5-epimerase and UDP-N-acetyglucosamine-4-epimerase of rabbit skin. *Biochim Biophys Acta* **73**, 145-151, doi:10.1016/0006-3002(63)90429-3 (1963).

68 Rabenstein, D. L. Heparin and heparan sulfate: structure and function. *Nat Prod Rep* **19**, 312-331, doi:10.1039/b100916h (2002).

69 Kunnas, T., Solakivi, T., Maatta, K. & Nikkari, S. T. Glucuronic Acid Epimerase (GLCE) Variant rs3865014 (A>G) Is Associated with BMI, Blood Hemoglobin, Hypertension, and Cerebrovascular Events, the TAMRISK Study. *Ann Hum Genet* **80**, 332-335, doi:10.1111/ahg.12166 (2016).

70 Wen, J., Yi, L., Wan, L. & Dong, X. Prognostic value of GLCE and infiltrating immune cells in Ewing sarcoma. *Heliyon* **9**, e19357, doi:10.1016/j.heliyon.2023.e19357 (2023).

71 Ardejani, M. S., Noodleman, L., Powers, E. T. & Kelly, J. W. Stereoelectronic effects in stabilizing protein-N-glycan interactions revealed by experiment and machine learning. *Nat Chem* **13**, 480-487, doi:10.1038/s41557-021-00646-w (2021).

72 Shental-Bechor, D. & Levy, Y. Effect of glycosylation on protein folding: a close look at thermodynamic stabilization. *Proc Natl Acad Sci U S A* **105**, 8256-8261, doi:10.1073/pnas.0801340105 (2008).

73 Darling, R. J. *et al.* Glycosylation of erythropoietin affects receptor binding kinetics: role of electrostatic interactions. *Biochemistry* **41**, 14524-14531, doi:10.1021/bi0265022 (2002).

74 Dalziel, M., Crispin, M., Scanlan, C. N., Zitzmann, N. & Dwek, R. A. Emerging principles for the therapeutic exploitation of glycosylation. *Science* **343**, 1235681, doi:10.1126/science.1235681 (2014).

75 An, H. J., Froehlich, J. W. & Lebrilla, C. B. Determination of glycosylation sites and site-specific heterogeneity in glycoproteins. *Curr Opin Chem Biol* **13**, 421-426, doi:10.1016/j.cbpa.2009.07.022 (2009).

76 Chu, C. S. *et al.* Profile of native N-linked glycan structures from human serum using high performance liquid chromatography on a microfluidic chip and time-of-flight mass spectrometry. *Proteomics* **9**, 1939-1951, doi:10.1002/pmic.200800249 (2009).

77 in *Essentials of Glycobiology* (eds A. Varki *et al.*) (2009).

78 Samuelsson, E. *et al.* Sialic Acid and Fucose Residues on the SARS-CoV-2 Receptor-Binding Domain Modulate IgG Antibody Reactivity. *ACS Infect Dis* **8**, 1883-1893, doi:10.1021/acsinfecdis.2c00155 (2022).

79 Breloy, I., Schwientek, T., Lehr, S. & Hanisch, F. G. Glucuronic acid can extend O-linked core 1 glycans, but it contributes only weakly to the negative surface charge of Drosophila melanogaster Schneider-2 cells. *FEBS Lett* **582**, 1593-1598, doi:10.1016/j.febslet.2008.04.003 (2008).

80 Iozzo, R. V. & Schaefer, L. Proteoglycan form and function: A comprehensive nomenclature of proteoglycans. *Matrix Biol* **42**, 11-55, doi:10.1016/j.matbio.2015.02.003 (2015).

81 Weigel, P. H. Hyaluronan Synthase: The Mechanism of Initiation at the Reducing End and a Pendulum Model for Polysaccharide Translocation to the Cell Exterior. *Int J Cell Biol* **2015**, 367579, doi:10.1155/2015/367579 (2015).

82 Minakata, S. *et al.* Protein C-Mannosylation and C-Mannosyl Tryptophan in Chemical Biology and Medicine. *Molecules* **26**, doi:10.3390/molecules26175258 (2021).

83 Holt, G. D. & Hart, G. W. The subcellular distribution of terminal N-acetylglucosamine moieties. Localization of a novel protein-saccharide linkage, O-linked GlcNAc. *J Biol Chem* **261**, 8049-8057 (1986).

84 Kreppel, L. K., Blomberg, M. A. & Hart, G. W. Dynamic glycosylation of nuclear and cytosolic proteins. Cloning and characterization of a unique O-GlcNAc transferase with multiple tetratricopeptide repeats. *J Biol Chem* **272**, 9308-9315, doi:10.1074/jbc.272.14.9308 (1997).

85 Clark, R. J. *et al.* Diabetes and the accompanying hyperglycemia impairs cardiomyocyte calcium cycling through increased nuclear O-GlcNAcylation. *J Biol Chem* **278**, 44230-44237, doi:10.1074/jbc.M303810200 (2003).

86 Ho, W. L., Hsu, W. M., Huang, M. C., Kadomatsu, K. & Nakagawara, A. Protein glycosylation in cancers and its potential therapeutic applications in neuroblastoma. *J Hematol Oncol* **9**, 100, doi:10.1186/s13045-016-0334-6 (2016).

87 Du, Z. & Lovly, C. M. Mechanisms of receptor tyrosine kinase activation in cancer. *Mol Cancer* **17**, 58, doi:10.1186/s12943-018-0782-4 (2018).

88 Ferreira, I. G. *et al.* Glycosylation as a Main Regulator of Growth and Death Factor Receptors Signaling. *Int J Mol Sci* **19**, doi:10.3390/ijms19020580 (2018).

89 Takahashi, M., Hasegawa, Y., Gao, C., Kuroki, Y. & Taniguchi, N. N-glycans of growth factor receptors: their role in receptor function and disease implications. *Clin Sci (Lond)* **130**, 1781-1792, doi:10.1042/CS20160273 (2016).

90 Whitson, K. B. *et al.* Functional effects of glycosylation at Asn-579 of the epidermal growth factor receptor. *Biochemistry* **44**, 14920-14931, doi:10.1021/bi050751j (2005).

91 Tsuda, T., Ikeda, Y. & Taniguchi, N. The Asn-420-linked sugar chain in human epidermal growth factor receptor suppresses ligand-independent spontaneous oligomerization. Possible role of a specific sugar chain in controllable receptor activation. *J Biol Chem* **275**, 21988-21994, doi:10.1074/jbc.M003400200 (2000).

92 Yokoe, S. *et al.* The Asn418-linked N-glycan of ErbB3 plays a crucial role in preventing spontaneous heterodimerization and tumor promotion. *Cancer Res* **67**, 1935-1942, doi:10.1158/0008-5472.CAN-06-3023 (2007).

93 Stuttfeld, E. & Ballmer-Hofer, K. Structure and function of VEGF receptors. *IUBMB Life* **61**, 915-922, doi:10.1002/iub.234 (2009).

94 Kovacs, K. *et al.* 2-Deoxy-Glucose Downregulates Endothelial AKT and ERK via Interference with N-Linked Glycosylation, Induction of Endoplasmic Reticulum Stress, and GSK3beta Activation. *Mol Cancer Ther* **15**, 264-275, doi:10.1158/1535-7163.MCT-14-0315 (2016).

95 Teven, C. M., Farina, E. M., Rivas, J. & Reid, R. R. Fibroblast growth factor (FGF) signaling in development and skeletal diseases. *Genes Dis* **1**, 199-213, doi:10.1016/j.gendis.2014.09.005 (2014).

96 Duchesne, L., Tissot, B., Rudd, T. R., Dell, A. & Fernig, D. G. N-glycosylation of fibroblast growth factor receptor 1 regulates ligand and heparan sulfate co-receptor binding. *J Biol Chem* **281**, 27178-27189, doi:10.1074/jbc.M601248200 (2006).

97 Cazet, A., Charest, J., Bennett, D. C., Sambrooks, C. L. & Contessa, J. N. Mannose phosphate isomerase regulates fibroblast growth factor receptor family signaling and glioma radiosensitivity. *PLoS One* **9**, e110345, doi:10.1371/journal.pone.0110345 (2014).

98 Tsang, K. Y. *et al.* Identification of the O-Glycan Epitope Targeted by the Anti-Human Carcinoma Monoclonal Antibody (mAb) NEO-201. *Cancers (Basel)* **14**, doi:10.3390/cancers14204999 (2022).

99 Chandler, K. B. & Costello, C. E. Glycomics and glycoproteomics of membrane proteins and cell-surface receptors: Present trends and future opportunities. *Electrophoresis* **37**, 1407-1419, doi:10.1002/elps.201500552 (2016).

100 Rho, J. H. *et al.* Discovery of sialyl Lewis A and Lewis X modified protein cancer biomarkers using high density antibody arrays. *J Proteomics* **96**, 291-299, doi:10.1016/j.jprot.2013.10.030 (2014).

101 Golgi, C. On the structure of nerve cells. 1898. *J Microsc* **155**, 3-7, doi:10.1111/j.1365-2818.1989.tb04294.x (1989).

102 Mogelsvang, S., Marsh, B. J., Ladinsky, M. S. & Howell, K. E. Predicting function from structure: 3D structure studies of the mammalian Golgi complex. *Traffic* **5**, 338-345, doi:10.1111/j.1398-9219.2004.00186.x (2004).

103 Rambourg, A., Clermont, Y., Chretien, M. & Olivier, L. Modulation of the Golgi apparatus in stimulated and nonstimulated prolactin cells of female rats. *Anat Rec* **235**, 353-362, doi:10.1002/ar.1092350304 (1993).

104 Nakamura, N. *et al.* Characterization of a cis-Golgi matrix protein, GM130. *J Cell Biol* **131**, 1715-1726, doi:10.1083/jcb.131.6.1715 (1995).
105 Mackenzie, J. M., Jones, M. K. & Westaway, E. G. Markers for trans-Golgi membranes and the intermediate compartment localize to induced membranes with distinct replication functions in flavivirus-infected cells. *J Virol* **73**, 9555-9567, doi:10.1128/JVI.73.11.9555-9567.1999 (1999).
106 Huang, Y. *et al.* Visualization of Protein Sorting at the Trans-Golgi Network and Endosomes Through Super-Resolution Imaging. *Front Cell Dev Biol* **7**, 181, doi:10.3389/fcell.2019.00181 (2019).
107 Ladinsky, M. S., Mastronarde, D. N., McIntosh, J. R., Howell, K. E. & Staehelin, L. A. Golgi structure in three dimensions: functional insights from the normal rat kidney cell. *J Cell Biol* **144**, 1135-1149, doi:10.1083/jcb.144.6.1135 (1999).
108 Orci, L. *et al.* Heterogeneous distribution of filipin--cholesterol complexes across the cisternae of the Golgi apparatus. *Proc Natl Acad Sci U S A* **78**, 293-297, doi:10.1073/pnas.78.1.293 (1981).
109 Rabouille, C. *et al.* Mapping the distribution of Golgi enzymes involved in the construction of complex oligosaccharides. *J Cell Sci* **108 (Pt 4)**, 1617-1627, doi:10.1242/jcs.108.4.1617 (1995).
110 Cantarel, B. L. *et al.* The Carbohydrate-Active EnZymes database (CAZy): an expert resource for Glycogenomics. *Nucleic Acids Res* **37**, D233-238, doi:10.1093/nar/gkn663 (2009).
111 Mesecke, N., Spang, A., Deponte, M. & Herrmann, J. M. A novel group of glutaredoxins in the cis-Golgi critical for oxidative stress resistance. *Mol Biol Cell* **19**, 2673-2680, doi:10.1091/mbc.e07-09-0896 (2008).
112 daCosta, C. J., Kaiser, D. E. & Baenziger, J. E. Role of glycosylation and membrane environment in nicotinic acetylcholine receptor stability. *Biophys J* **88**, 1755-1764, doi:10.1529/biophysj.104.052944 (2005).
113 Hassan, H. *et al.* The lectin domain of UDP-N-acetyl-D-galactosamine: polypeptide N-acetylgalactosaminyltransferase-T4 directs its glycopeptide specificities. *J Biol Chem* **275**, 38197-38205, doi:10.1074/jbc.M005783200 (2000).
114 Fritz, T. A., Raman, J. & Tabak, L. A. Dynamic association between the catalytic and lectin domains of human UDP-GalNAc:polypeptide alpha-N-acetylgalactosaminyltransferase-2. *J Biol Chem* **281**, 8613-8619, doi:10.1074/jbc.M513590200 (2006).
115 Shifley, E. T. & Cole, S. E. Lunatic fringe protein processing by proprotein convertases may contribute to the short protein half-life in the segmentation clock. *Biochim Biophys Acta* **1783**, 2384-2390, doi:10.1016/j.bbamcr.2008.07.009 (2008).
116 Capasso, J. M., Keenan, T. W., Abeijon, C. & Hirschberg, C. B. Mechanism of phosphorylation in the lumen of the Golgi apparatus. Translocation of adenosine 5'-triphosphate into Golgi vesicles from rat liver and mammary gland. *J Biol Chem* **264**, 5233-5240 (1989).
117 Baeuerle, P. A. & Huttner, W. B. Tyrosine sulfation is a trans-Golgi-specific protein modification. *J Cell Biol* **105**, 2655-2664, doi:10.1083/jcb.105.6.2655 (1987).
118 Young, R. W. The role of the Golgi complex in sulfate metabolism. *J Cell Biol* **57**, 175-189, doi:10.1083/jcb.57.1.175 (1973).

119 Tang, B. L., Wang, Y., Ong, Y. S. & Hong, W. COPII and exit from the endoplasmic reticulum. *Biochim Biophys Acta* **1744**, 293-303, doi:10.1016/j.bbamcr.2005.02.007 (2005).

120 Marcusson, E. G., Horazdovsky, B. F., Cereghino, J. L., Gharakhanian, E. & Emr, S. D. The sorting receptor for yeast vacuolar carboxypeptidase Y is encoded by the VPS10 gene. *Cell* **77**, 579-586, doi:10.1016/0092-8674(94)90219-4 (1994).

121 Gu, F., Crump, C. M. & Thomas, G. Trans-Golgi network sorting. *Cell Mol Life Sci* **58**, 1067-1084, doi:10.1007/PL00000922 (2001).

122 Hadlington, J. L. & Denecke, J. Sorting of soluble proteins in the secretory pathway of plants. *Curr Opin Plant Biol* **3**, 461-468, doi:10.1016/s1369-5266(00)00114-x (2000).

123 Munro, S. & Pelham, H. R. A C-terminal signal prevents secretion of luminal ER proteins. *Cell* **48**, 899-907, doi:10.1016/0092-8674(87)90086-9 (1987).

124 Lewis, M. J., Sweet, D. J. & Pelham, H. R. The ERD2 gene determines the specificity of the luminal ER protein retention system. *Cell* **61**, 1359-1363, doi:10.1016/0092-8674(90)90699-f (1990).

125 Tu, L. & Banfield, D. K. Localization of Golgi-resident glycosyltransferases. *Cell Mol Life Sci* **67**, 29-41, doi:10.1007/s00018-009-0126-z (2010).

126 Chen, Y., Gershlick, D. C., Park, S. Y. & Bonifacino, J. S. Segregation in the Golgi complex precedes export of endolysosomal proteins in distinct transport carriers. *J Cell Biol* **216**, 4141-4151, doi:10.1083/jcb.201707172 (2017).

127 Stalder, D. & Gershlick, D. C. Direct trafficking pathways from the Golgi apparatus to the plasma membrane. *Semin Cell Dev Biol* **107**, 112-125, doi:10.1016/j.semcdb.2020.04.001 (2020).

128 Sasaki, K. & Yoshida, H. Organelle autoregulation-stress responses in the ER, Golgi, mitochondria and lysosome. *J Biochem* **157**, 185-195, doi:10.1093/jb/mvv010 (2015).

129 Sasaki, K. & Yoshida, H. Golgi stress response and organelle zones. *FEBS Lett* **593**, 2330-2340, doi:10.1002/1873-3468.13554 (2019).

130 Oku, M. *et al.* Novel cis-acting element GASE regulates transcriptional induction by the Golgi stress response. *Cell Struct Funct* **36**, 1-12, doi:10.1247/csf.10014 (2011).

131 Taniguchi, M. *et al.* TFE3 is a bHLH-ZIP-type transcription factor that regulates the mammalian Golgi stress response. *Cell Struct Funct* **40**, 13-30, doi:10.1247/csf.14015 (2015).

132 Kim, W. K., Choi, W., Deshar, B., Kang, S. & Kim, J. Golgi Stress Response: New Insights into the Pathogenesis and Therapeutic Targets of Human Diseases. *Mol Cells* **46**, 191-199, doi:10.14348/molcells.2023.2152 (2023).

133 Sasaki, K. *et al.* PGSE Is a Novel Enhancer Regulating the Proteoglycan Pathway of the Mammalian Golgi Stress Response. *Cell Struct Funct* **44**, 1-19, doi:10.1247/csf.18031 (2019).

134 Helms, J. B. & Rothman, J. E. Inhibition by brefeldin A of a Golgi membrane enzyme that catalyses exchange of guanine nucleotide bound to ARF. *Nature* **360**, 352-354, doi:10.1038/360352a0 (1992).

135 Howley, B. V., Link, L. A., Grelet, S., El-Sabban, M. & Howe, P. H. A CREB3-regulated ER-Golgi trafficking signature promotes metastatic progression in breast cancer. *Oncogene* **37**, 1308-1325, doi:10.1038/s41388-017-0023-0 (2018).

136 Reiling, J. H. *et al.* A CREB3-ARF4 signalling pathway mediates the response to Golgi stress and susceptibility to pathogens. *Nat Cell Biol* **15**, 1473-1485, doi:10.1038/ncb2865 (2013).

137 Miyata, S., Mizuno, T., Koyama, Y., Katayama, T. & Tohyama, M. The endoplasmic reticulum-resident chaperone heat shock protein 47 protects the Golgi apparatus from the effects of O-glycosylation inhibition. *PLoS One* **8**, e69732, doi:10.1371/journal.pone.0069732 (2013).

138 Boss, W. F., Morre, D. J. & Mollenhauer, H. H. Monensin-induced swelling of Golgi apparatus cisternae mediated by a proton gradient. *Eur J Cell Biol* **34**, 1-8 (1984).

139 Suga, K., Saito, A., Mishima, T. & Akagawa, K. Data for the effects of ER and Golgi stresses on the ER-Golgi SNARE Syntaxin5 expression and on the betaAPP processing in cultured hippocampal neurons. *Data Brief* **5**, 114-123, doi:10.1016/j.dib.2015.08.023 (2015).

140 Raphemot, R., Toro-Moreno, M., Lu, K. Y., Posfai, D. & Derbyshire, E. R. Discovery of Druggable Host Factors Critical to Plasmodium Liver-Stage Infection. *Cell Chem Biol* **26**, 1253-1262 e1255, doi:10.1016/j.chembiol.2019.05.011 (2019).

141 Feng, Y. *et al.* Retrograde transport of cholera toxin from the plasma membrane to the endoplasmic reticulum requires the trans-Golgi network but not the Golgi apparatus in Exo2-treated cells. *EMBO Rep* **5**, 596-601, doi:10.1038/sj.embor.7400152 (2004).

142 Sbodio, J. I., Snyder, S. H. & Paul, B. D. Golgi stress response reprograms cysteine metabolism to confer cytoprotection in Huntington's disease. *Proc Natl Acad Sci U S A* **115**, 780-785, doi:10.1073/pnas.1717877115 (2018).

143 Wishart, D. S. *et al.* HMDB: the Human Metabolome Database. *Nucleic Acids Res* **35**, D521-526, doi:10.1093/nar/gkl923 (2007).

144 Nelsestuen, G. L. & Kirkwood, S. The mechanism of action of uridine diphosphoglucose dehydrogenase. Uridine diphosphohexodialdoses as intermediates. *J Biol Chem* **246**, 3824-3834 (1971).

145 Sze, J. H., Brownlie, J. C. & Love, C. A. Biotechnological production of hyaluronic acid: a mini review. *3 Biotech* **6**, 67, doi:10.1007/s13205-016-0379-9 (2016).

146 Liu, Y. & Coughtrie, M. W. H. Revisiting the Latency of Uridine Diphosphate-Glucuronosyltransferases (UGTs)-How Does the Endoplasmic Reticulum Membrane Influence Their Function? *Pharmaceutics* **9**, doi:10.3390/pharmaceutics9030032 (2017).

147 Kuang, B. *et al.* Role of UDP-Glucuronic Acid Decarboxylase in Xylan Biosynthesis in Arabidopsis. *Mol Plant* **9**, 1119-1131, doi:10.1016/j.molp.2016.04.013 (2016).

148 Lehner, N. D., Bullock, B. C. & Clarkson, T. B. Ascorbic acid deficiency in the squirrel monkey. *Proc Soc Exp Biol Med* **128**, 512-514, doi:10.3181/00379727-128-33053 (1968).

149 Nishikimi, M. & Yagi, K. Molecular basis for the deficiency in humans of gulonolactone oxidase, a key enzyme for ascorbic acid biosynthesis. *Am J Clin Nutr* **54**, 1203S-1208S, doi:10.1093/ajcn/54.6.1203s (1991).

150 Smirnoff, N. L-ascorbic acid biosynthesis. *Vitam Horm* **61**, 241-266, doi:10.1016/s0083-6729(01)61008-2 (2001).

151 Idle, J. R. & Gonzalez, F. J. Metabolomics. *Cell Metab* **6**, 348-351, doi:10.1016/j.cmet.2007.10.005 (2007).

152 Patterson, A. D., Gonzalez, F. J. & Idle, J. R. Xenobiotic metabolism: a view through the metabolometer. *Chem Res Toxicol* **23**, 851-860, doi:10.1021/tx100020p (2010).

153 David Josephy, P., Peter Guengerich, F. & Miners, J. O. "Phase I and Phase II" drug metabolism: terminology that we should phase out? *Drug Metab Rev* **37**, 575-580, doi:10.1080/03602530500251220 (2005).
154 Oda, S., Fukami, T., Yokoi, T. & Nakajima, M. A comprehensive review of UDP-glucuronosyltransferase and esterases for drug development. *Drug Metab Pharmacokinet* **30**, 30-51, doi:10.1016/j.dmpk.2014.12.001 (2015).
155 Fedejko, B. & Mazerska, Z. [UDP-glucuronyltransferases in detoxification and activation metabolism of endogenous compounds and xenobiotics]. *Postepy Biochem* **57**, 49-62 (2011).
156 Burchell, B., Brierley, C. H. & Rance, D. Specificity of human UDP-glucuronosyltransferases and xenobiotic glucuronidation. *Life Sci* **57**, 1819-1831, doi:10.1016/0024-3205(95)02073-r (1995).
157 Kiang, T. K., Ensom, M. H. & Chang, T. K. UDP-glucuronosyltransferases and clinical drug-drug interactions. *Pharmacol Ther* **106**, 97-132, doi:10.1016/j.pharmthera.2004.10.013 (2005).
158 Miners, J. O., Mackenzie, P. I. & Knights, K. M. The prediction of drug-glucuronidation parameters in humans: UDP-glucuronosyltransferase enzyme-selective substrate and inhibitor probes for reaction phenotyping and in vitro-in vivo extrapolation of drug clearance and drug-drug interaction potential. *Drug Metab Rev* **42**, 196-208, doi:10.3109/03602530903210716 (2010).
159 Cerny, M. A. Prevalence of Non-Cytochrome P450-Mediated Metabolism in Food and Drug Administration-Approved Oral and Intravenous Drugs: 2006-2015. *Drug Metab Dispos* **44**, 1246-1252, doi:10.1124/dmd.116.070763 (2016).
160 Mazerska, Z., Mroz, A., Pawlowska, M. & Augustin, E. The role of glucuronidation in drug resistance. *Pharmacol Ther* **159**, 35-55, doi:10.1016/j.pharmthera.2016.01.009 (2016).
161 Mays, D. C. *et al.* A nonprimate animal model applicable to zidovudine pharmacokinetics in humans: inhibition of glucuronidation and renal excretion of zidovudine by probenecid in rats. *J Pharmacol Exp Ther* **259**, 1261-1270 (1991).
162 Court, M. H. *et al.* Quantitative distribution of mRNAs encoding the 19 human UDP-glucuronosyltransferase enzymes in 26 adult and 3 fetal tissues. *Xenobiotica* **42**, 266-277, doi:10.3109/00498254.2011.618954 (2012).
163 Ohno, S. & Nakajin, S. Determination of mRNA expression of human UDP-glucuronosyltransferases and application for localization in various human tissues by real-time reverse transcriptase-polymerase chain reaction. *Drug Metab Dispos* **37**, 32-40, doi:10.1124/dmd.108.023598 (2009).
164 Rowland, A., Miners, J. O. & Mackenzie, P. I. The UDP-glucuronosyltransferases: their role in drug metabolism and detoxification. *Int J Biochem Cell Biol* **45**, 1121-1132, doi:10.1016/j.biocel.2013.02.019 (2013).
165 Tcaciuc, E., Podurean, M. & Tcaciuc, A. Management of Crigler-Najjar syndrome. *Med Pharm Rep* **94**, S64-S67, doi:10.15386/mpr-2234 (2021).
166 Bhandari, J., Thada, P. K. & Yadav, D. in *StatPearls* (2023).
167 Muraoka, M., Kawakita, M. & Ishida, N. Molecular characterization of human UDP-glucuronic acid/UDP-N-acetylgalactosamine transporter, a novel nucleotide sugar transporter with dual substrate specificity. *FEBS Lett* **495**, 87-93, doi:10.1016/s0014-5793(01)02358-4 (2001).

168 Kobayashi, T., Sleeman, J. E., Coughtrie, M. W. & Burchell, B. Molecular and functional characterization of microsomal UDP-glucuronic acid uptake by members of the nucleotide sugar transporter (NST) family. *Biochem J* **400**, 281-289, doi:10.1042/BJ20060429 (2006).

169 Hiraoka, S. *et al.* Nucleotide-sugar transporter SLC35D1 is critical to chondroitin sulfate synthesis in cartilage and skeletal development in mouse and human. *Nat Med* **13**, 1363-1367, doi:10.1038/nm1655 (2007).

170 Ishida, N. *et al.* Identification and characterization of human Golgi nucleotide sugar transporter SLC35D2, a novel member of the SLC35 nucleotide sugar transporter family. *Genomics* **85**, 106-116, doi:10.1016/j.ygeno.2004.09.010 (2005).

171 Ishida, N. & Kawakita, M. Molecular physiology and pathology of the nucleotide sugar transporter family (SLC35). *Pflugers Arch* **447**, 768-775, doi:10.1007/s00424-003-1093-0 (2004).

172 Parker, J. L. & Newstead, S. Gateway to the Golgi: molecular mechanisms of nucleotide sugar transporters. *Curr Opin Struct Biol* **57**, 127-134, doi:10.1016/j.sbi.2019.03.019 (2019).

173 Muraoka, M., Miki, T., Ishida, N., Hara, T. & Kawakita, M. Variety of nucleotide sugar transporters with respect to the interaction with nucleoside mono- and diphosphates. *J Biol Chem* **282**, 24615-24622, doi:10.1074/jbc.M611358200 (2007).

174 Berninsone, P., Hwang, H. Y., Zemtseva, I., Horvitz, H. R. & Hirschberg, C. B. SQV-7, a protein involved in Caenorhabditis elegans epithelial invagination and early embryogenesis, transports UDP-glucuronic acid, UDP-N- acetylgalactosamine, and UDP-galactose. *Proc Natl Acad Sci U S A* **98**, 3738-3743, doi:10.1073/pnas.061593098 (2001).

175 Ondo, K., Arakawa, H., Nakano, M., Fukami, T. & Nakajima, M. SLC35B1 significantly contributes to the uptake of UDPGA into the endoplasmic reticulum for glucuronidation catalyzed by UDP-glucuronosyltransferases. *Biochem Pharmacol* **175**, 113916, doi:10.1016/j.bcp.2020.113916 (2020).

176 Sosicka, P. *et al.* SLC35A5 Protein-A Golgi Complex Member with Putative Nucleotide Sugar Transport Activity. *Int J Mol Sci* **20**, doi:10.3390/ijms20020276 (2019).

177 Zhou, T. *et al.* Comparison of First-Line Treatments for Patients With Extensive-Stage Small Cell Lung Cancer: A Systematic Review and Network Meta-analysis. *JAMA Netw Open* **3**, e2015748, doi:10.1001/jamanetworkopen.2020.15748 (2020).

178 Takashima, A. *et al.* Standard First-Line Chemotherapy for Metastatic Gastric Cancer in Japan Has Met the Global Standard: Evidence From Recent Phase III Trials. *Gastrointest Cancer Res* **3**, 239-244 (2009).

179 Pfister, D. *et al.* First-line salvage treatment options for germ cell tumor patients failing stage-adapted primary treatment : A comprehensive review compiled by the German Testicular Cancer Study Group. *World J Urol* **40**, 2853-2861, doi:10.1007/s00345-022-03959-8 (2022).

180 Ramos, A., Sadeghi, S. & Tabatabaeian, H. Battling Chemoresistance in Cancer: Root Causes and Strategies to Uproot Them. *Int J Mol Sci* **22**, doi:10.3390/ijms22179451 (2021).

181 Harris, L. N. *et al.* Molecular subtypes of breast cancer in relation to paclitaxel response and outcomes in women with metastatic disease: results from CALGB 9342. *Breast Cancer Res* **8**, R66, doi:10.1186/bcr1622 (2006).

182 Szakacs, G., Paterson, J. K., Ludwig, J. A., Booth-Genthe, C. & Gottesman, M. M. Targeting multidrug resistance in cancer. *Nat Rev Drug Discov* **5**, 219-234, doi:10.1038/nrd1984 (2006).
183 Galluzzi, L. *et al.* Systems biology of cisplatin resistance: past, present and future. *Cell Death Dis* **5**, e1257, doi:10.1038/cddis.2013.428 (2014).
184 Longley, D. B. & Johnston, P. G. Molecular mechanisms of drug resistance. *J Pathol* **205**, 275-292, doi:10.1002/path.1706 (2005).
185 Trusolino, L. & Bertotti, A. Compensatory pathways in oncogenic kinase signaling and resistance to targeted therapies: six degrees of separation. *Cancer Discov* **2**, 876-880, doi:10.1158/2159-8290.CD-12-0400 (2012).
186 Holohan, C., Van Schaeybroeck, S., Longley, D. B. & Johnston, P. G. Cancer drug resistance: an evolving paradigm. *Nat Rev Cancer* **13**, 714-726, doi:10.1038/nrc3599 (2013).
187 Zheng, H. C. The molecular mechanisms of chemoresistance in cancers. *Oncotarget* **8**, 59950-59964, doi:10.18632/oncotarget.19048 (2017).
188 Bertino, J. R. Karnofsky memorial lecture. Ode to methotrexate. *J Clin Oncol* **11**, 5-14, doi:10.1200/JCO.1993.11.1.5 (1993).
189 Kinahan, C. *et al.* The anti-tumor activity of pralatrexate (PDX) correlates with the expression of RFC and DHFR mRNA in preclinical models of multiple myeloma. *Oncotarget* **11**, 1576-1589, doi:10.18632/oncotarget.27516 (2020).
190 Kaufman, Y., Ifergan, I., Rothem, L., Jansen, G. & Assaraf, Y. G. Coexistence of multiple mechanisms of PT523 resistance in human leukemia cells harboring 3 reduced folate carrier alleles: transcriptional silencing, inactivating mutations, and allele loss. *Blood* **107**, 3288-3294, doi:10.1182/blood-2005-10-4048 (2006).
191 Guo, W. *et al.* Mechanisms of methotrexate resistance in osteosarcoma. *Clin Cancer Res* **5**, 621-627 (1999).
192 Ughachukwu, P. & Unekwe, P. Efflux pump-mediated resistance in chemotherapy. *Ann Med Health Sci Res* **2**, 191-198, doi:10.4103/2141-9248.105671 (2012).
193 Vasiliou, V., Vasiliou, K. & Nebert, D. W. Human ATP-binding cassette (ABC) transporter family. *Hum Genomics* **3**, 281-290, doi:10.1186/1479-7364-3-3-281 (2009).
194 Smyth, M. J., Krasovskis, E., Sutton, V. R. & Johnstone, R. W. The drug efflux protein, P-glycoprotein, additionally protects drug-resistant tumor cells from multiple forms of caspase-dependent apoptosis. *Proc Natl Acad Sci U S A* **95**, 7024-7029, doi:10.1073/pnas.95.12.7024 (1998).
195 Kurimchak, A. M. *et al.* The drug efflux pump MDR1 promotes intrinsic and acquired resistance to PROTACs in cancer cells. *Sci Signal* **15**, eabn2707, doi:10.1126/scisignal.abn2707 (2022).
196 Cole, S. P. Multidrug resistance protein 1 (MRP1, ABCC1), a "multitasking" ATP-binding cassette (ABC) transporter. *J Biol Chem* **289**, 30880-30888, doi:10.1074/jbc.R114.609248 (2014).
197 Kang, J. *et al.* Plant ABC Transporters. *Arabidopsis Book* **9**, e0153, doi:10.1199/tab.0153 (2011).
198 Szymczyk, J. *et al.* FGF/FGFR-Dependent Molecular Mechanisms Underlying Anti-Cancer Drug Resistance. *Cancers (Basel)* **13**, doi:10.3390/cancers13225796 (2021).

199 Fatemian, T. & Chowdhury, E. H. Targeting oncogenes and tumor suppressors genes to mitigate chemoresistance. *Curr Cancer Drug Targets* **14**, 599-609, doi:10.2174/1568009614071409261044458 (2014).
200 Gazdar, A. F. Activating and resistance mutations of EGFR in non-small-cell lung cancer: role in clinical response to EGFR tyrosine kinase inhibitors. *Oncogene* **28 Suppl 1**, S24-31, doi:10.1038/onc.2009.198 (2009).
201 Kaboli, P. J., Imani, S., Jomhori, M. & Ling, K. H. Chemoresistance in breast cancer: PI3K/Akt pathway inhibitors vs the current chemotherapy. *Am J Cancer Res* **11**, 5155-5183 (2021).
202 Baugh, E. H., Ke, H., Levine, A. J., Bonneau, R. A. & Chan, C. S. Why are there hotspot mutations in the TP53 gene in human cancers? *Cell Death Differ* **25**, 154-160, doi:10.1038/cdd.2017.180 (2018).
203 Williams, A. B. & Schumacher, B. p53 in the DNA-Damage-Repair Process. *Cold Spring Harb Perspect Med* **6**, doi:10.1101/cshperspect.a026070 (2016).
204 Ozaki, T. & Nakagawara, A. Role of p53 in Cell Death and Human Cancers. *Cancers (Basel)* **3**, 994-1013, doi:10.3390/cancers3010994 (2011).
205 Parrales, A. & Iwakuma, T. Targeting Oncogenic Mutant p53 for Cancer Therapy. *Front Oncol* **5**, 288, doi:10.3389/fonc.2015.00288 (2015).
206 Letai, A. G. Diagnosing and exploiting cancer's addiction to blocks in apoptosis. *Nat Rev Cancer* **8**, 121-132, doi:10.1038/nrc2297 (2008).
207 Oltersdorf, T. *et al.* An inhibitor of Bcl-2 family proteins induces regression of solid tumours. *Nature* **435**, 677-681, doi:10.1038/nature03579 (2005).
208 Konopleva, M. *et al.* Mechanisms of apoptosis sensitivity and resistance to the BH3 mimetic ABT-737 in acute myeloid leukemia. *Cancer Cell* **10**, 375-388, doi:10.1016/j.ccr.2006.10.006 (2006).
209 Garcia, J. S. Navitoclax, Venetoclax, and Decitabine for the Treatment of High-Risk Myeloid Malignancies. (Dana-Farber Harvard Cancer Center, 2005-active).
210 Lin, X. *et al.* 'Seed' analysis of off-target siRNAs reveals an essential role of Mcl-1 in resistance to the small-molecule Bcl-2/Bcl-XL inhibitor ABT-737. *Oncogene* **26**, 3972-3979, doi:10.1038/sj.onc.1210166 (2007).
211 Wang, H., Guo, M., Wei, H. & Chen, Y. Targeting MCL-1 in cancer: current status and perspectives. *J Hematol Oncol* **14**, 67, doi:10.1186/s13045-021-01079-1 (2021).
212 Phi, L. T. H. *et al.* Cancer Stem Cells (CSCs) in Drug Resistance and their Therapeutic Implications in Cancer Treatment. *Stem Cells Int* **2018**, 5416923, doi:10.1155/2018/5416923 (2018).
213 Zhou, H. M., Zhang, J. G., Zhang, X. & Li, Q. Targeting cancer stem cells for reversing therapy resistance: mechanism, signaling, and prospective agents. *Signal Transduct Target Ther* **6**, 62, doi:10.1038/s41392-020-00430-1 (2021).
214 Zhang, A., Miao, K., Sun, H. & Deng, C. X. Tumor heterogeneity reshapes the tumor microenvironment to influence drug resistance. *Int J Biol Sci* **18**, 3019-3033, doi:10.7150/ijbs.72534 (2022).
215 Dagogo-Jack, I. & Shaw, A. T. Tumour heterogeneity and resistance to cancer therapies. *Nat Rev Clin Oncol* **15**, 81-94, doi:10.1038/nrclinonc.2017.166 (2018).
216 Novoa Diaz, M. B., Martin, M. J. & Gentili, C. Tumor microenvironment involvement in colorectal cancer progression via Wnt/beta-catenin pathway: Providing understanding of

the complex mechanisms of chemoresistance. *World J Gastroenterol* **28**, 3027-3046, doi:10.3748/wjg.v28.i26.3027 (2022).

217 Zhang, Q., Ding, J., Wang, Y., He, L. & Xue, F. Tumor microenvironment manipulates chemoresistance in ovarian cancer (Review). *Oncol Rep* **47**, doi:10.3892/or.2022.8313 (2022).

218 Strassburg, C. P., Manns, M. P. & Tukey, R. H. Differential down-regulation of the UDP-glucuronosyltransferase 1A locus is an early event in human liver and biliary cancer. *Cancer Res* **57**, 2979-2985 (1997).

219 Hu, D. G., Marri, S., McKinnon, R. A., Mackenzie, P. I. & Meech, R. Deregulation of the Genes that Are Involved in Drug Absorption, Distribution, Metabolism, and Excretion in Hepatocellular Carcinoma. *J Pharmacol Exp Ther* **368**, 363-381, doi:10.1124/jpet.118.255018 (2019).

220 Beyerle, J. *et al.* Expression Patterns of Xenobiotic-Metabolizing Enzymes in Tumor and Adjacent Normal Mucosa Tissues among Patients with Colorectal Cancer: The ColoCare Study. *Cancer Epidemiol Biomarkers Prev* **29**, 460-469, doi:10.1158/1055-9965.EPI-19-0449 (2020).

221 Chen, X. *et al.* Variation in gene expression patterns in human gastric cancers. *Mol Biol Cell* **14**, 3208-3215, doi:10.1091/mbc.e02-12-0833 (2003).

222 Hou, J. *et al.* Gene expression-based classification of non-small cell lung carcinomas and survival prediction. *PLoS One* **5**, e10312, doi:10.1371/journal.pone.0010312 (2010).

223 Welsh, J. B. *et al.* Analysis of gene expression identifies candidate markers and pharmacological targets in prostate cancer. *Cancer Res* **61**, 5974-5978 (2001).

224 Sodani, K., Patel, A., Kathawala, R. J. & Chen, Z. S. Multidrug resistance associated proteins in multidrug resistance. *Chin J Cancer* **31**, 58-72, doi:10.5732/cjc.011.10329 (2012).

225 Cuff, R. L., Wade, L. T., Rychlik, B., Jedlitschky, G. A. & Burchell, B. Characterisation of glucuronidation and transport in V79 cells co-expressing UGT1A1 and MRP1. *Toxicol Lett* **120**, 43-49, doi:10.1016/s0378-4274(01)00305-8 (2001).

226 Josephy, P. D. Re: Feigelson, H.S. and Henderson, B.E. (1996) Estrogens and breast cancer. Carcinogenesis, 17, 2279-2284. *Carcinogenesis* **18**, 1859-1860, doi:10.1093/carcin/18.9.1859 (1997).

227 Cengiz, B. *et al.* Differential expression of the UGT1A family of genes in stomach cancer tissues. *Tumour Biol* **36**, 5831-5837, doi:10.1007/s13277-015-3253-1 (2015).

228 Naor, D., Nedvetzki, S., Golan, I., Melnik, L. & Faitelson, Y. CD44 in cancer. *Crit Rev Clin Lab Sci* **39**, 527-579, doi:10.1080/10408360290795574 (2002).

229 Misra, S., Hascall, V. C., Markwald, R. R. & Ghatak, S. Interactions between Hyaluronan and Its Receptors (CD44, RHAMM) Regulate the Activities of Inflammation and Cancer. *Front Immunol* **6**, 201, doi:10.3389/fimmu.2015.00201 (2015).

230 Chaudhry, G. E. *et al.* Understanding Hyaluronan Receptor (CD44) Interaction, HA-CD44 Activated Potential Targets in Cancer Therapeutics. *Adv Pharm Bull* **11**, 426-438, doi:10.34172/apb.2021.050 (2021).

231 Iozzo, R. V. & Sanderson, R. D. Proteoglycans in cancer biology, tumour microenvironment and angiogenesis. *J Cell Mol Med* **15**, 1013-1031, doi:10.1111/j.1582-4934.2010.01236.x (2011).

232 Hanahan, D. & Weinberg, R. A. Hallmarks of cancer: the next generation. *Cell* **144**, 646-674, doi:10.1016/j.cell.2011.02.013 (2011).

233 Meyers, R. M. *et al.* Computational correction of copy number effect improves specificity of CRISPR-Cas9 essentiality screens in cancer cells. *Nat Genet* **49**, 1779-1784, doi:10.1038/ng.3984 (2017).

234 Barretina, J. *et al.* The Cancer Cell Line Encyclopedia enables predictive modelling of anticancer drug sensitivity. *Nature* **483**, 603-607, doi:10.1038/nature11003 (2012).

235 Barger, C. J., Branick, C., Chee, L. & Karpf, A. R. Pan-Cancer Analyses Reveal Genomic Features of FOXM1 Overexpression in Cancer. *Cancers (Basel)* **11**, doi:10.3390/cancers11020251 (2019).

236 Axelrod, J., Kalckar, H. M., Maxwell, E. S. & Strominger, J. L. Enzymatic formation of uridine diphosphoglucuronic acid. *J Biol Chem* **224**, 79-90 (1957).

237 Prydz, K. & Dalen, K. T. Synthesis and sorting of proteoglycans. *Journal of cell science* **113**, 193-205 (2000).

238 Mulder, G. J. Glucuronidation and its role in regulation of biological activity of drugs. *Annu Rev Pharmacol Toxicol* **32**, 25-49, doi:10.1146/annurev.pa.32.040192.000325 (1992).

239 Moriarity, J. L. *et al.* UDP-glucuronate decarboxylase, a key enzyme in proteoglycan synthesis: cloning, characterization, and localization. *J Biol Chem* **277**, 16968-16975, doi:10.1074/jbc.M109316200 (2002).

240 Kjellen, L. & Lindahl, U. Proteoglycans: structures and interactions. *Annu Rev Biochem* **60**, 443-475, doi:10.1146/annurev.bi.60.070191.002303 (1991).

241 Winkler, J., Abisoye-Ogunniyan, A., Metcalf, K. J. & Werb, Z. Concepts of extracellular matrix remodelling in tumour progression and metastasis. *Nat Commun* **11**, 5120, doi:10.1038/s41467-020-18794-x (2020).

242 Vitale, D. *et al.* Proteoglycans and glycosaminoglycans as regulators of cancer stem cell function and therapeutic resistance. *FEBS J* **286**, 2870-2882, doi:10.1111/febs.14967 (2019).

243 Neufeld, E. F. & Hall, C. W. Inhibition of Udp-D-Glucose Dehydrogenase by Udp-D-Xylose: A Possible Regulatory Mechanism. *Biochem Biophys Res Commun* **19**, 456-461, doi:10.1016/0006-291x(65)90146-4 (1965).

244 Gainey, P. A. & Phelps, C. F. Interactions of urdine diphosphate glucose dehydrogenase with the inhibitor urdine diphosphate xylose. *Biochem J* **145**, 129-134, doi:10.1042/bj1450129 (1975).

245 Beattie, N. R., Keul, N. D., Sidlo, A. M. & Wood, Z. A. Allostery and Hysteresis Are Coupled in Human UDP-Glucose Dehydrogenase. *Biochemistry* **56**, 202-211, doi:10.1021/acs.biochem.6b01044 (2017).

246 Ignashkova, T. I. *et al.* Cell survival and protein secretion associated with Golgi integrity in response to Golgi stress-inducing agents. *Traffic* **18**, 530-544, doi:10.1111/tra.12493 (2017).

247 Stanley, P. Golgi glycosylation. *Cold Spring Harb Perspect Biol* **3**, doi:10.1101/cshperspect.a005199 (2011).

248 Varki, A. Factors controlling the glycosylation potential of the Golgi apparatus. *Trends Cell Biol* **8**, 34-40, doi:10.1016/s0962-8924(97)01198-7 (1998).

249 Tarentino, A. L., Gomez, C. M. & Plummer, T. H., Jr. Deglycosylation of asparagine-linked glycans by peptide:N-glycosidase F. *Biochemistry* **24**, 4665-4671, doi:10.1021/bi00338a028 (1985).
250 Unal, E. S., Zhao, R., Qiu, A. & Goldman, I. D. N-linked glycosylation and its impact on the electrophoretic mobility and function of the human proton-coupled folate transporter (HsPCFT). *Biochim Biophys Acta* **1778**, 1407-1414, doi:10.1016/j.bbamem.2008.03.009 (2008).
251 Contessa, J. N., Bhojani, M. S., Freeze, H. H., Rehemtulla, A. & Lawrence, T. S. Inhibition of N-linked glycosylation disrupts receptor tyrosine kinase signaling in tumor cells. *Cancer Res* **68**, 3803-3809, doi:10.1158/0008-5472.CAN-07-6389 (2008).
252 Ornitz, D. M. & Itoh, N. The Fibroblast Growth Factor signaling pathway. *Wiley Interdiscip Rev Dev Biol* **4**, 215-266, doi:10.1002/wdev.176 (2015).
253 Hakuno, F. & Takahashi, S. I. IGF1 receptor signaling pathways. *J Mol Endocrinol* **61**, T69-T86, doi:10.1530/JME-17-0311 (2018).
254 Ouhtit, A., Rizeq, B., Saleh, H. A., Rahman, M. M. & Zayed, H. Novel CD44-downstream signaling pathways mediating breast tumor invasion. *Int J Biol Sci* **14**, 1782-1790, doi:10.7150/ijbs.23586 (2018).
255 Normanno, N. *et al.* Epidermal growth factor receptor (EGFR) signaling in cancer. *Gene* **366**, 2-16, doi:10.1016/j.gene.2005.10.018 (2006).
256 Jayaprakash, N. G. & Surolia, A. Role of glycosylation in nucleating protein folding and stability. *Biochem J* **474**, 2333-2347, doi:10.1042/BCJ20170111 (2017).
257 Lis, H. & Sharon, N. Protein glycosylation. Structural and functional aspects. *Eur J Biochem* **218**, 1-27, doi:10.1111/j.1432-1033.1993.tb18347.x (1993).
258 Taylor, E. S., Pol-Fachin, L., Lins, R. D. & Lower, S. K. Conformational stability of the epidermal growth factor (EGF) receptor as influenced by glycosylation, dimerization and EGF hormone binding. *Proteins* **85**, 561-570, doi:10.1002/prot.25220 (2017).
259 Saha, S. *et al.* UDP-glucose 6-dehydrogenase expression as a predictor of survival in patients with pulmonary adenocarcinoma. *IJS Oncology* **5**, e85 (2020).
260 Hagiuda, D. *et al.* Clinicopathological and prognostic significance of nuclear UGDH localization in lung adenocarcinoma. *Biomed Res* **40**, 17-27, doi:10.2220/biomedres.40.17 (2019).
261 Arnold, J. M. *et al.* UDP-glucose 6-dehydrogenase regulates hyaluronic acid production and promotes breast cancer progression. *Oncogene* **39**, 3089-3101, doi:10.1038/s41388-019-0885-4 (2020).
262 Teoh, S. T., Ogrodzinski, M. P. & Lunt, S. Y. UDP-glucose 6-dehydrogenase knockout impairs migration and decreases in vivo metastatic ability of breast cancer cells. *Cancer Lett* **492**, 21-30, doi:10.1016/j.canlet.2020.07.031 (2020).
263 Lin, L. H. *et al.* Targeting UDP-glucose dehydrogenase inhibits ovarian cancer growth and metastasis. *J Cell Mol Med* **24**, 11883-11902, doi:10.1111/jcmm.15808 (2020).
264 Tang, T. *et al.* A mouse knockout library for secreted and transmembrane proteins. *Nat Biotechnol* **28**, 749-755, doi:10.1038/nbt.1644 (2010).
265 Tang, Z. *et al.* GEPIA: a web server for cancer and normal gene expression profiling and interactive analyses. *Nucleic Acids Res* **45**, W98-W102, doi:10.1093/nar/gkx247 (2017).
266 Vitale, D. L. *et al.* Initial Identification of UDP-Glucose Dehydrogenase as a Prognostic Marker in Breast Cancer Patients, Which Facilitates Epirubicin Resistance and Regulates

Hyaluronan Synthesis in MDA-MB-231 Cells. *Biomolecules* **11**, doi:10.3390/biom11020246 (2021).

267 Ahmed, N. *et al.* Unique proteome signature of post-chemotherapy ovarian cancer ascites-derived tumor cells. *Sci Rep* **6**, 30061, doi:10.1038/srep30061 (2016).

268 Paul, D. *et al.* Global proteomic profiling identifies etoposide chemoresistance markers in non-small cell lung carcinoma. *J Proteomics* **138**, 95-105, doi:10.1016/j.jprot.2016.02.008 (2016).

269 Corsello, S. M. *et al.* Discovering the anti-cancer potential of non-oncology drugs by systematic viability profiling. *Nat Cancer* **1**, 235-248, doi:10.1038/s43018-019-0018-6 (2020).

270 Radominska-Pandya, A., Bratton, S. M., Redinbo, M. R. & Miley, M. J. The crystal structure of human UDP-glucuronosyltransferase 2B7 C-terminal end is the first mammalian UGT target to be revealed: the significance for human UGTs from both the 1A and 2B families. *Drug Metab Rev* **42**, 133-144, doi:10.3109/03602530903209049 (2010).

271 Mackenzie, P. I. *et al.* Regulation of UDP glucuronosyltransferase genes. *Curr Drug Metab* **4**, 249-257, doi:10.2174/1389200033489442 (2003).

272 Nagar, S. & Blanchard, R. L. Pharmacogenetics of uridine diphosphoglucuronosyltransferase (UGT) 1A family members and its role in patient response to irinotecan. *Drug Metab Rev* **38**, 393-409, doi:10.1080/03602530600739835 (2006).

273 Wang, T., Wei, J. J., Sabatini, D. M. & Lander, E. S. Genetic screens in human cells using the CRISPR-Cas9 system. *Science* **343**, 80-84, doi:10.1126/science.1246981 (2014).

274 Sanjana, N. E., Shalem, O. & Zhang, F. Improved vectors and genome-wide libraries for CRISPR screening. *Nat Methods* **11**, 783-784, doi:10.1038/nmeth.3047 (2014).

275 Nonnenmacher, Y. *et al.* Analysis of mitochondrial metabolism in situ: Combining stable isotope labeling with selective permeabilization. *Metab Eng* **43**, 147-155, doi:10.1016/j.ymben.2016.12.005 (2017).

276 Vercesi, A. E., Bernardes, C. F., Hoffmann, M. E., Gadelha, F. R. & Docampo, R. Digitonin permeabilization does not affect mitochondrial function and allows the determination of the mitochondrial membrane potential of Trypanosoma cruzi in situ. *J Biol Chem* **266**, 14431-14434 (1991).

277 Sachs, N. *et al.* A Living Biobank of Breast Cancer Organoids Captures Disease Heterogeneity. *Cell* **172**, 373-386 e310, doi:10.1016/j.cell.2017.11.010 (2018).

278 Couchman, J. R. Transmembrane signaling proteoglycans. *Annu Rev Cell Dev Biol* **26**, 89-114, doi:10.1146/annurev-cellbio-100109-104126 (2010).

279 Mythreye, K. & Blobe, G. C. Proteoglycan signaling co-receptors: roles in cell adhesion, migration and invasion. *Cell Signal* **21**, 1548-1558, doi:10.1016/j.cellsig.2009.05.001 (2009).

280 Karagiorgou, Z., Fountas, P. N., Manou, D., Knutsen, E. & Theocharis, A. D. Proteoglycans Determine the Dynamic Landscape of EMT and Cancer Cell Stemness. *Cancers (Basel)* **14**, doi:10.3390/cancers14215328 (2022).

281 Beattie, N. R., Pioso, B. J., Sidlo, A. M., Keul, N. D. & Wood, Z. A. Hysteresis and Allostery in Human UDP-Glucose Dehydrogenase Require a Flexible Protein Core. *Biochemistry* **57**, 6848-6859, doi:10.1021/acs.biochem.8b00497 (2018).

282 Chen, J., Yu, Y., Gao, J. & Yang, S. UDP-glucose Dehydrogenase: The First-step Oxidation Is an NAD(+)-dependent Bimolecular Nucleophilic Substitution Reaction (S(N)2). *Int J Biol Sci* **15**, 341-350, doi:10.7150/ijbs.28904 (2019).

283 Hadley, B. *et al.* Nucleotide Sugar Transporter SLC35 Family Structure and Function. *Comput Struct Biotechnol J* **17**, 1123-1134, doi:10.1016/j.csbj.2019.08.002 (2019).

284 Burchell, B. & Coughtrie, M. W. Genetic and environmental factors associated with variation of human xenobiotic glucuronidation and sulfation. *Environ Health Perspect* **105 Suppl 4**, 739-747, doi:10.1289/ehp.97105s4739 (1997).

285 Van Vleet, T. R., Liu, H., Lee, A. & Blomme, E. A. G. Acyl glucuronide metabolites: Implications for drug safety assessment. *Toxicol Lett* **272**, 1-7, doi:10.1016/j.toxlet.2017.03.003 (2017).

286 Triggs-Raine, B. & Natowicz, M. R. Biology of hyaluronan: Insights from genetic disorders of hyaluronan metabolism. *World J Biol Chem* **6**, 110-120, doi:10.4331/wjbc.v6.i3.110 (2015).

287 Rautengarten, C. *et al.* A hypomorphic allele of SLC35D1 results in Schneckenbecken-like dysplasia. *Hum Mol Genet* **28**, 3543-3551, doi:10.1093/hmg/ddz200 (2019).

288 Hirschberg, C. B., Robbins, P. W. & Abeijon, C. Transporters of nucleotide sugars, ATP, and nucleotide sulfate in the endoplasmic reticulum and Golgi apparatus. *Annu Rev Biochem* **67**, 49-69, doi:10.1146/annurev.biochem.67.1.49 (1998).

289 Wang, Q. *et al.* UDP-glucose dehydrogenase expression is upregulated following EMT and differentially affects intracellular glycerophosphocholine and acetylaspartate levels in breast mesenchymal cell lines. *Mol Oncol* **16**, 1816-1840, doi:10.1002/1878-0261.13172 (2022).

290 Ahrens, T. D. *et al.* The Role of Proteoglycans in Cancer Metastasis and Circulating Tumor Cell Analysis. *Front Cell Dev Biol* **8**, 749, doi:10.3389/fcell.2020.00749 (2020).

291 Miletti-Gonzalez, K. E. *et al.* The CD44 receptor interacts with P-glycoprotein to promote cell migration and invasion in cancer. *Cancer Res* **65**, 6660-6667, doi:10.1158/0008-5472.CAN-04-3478 (2005).

292 Colone, M. *et al.* The multidrug transporter P-glycoprotein: a mediator of melanoma invasion? *J Invest Dermatol* **128**, 957-971, doi:10.1038/sj.jid.5701082 (2008).

293 Baumgartner, G., Gomar-Hoss, C., Sakr, L., Ulsperger, E. & Wogritsch, C. The impact of extracellular matrix on the chemoresistance of solid tumors--experimental and clinical results of hyaluronidase as additive to cytostatic chemotherapy. *Cancer Lett* **131**, 85-99 (1998).

294 Cummings, J. *et al.* Glucuronidation as a mechanism of intrinsic drug resistance in human colon cancer: reversal of resistance by food additives. *Cancer Res* **63**, 8443-8450 (2003).

295 Watkins, A. R. & Reesink, H. L. Lubricin in experimental and naturally occurring osteoarthritis: a systematic review. *Osteoarthritis Cartilage* **28**, 1303-1315, doi:10.1016/j.joca.2020.05.009 (2020).

296 Gupta, R. C., Lall, R., Srivastava, A. & Sinha, A. Hyaluronic Acid: Molecular Mechanisms and Therapeutic Trajectory. *Front Vet Sci* **6**, 192, doi:10.3389/fvets.2019.00192 (2019).

297 Lemberg, K. M., Gori, S. S., Tsukamoto, T., Rais, R. & Slusher, B. S. Clinical development of metabolic inhibitors for oncology. *J Clin Invest* **132**, doi:10.1172/JCI148550 (2022).

298 Gasparrini, M. & Audrito, V. NAMPT: A critical driver and therapeutic target for cancer. *Int J Biochem Cell Biol* **145**, 106189, doi:10.1016/j.biocel.2022.106189 (2022).

299 Stine, Z. E., Schug, Z. T., Salvino, J. M. & Dang, C. V. Targeting cancer metabolism in the era of precision oncology. *Nat Rev Drug Discov* **21**, 141-162, doi:10.1038/s41573-021-00339-6 (2022).

300 Eixelsberger, T. *et al.* Structure and mechanism of human UDP-xylose synthase: evidence for a promoting role of sugar ring distortion in a three-step catalytic conversion of UDP-glucuronic acid. *J Biol Chem* **287**, 31349-31358, doi:10.1074/jbc.M112.386706 (2012).

301 Wolfert, M. A. & Boons, G. J. Adaptive immune activation: glycosylation does matter. *Nat Chem Biol* **9**, 776-784, doi:10.1038/nchembio.1403 (2013).

302 Bassani-Sternberg, M. & Coukos, G. Mass spectrometry-based antigen discovery for cancer immunotherapy. *Curr Opin Immunol* **41**, 9-17, doi:10.1016/j.coi.2016.04.005 (2016).

303 Guan, H. *et al.* Tumor neoantigens: Novel strategies for application of cancer immunotherapy. *Oncol Res* **31**, 437-448, doi:10.32604/or.2023.029924 (2023).